A New Particle Model

XiaoHua Ye[1]

9140 Leslie Street, Richmond Hill, ON, L4B 0A9, Canada

Contents

[1] Email: yeshowhua@proton.me

Abstract

The Standard Model (SM) does not provide an empirical explanation for the variation in properties such as mass, charge, and spin among point-like fundamental particles. It also does not explain certain phenomena, including dark energy, dark matter, the observed asymmetry between matter and antimatter, neutrino mass and oscillation, and gravity. Additionally, some experimental observations differ from its predictions. This paper presents a new particle model (NPM), which characterizes fundamental particles as composite entities with internal structure. The NPM aims to address major anomalies and unresolved puzzles in the SM and offers testable predictions that extend beyond the SM.

1. Introduction

The Standard Model (SM) describes fundamental particles and forces over various energy scales, but remains incomplete, failing to explain many phenomena and conflicting with some experimental results. In addition, its accuracy relies on techniques like renormalizations, simulations, ongoing corrections and calibrations, etc. The SM has over 19 free parameters (*1*, *2*) —such as masses, coupling constants, and mixing angles—that are set by experiment rather than theory. Measurement reliability often depends on the model and methods used, highlighting that the Standard Model is more of a patchwork than a unified theory.

The SM uses elements and operators in the virtual Hilbert space to mathematically describe the features of fundamental particles and forces due to lack of knowledge of the interior structures of particles. Although it provides statistical accuracy in various sectors, it lacks the power to explain the underlying mechanisms of phenomena. For example, describing particles as point-like conflicts with the concept of their infinitely extended fields and their intrinsic properties like spin and mass.

Since the experimental discovery of neutrino oscillation and the confirmation of neutrino mass by the Super-Kamiokande Observatory and the Sudbury Neutrino Observatory (*3*), the pursuit of physics beyond the Standard Model (SM) has gained significant traction within the physics community, leading to numerous advancements. We have developed a new particle model (NPM) based on a generation principle. While still in the phenomenological stage, it offers unified solutions for Standard Model issues and predicts testable physics beyond the SM.

The following are key insights from the NPM:

- The elementary particles described in the Standard Model (SM) may not originate from a single event like the Big Bang; instead, they could be produced sequentially from more fundamental particles. Each particle possesses internal constituents that govern properties including mass, spin, and charge. The orbital coupling and spin of constituents determines the flavour of the particles.
- Electromagnetic forces are suggested to arise from gravitational interactions, with strong forces forming atop electromagnetic forces, and weak interactions representing the disruption of strong forces.
- According to the NPM, a quark is defined as a charged lepton bound by a gluon, sharing the same electric charge as its corresponding lepton, which explains matter-antimatter asymmetry. This perspective prompts a need to reevaluate theories regarding quark fractional charges and quark confinement. Therefore, quark is unnecessary in particle physics.
- The compositions of many charged mesons proposed in the SM are not supported by the NPM that offers alternative compositions for these particles, which allows better explanation for meson properties and behaviours like meson decay and meson oscillation.
- In the NPM framework, the neutron is made up of four valence quarks in a uud-d core structure, which breaks isospin symmetry but better explains beta decay, nuclear forces, and observed data.
- In NPM, gluons are made of two photons and have mass and flavor, offering an empirical view of QCD. Free gluons explain many dark matter behaviors, while bonded gluons are found in hadrons.
- According to the NPM, neutrinos are emitted photons that keep coupling traits and inherit flavors from parent particles like gluons and leptons. Neutrino oscillation occurs through their interactions with free gluons (dark matters).

The NPM was initially developed from both speculation and analysis of inconsistencies between the Standard Model (SM) and observations. Except for the introductory sections, most of the paper addresses experiments where the SM either conflicts with or does not explain observed phenomena, while the NPM offers potential explanations.

Section 2 presents that elementary particles in the Standard Model (SM) are generated from more basic particles and how fundamental forces and fields are formed, which lays a foundation to connect dark energy, gravitation, electromagnetic field and dark matters, and explain the matter and antimatter asymmetry and the formation of particle families.

Section 3 explores a particle's spin, composition issues, specific spin numbers, and new findings such as neutrinos not being spin-1/2 particles and uses layer associated spin to address the proton spin crisis.

Section 4 introduces the mass origin of particles, different from the Higgs mechanism, and analyzes mass anomalies in the SM.

Section 5 discusses why quarks should have integer charges instead of fractional ones and why free particles with fractional charges haven't been detected, addressing issues like muon and quark anomalous magnetic moments (AMM) and proton antimatter asymmetry.

Section 6 covers new findings about gluons and strong interaction beyond the SM and provides empirical interpretation of QCD.

Section 7 predicts new compositions of common mesons and reveals mechanisms behind their decay and oscillations, and provides better explanations for observations like the $\eta - \eta'$ puzzle, parity violation in the τ–θ puzzle and the isospin-symmetry violation in K decays, etc.

Section 8 details the actual sources and properties of neutrinos and reveals the mechanism of neutrino oscillation and addresses various phenomena in astrophysics.

Section 9 addresses problems in weak interaction theory, including violations of charge conservation and energy conservation laws, and presents updated models for neutrino-induced beta decays.

Section 10 provides qualitative explanations for several neutrino anomalies found in experiments.

Section 11 provides insight into element formation and transmutation, revealing types of nuclear forces and block structures of nuclear binding. It also deduces binding structures for isotopes from ^{2}H to ^{22}C (detailed in **Appendix 1**), explaining associated nuclear behaviors with details and resolving some longstanding astrophysical issues.

Section 12 provides our conclusion and outlook for further research.

2. New Particle Model (NPM)

The New Particle Model (NPM) was established in 2021, and significant advancements have been made over the past four years. Figure 1 illustrates the latest version of the model.

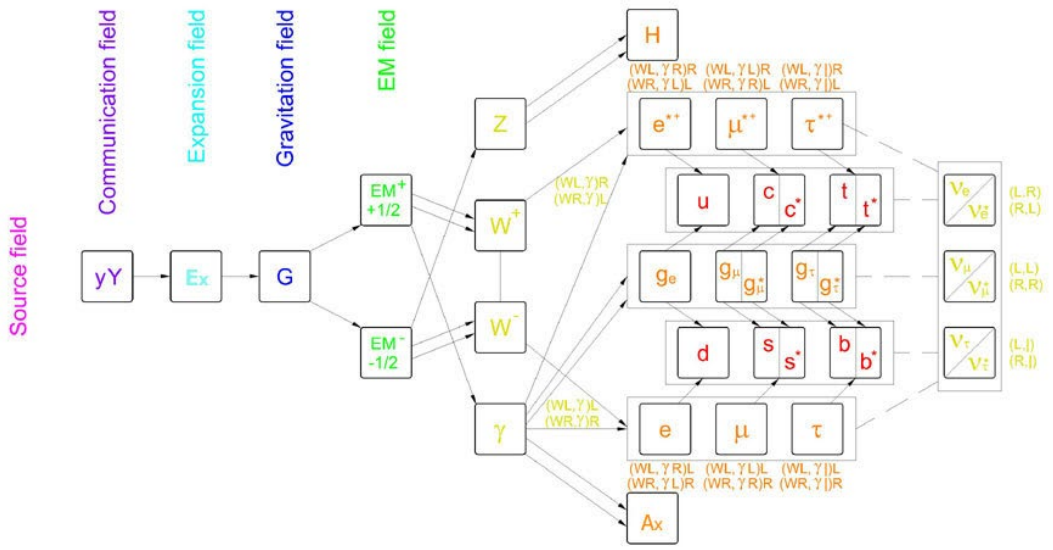

Fig.1| New Particle Model (NPM). Additional particles are proposed beyond the Standard Model: yY (Ying & Yang particle that forms the communication field), Ex (expandon, the dark energy particle that forms the expansion field), G (graviton that forms the gravitation field), EM (the electromagnetic particle that forms EM field), Ax (Axion, the cold dark matter particle), gluons (with three flavours and their heavy-states: g_e, g_μ, g_τ, g^*_μ, g^*_τ), heavy-state leptons (e*, μ*,τ*), heavy-state quarks (s*,c*,b*,t*), heavy-state neutrinos (ν^*_e, ν^*_μ ,ν^*_τ).

The diagram indicates that elementary particles in the Standard Model are not fundamental in the New Particle Model, as they are generated from and composed of more basic particles.

2.1 Formation of Fundamental Fields

At the inception of the universe, countless yY particles emerged from the source field exhibiting zero-dimensional movement (point vibration). Subsequently, the universe evolved into symmetrical multiverses with varying densities of yY particles within each distinct universe. The universe we stay is part of a broader multiverse formation. The periodic multiverse model adheres to symmetry principles, the law of energy conservation, the fine structure constant, and Lorentz transformation, among other rules, which will be elaborated upon in a separate paper.

yY particles are extremely short-lived but can instantly revive, enabling them to create a communication field across the multiverse. Some longer living yY particles form Ex particles or expandons, which move in one dimension and develop a dynamic expansion field known as dark energy.

A single expandon is a very short-lived particle. Some expandons that lasted longer attracted each other to form gravitons, which rotate in two dimensions and collectively created a stable gravitational field.

Like yY particles and expandons, gravitons are fleeting. Some, however, interact in a spiral path, forming new electromagnetic particles (EMs) with chirality and charge. Right-handed motion creates positive EM^+ with a +1/2e charge, while left-handed motion forms negative EM^- with a -1/2e charge.

EM particles are transient and can quickly reappear. There are two types: ground-state and excited-state EMs. Ground-state EMs form a dynamic, isotropic EM field. Pairs of ground-state EM^+ and EM^- create ground-state photons, which make up the EM field in a quadrupole structure (see Fig. 2).

All fundamental particles exhibit particle-wave duality, and their wave properties can be effectively described using Euler's formula variations:

$$e^{it} = \mathrm{Cos}(t) + i\mathrm{Sin}(t) \qquad (2.1)$$

The functions of fundamental forces through wave interaction and resonance can also be described using various forms of Euler's formula, which will be covered in another work. This paper focuses on the internal structures and interactions of particles.

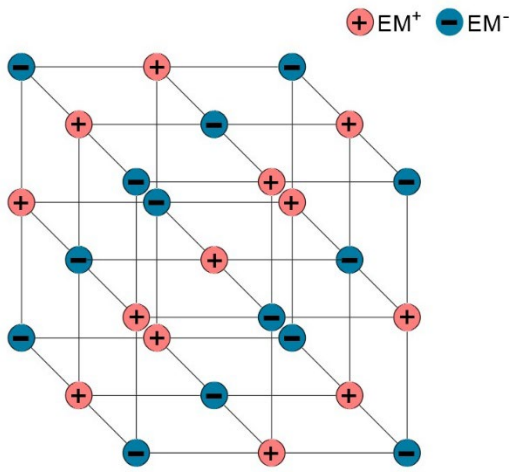

Fig. 2|EM field: A dynamic grid composed of numerous pairs of fleeting ground-state EM^+ and EM^-, arranged in an electromagnetic quadrupole structure.

2.2 1st Generation of Detectable Particles: γ, W and Z

Numerous excited-state EMs were released from the EM field and interacted with each other to form four different particles: $W^+(EM^+{+}EM^+,+1e)$, $W^-(EM^-{+}EM^-,-1e)$, $\gamma(EM^-{+}EM^+$, stable neutral) and $Z(EM^-{+}EM^+$, unstable neutral).

Inside photons (γ), gravitational attraction and centrifugal force balance at a distance possibly less than the Planck length. The coupling chirality of interior EMs determines the γ's polarization: the left-handed γL, the right-handed γR, and the linear γ|. Within γL and γR, EMs have orbital planes perpendicular to the axial direction; in linear γ|, their orbits and the axial are coplanar, which is different from the linear polarization of light (photon beam).

Within W bosons, gravitational attraction and electromagnetic repulsion balance at a tiny scale, possibly smaller than the Planck length. W bosons exhibit only left- or right-handed chirality, lacking linear polarization likely due to internal EM repulsion. Contrary to the Standard Model, W bosons do not decay; their short lifespan is due to interactions with gluons (see details in Sec. 9.1).

The Z boson is an unstable state of the photon (γ) caused by a high-energy event like a particle collision that disrupts the equilibrium of internal electromagnetic forces.

In the Standard Model (SM), W, Z, and γ bosons act as virtual particles delivering fundamental forces. In the New Particle Model (NPM), they behave as real particles, forming new particles through coupling or resonating in extreme conditions like the universe's early stage. As components of fermions and gluons, they influence strong and weak interactions (see Sections 6-9).

2.3 2nd Generation of Detectable Particles: Gluons, Leptons, Axions and Higgs

When two photons (γ) interact, they can form particles such as axions(Ax) and gluons(g).

Inside axions, two photons (or four EMs) interact dynamically, resulting in an almost isotropic electric distribution. Therefore, axions are chargeless, have negligible mass (*4*) and possess an electric dipole moment (EDM). As hypothetical dark matter candidates in the SM, axions only respond to gravity and have very low interaction cross-sections for electromagnetic, weak, and strong forces.

Gluons, composed of two identical photons rotating around each other with regular frequency, thus have a spin number of 1(See Sec. 3 for more on spin). In NPM, there are three flavours of gluons: g_e, g_μ and g_τ. Electron gluons (g_e) consist of two γs with different chirality, muon gluons (g_μ) have two γs with the same chirality, and tau gluons (g_τ) are formed by one left- or right-handed γ rotating with one linear γ, which can be expressed accordingly as follows:

$g_e \equiv \gamma L{+}\gamma R$;

$g_\mu \equiv \gamma L{+}\gamma L$ or $\gamma R{+}\gamma R$;

$g_\tau \equiv \gamma L+\gamma|$ or $\gamma R+\gamma|$.

The two internal photons of a gluon orbit each other, exhibiting either left-handed or right-handed orbital chirality. If one of the two photons possesses chirality that matches the orbital chirality, the gluon is classified as a light state gluon (g). Conversely, if the chirality differs, it is referred to as a heavy state gluon (g*). The electron gluon g_e lacks a heavy state.

Therefore, considering both spin chirality and orbiting chirality, gluons are classified as follows:

$$g_eL \equiv (\gamma L+\gamma R)L \text{ or } g_eR \equiv (\gamma L+\gamma R)R \quad (2.2)$$

$$g_\mu L \equiv (\gamma L+\gamma L)L \text{ or } g_\mu R \equiv (\gamma R+\gamma R)R \quad (2.3)$$

$$g_\tau L \equiv (\gamma L+\gamma|)L \text{ or } g_\tau R \equiv (\gamma R+\gamma|)R \quad (2.4)$$

$$g^*_\mu L \equiv (\gamma R+\gamma R)L \text{ or } g^*_\mu R \equiv (\gamma L+\gamma L)R \quad (2.5)$$

$$g^*_\tau L \equiv (\gamma R+\gamma|)L \text{ or } g^*_\tau R \equiv (\gamma L+\gamma|)R \quad (2.6)$$

When a γ combines with a W^-, they form three types (flavors) of charged leptons: an electron ($e(W^-L+\gamma R)$ or $e(W^-R+\gamma L)$); a muon ($\mu(W^-L+\gamma L)$ or $\mu(W^-R+\gamma R)$); a tau ($\tau(W^-L+\gamma|)$ or $\tau(W^-R+\gamma|)$).

Similarly, when considering orbiting chirality, charged leptons also exhibit two energy states that are influenced by the chirality of the W boson. If the orbiting chirality matches the W boson's chirality, the lepton is in a light state; otherwise, it is in a heavy state. Therefore, charged leptons and their anti-particles can be classified and described accordingly:

$$eL \equiv (W^-L+\gamma R)L \text{ or } eR \equiv (W^-R+\gamma L)R \quad (2.7)$$

$$\mu L \equiv (W^-L+\gamma L)L \text{ or } \mu R \equiv (W^-R+\gamma R)R \quad (2.8)$$

$$\tau L \equiv (W^-L+\gamma|)L \text{ or } \tau R \equiv (W^-R+\gamma|)R \quad (2.9)$$

$$e^+L \equiv (W^+L+\gamma R)L \text{ or } e^+R \equiv (W^+R+\gamma L)R \quad (2.10)$$

$$\mu^+L \equiv (W^+L+\gamma L)L \text{ or } \mu^+R \equiv (W^+R+\gamma R)R \quad (2.11)$$

$$\tau^+L \equiv (W^+L+\gamma|)L \text{ or } \tau^+R \equiv (W^+R+\gamma|)R \quad (2.12)$$

$$e^*L \equiv (W^-R+\gamma L)L \text{ or } e^*R \equiv (W^-L+\gamma R)R \quad (2.13)$$

$$\mu^*L \equiv (W^-R+\gamma R)L \text{ or } \mu^*R \equiv (W^-L+\gamma L)R \quad (2.14)$$

$$\tau^*L \equiv (W^-R+\gamma|)L \text{ or } \tau^*R \equiv (W^-L+\gamma|)R \quad (2.15)$$

$$e^{*+}L \equiv (W^{+}R+\gamma L)L \text{ or } e^{*+}R \equiv (W^{+}L+\gamma R)R \quad (2.16)$$

$$\mu^{*+}L \equiv (W^{+}R+\gamma R)L \text{ or } \mu^{*+}R \equiv (W^{+}L+\gamma L)R \quad (2.17)$$

$$\tau^{*+}L \equiv (W^{+}R+\gamma|)L \text{ or } \tau^{*+}R \equiv (W^{+}L+\gamma|)R \quad (2.18)$$

Although the heavy state leptons are not currently recognized by the physics community, they are essential for understanding the compositions of quarks and mesons (see details in Section 7).

In NPM, a Higgs boson (H) is an unstable combination of two Z bosons, which can be produced in high-energy events such as particle and antiparticle collisions. As 3rd generation excited particles, Higgs bosons are not involved in the mass origination of particles (see details in Sec. 4.1).

2.4 3rd Generation of Detectable Particles: Quarks

In the early stages of particle formation, particles like W bosons, electrons, muons, taus, and their antiparticles collided, releasing immense energy. The remaining particles formed a dense, hot plasma. As the universe expanded and cooled, gluons began combining leptons and their antiparticles to form quarks.

Quarks are charged leptons bound by gluons. Light state gluons bind e, μ, τ leptons to form d, s, b quarks and their anti-particles:

$$dL \equiv (g_e)(W^{-}L+\gamma R)L \text{ or } dR \equiv (g_e)(W^{-}R+\gamma L)R \quad (2.19)$$

$$sL \equiv (g_\mu)(W^{-}L+\gamma L)L \text{ or } sR \equiv (g_\mu)(Ws^{-}R+\gamma R)R \quad (2.20)$$

$$bL \equiv (g_\tau)(W^{-}L+\gamma|)L \text{ or } bR \equiv (g_\tau)(W^{-}R+\gamma|)R \quad (2.21)$$

$$d^{+}L \equiv (g_e)(W^{+}L+\gamma R)L \text{ or } d^{+}R \equiv (g_e)(W^{+}R+\gamma L)R \quad (2.22)$$

$$s^{+}L \equiv (g_\mu)(W^{+}L+\gamma L)L \text{ or } s^{+}R \equiv (g_\mu)(W^{+}R+\gamma R)R \quad (2.23)$$

$$b^{+}L \equiv (g_\tau)(W^{+}L+\gamma|)L \text{ or } b^{+}R \equiv (g_\tau)(W^{+}R+\gamma|)R \quad (2.24)$$

Similarly, light state gluons bind heavy leptons e^{*+}, μ^{*+}, τ^{*+} to form u, c, t quarks and their anti-particles:

$$uL \equiv (g_e)(W^{+}R+\gamma L)L \text{ or } uR \equiv (g_e)(W^{+}L+\gamma R)R \quad (2.25)$$

$$cL \equiv (g_\mu)(W^{+}R+\gamma R)L \text{ or } cR \equiv (g_\mu)(W^{+}L+\gamma L)R \quad (2.26)$$

$$tL \equiv (g\tau)(W^{+}R+\gamma|)L \text{ or } tR \equiv (g\tau)(W^{+}L+\gamma|)R \quad (2.27)$$

$$u^{-}L \equiv (g_e)(W^{-}R+\gamma L)L \text{ or } u^{-}R \equiv (g_e)(W^{-}L+\gamma R)R \quad (2.28)$$

$$c^{-}L \equiv (g_\mu)(W^{-}R+\gamma R)L \text{ or } c^{-}R \equiv (g_\mu)(W^{-}L+\gamma L)R \quad (2.29)$$

$$t^{-}L \equiv (g\tau)(W^{-}R+\gamma|)L \text{ or } t^{-}R \equiv (g\tau)(W^{-}L+\gamma|)R \quad (2.30)$$

When light state leptons bind with a heavy state gluon g*, they form down heavy state quarks and their antiquarks, which can be classified and expressed as follows:

$$s^{*}L \equiv (g_\mu^{*})(W^{-}L+\gamma L)L \text{ or } s^{*}R \equiv (g_\mu^{*})(Ws^{-}R+\gamma R)R \quad (2.31)$$

$$b^{*}L \equiv (g\tau^{*})(W^{-}L+\gamma|)L \text{ or } b^{*}R \equiv (g\tau^{*})(W^{-}R+\gamma|)R \quad (2.32)$$

$$s^{*+}L \equiv (g_\mu^{*})(W^{+}L+\gamma L)L \text{ or } s^{*+}R \equiv (g_\mu^{*})(W^{+}R+\gamma R)R \quad (2.33)$$

$$b^{*+}L \equiv (g\tau^{*})(W^{+*}+\gamma|)L \text{ or } b^{*+}R \equiv (g\tau^{*})(W^{+}R+\gamma|)R \quad (2.34)$$

Similarly, when heavy state leptons bind with a heavy state gluon g*, they form up heavy state quarks and their antiquarks, which can be expressed as follows:

$$c^{*}L \equiv (g_\mu^{*})(W^{+}R+\gamma R)L \text{ or } c^{*}R \equiv (g_\mu^{*})(W^{+}L+\gamma L)R \quad (2.35)$$

$$t^{*}L \equiv (g\tau^{*})(W^{+}R+\gamma|)L \text{ or } t^{*}R \equiv (g\tau^{*})(W^{+}L+\gamma|)R \quad (2.36)$$

$$c^{*-}L \equiv (g_\mu^{*})(W^{-}R+\gamma R)L \text{ or } c^{*-}R \equiv (g_\mu^{*})(W^{-}L+\gamma L)R \quad (2.37)$$

$$t^{*-}L \equiv (g\tau^{*})(W^{-}R+\gamma|)L \text{ or } t^{*-}R \equiv (g\tau^{*})(W^{-}L+\gamma|)R \quad (2.38)$$

Many of the heavy state quarks mentioned above are considered intermediate mesons in the Standard Model, as will be discussed in Section 7.

2.5 4th Generation of Detectable Particles: Hadrons

As the universe continued to cool and expand, gluons and leptons combined to form quarks and hadrons, such as mesons, protons, neutrons, and other baryons in a plasma soup filled with charged leptons and bosons. During this period, numerous collisions and annihilations occurred between charged particles and their respective anti-particles. Additionally, during this phase, an unexplained minor symmetry breaking event resulted in that more positrons and heavy positrons than electrons and heavy electrons were captured by gluons to form the uud core structure of protons, thus there were more protons than anti-protons while more electrons and heavy

electrons than positrons and heavy positrons were left free and moving around protons or captured by protons to form neutrons (uud+d). This explains why protons and electrons are nearly equal in number and marks the earliest examples of C violation in the universe.

After numerous annihilations of particles and anti-particles, most remaining hadrons and leptons include particles like protons, neutrons, electrons, and mesons. The apparent predominance of matter over antimatter is misleading; missing antimatter like positrons and heavy positrons exist as the excess up quarks within protons. When counting the number of positive and negative fermions (leptons and bound leptons) of any atoms there is no matter and antimatter asymmetry. Current technology cannot distinguish between electrons and heavy electrons (or between positrons and heavy positrons) due to the tiny difference of their masses (see Sec. 4.3 for details).

In NPM, protons have a uud core structure like the SM. However, neutrons differ with a core structure of uud+d, having an extra down quark (electron or heavy electron bound by a gluon, see Fig. 3). The binding force between this extra down quark and the uud is weaker than the binding forces within the uud structure (see details on strong force in Sec. 6 and nuclear force in Sec.11). This difference explains the varying behaviors of protons and neutrons in beta decay (see Sec. 9 for more information).

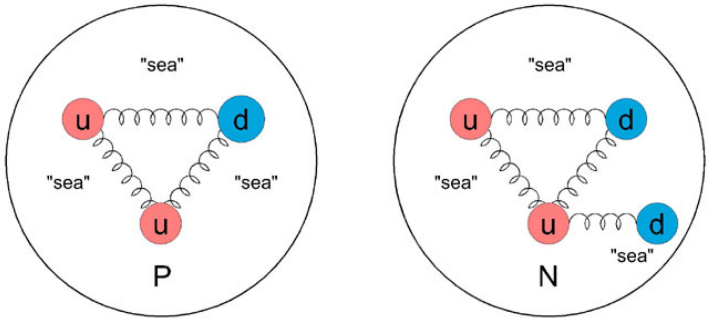

Fig. 3| Main components of proton and neutron: u can be $\bar{d}$ (a gluon bound positron or heavy positron), and d can be $\bar{u}$ (a gluon bound electron or heavy electron). The "sea" consists of quantum fluctuations of (anti)quarks and gluons.

The proposed uud+d structure of the neutron aligns with the structures and compositions of tetraquarks recently observed in various experiments (5-7). On the other hand, recent nEDM experiments have indicated a discrepancy of 13 orders of magnitude between the precision of measurement of the neutron EDM and the expected quantum uncertainty for this quantity (8, 9), which suggests that the current model of the internal structure and composition of the neutron requires considerable modification.

The recent high-energy collisions between argon and scandium atomic nuclei at CERN SPS implicate isospin asymmetry with proton and neutron. The isotope ^{40}Ar has 18 protons and 22 neutrons, and the isotope ^{45}Sc has 21 protons and 24 neutrons. As mentioned, in the Standard Model (SM), protons are composed of two up quarks and one down quark, while neutrons have one up quark and two down quarks. Therefore, more down quarks are expected in the systems before and after collision. However, the experiment result suggests more up quarks post-collision (*10*). According to NPM, this result corresponds to the anticipated uud core structure of protons and the uud-d core structure of neutrons, which clearly shows the isospin asymmetry between proton and neutron because neutron has one more up quark in the core than the udd core suggested by the current theory. Further analysis is in Sec. 7.3.

We predict that similar outcome will occur in other neutron-rich isotope collisions, and the more neutrons in the system, the more charged K quarks (thus more up quarks) will be produced than the SM suggests. For example, colliding ^{41}Ar with ^{47}Sc will yield even more charged K quarks than the current experiments, deviating further from the current theorical prediction.

As the universe continued to expand and cool, it formed primary elements, molecule gas, black holes, stars, and galaxies through processes such as nucleosynthesis, radioactive decay, photodisintegration, cosmic ray spallation, gravitational accumulation, and stellar merging.

2.6 Emitted Photons with Flavors: Neutrinos

In addition to particle and antiparticle annihilation, numerous processes during the evolution of the universe may result in the release of photons from particles like gluons, quarks and charged leptons. In certain scenarios, these internal photons may be emitted as a specific type of photons that retains the coupling characteristics of its previous combination. These are neutrinos, which exist in three flavors: ν_e, ν_μ ,ν_τ, along with their corresponding heavy states ν^*_e, ν^*_μ ,ν^*_τ. These correspond to the three flavors of gluons, quarks, and charged leptons, respectively. For example, the ν_μ/ν^*_μ could represent the internal “γ” released from μ/μ^*, g_μ/g^*_μ, s/s* quarks, and c/c* quarks.

In equations involving neutrino interactions, replacing the particle's internal "γ" with "ν" does not affect validity. Details on neutrinos are covered in Section 8.

3. About Particle Spin

3.1 What Causes Spin

In the Standard Model, elementary particles are indivisible point-like entities that oddly exhibit different spin and spin numbers, as well as varying masses and charges.

Physicists often use Dirac's equation (11) to describe charged fermions with spin, viewing the four-dimensional spinors as the mathematical form of charged (anti) fermion with left-handed and right-handed spin, or up-state spin and down-state spin in an abstract state space. However, Roger Penrose suggested that these four-dimensional spinors can be interpreted as pairs of two-dimensional spinors, each representing a massless particle with left-handed (Zig) or right-handed (Zag) spin. These particles move at the speed of light in a zigzag pattern, alternating between forward and backward motions (12), suggesting they are composite with internal physical spinors.

A recent study suggested that an electron's spin is due to angular momentum from energy circulation in its wave field, and its magnetic moment arises from a circulating charge, though the author thought this is not a description about the internal structure of electrons (13).

In NPM, elementary particles are composed of pair of more fundamental particles. The spin state of a particle is determined by the coupling state of the two interior particles, including factors such as their shape, whether they are spinning regularly, whether they are orbiting each other, and their distance from one another, etc.

If the two interior particles only vibrate without spinning, the particle's spin state depends on the relative position and velocity of the interior particles. When the two interior particles are identical and their spins are synchronized, the particle's overall spin matches theirs. If they differ and have unsynchronized spins, the faster-spinning interior particle dominates the spin state. If a particle returns to its original spin state after the interior particles complete n rotations ($n2\pi$), its spin number is 1/n, reflecting the coupling of interior particles; thus, this spin number is a discrete quantum value.

In the Standard Model (SM), the spin state of a particle is a superposition state; while the magnitude of the spin remains constant, the spin direction can change and switch between up direction and down direction. In contrast, in the New Particle Model (NPM), both the spin magnitude and spin direction of a particle remain unchanged because they are intrinsic properties of the particle, similar to its charge and mass. As a result, the spin number of a particle does not change. This principle applies to all elementary particles and their internal particles.

The Stern-Gerlach experiment first demonstrated quantization of magnetic moment and angular momentum (14, 15), though its interpretation was flawed. It is the direction of silver atoms' spin axes, not their chirality that is indeterminate until exposed to a magnetic field. In a vertical magnetic field, they deflect up or down without changing chirality; in a horizontal field, they move left or right, again retaining chirality. As discussed in Sec.3.3, the silver atom's spin is a layer-associated property, rather than just the sum of its quark and electron spins.

A recent SPDC experiment demonstrated that orbital angular momentum (OAM) is conserved when a single photon splits into entangled pairs (16), indicating OAM and spin cannot exist as a superposition value.

The Pauli exclusion principle states that an atomic orbital can contain a maximum of two electrons, each with opposite spins. This means electron spin states within an orbital cannot be combined or superposed—they must remain distinct and stable.

3.2 Spin of Common Particles

Spin-2 particles

In NPM, gravitons are the first generation of excited particles with interior particles orbiting each other. Gravitons consist of two identical, non-spinning expandons, resuming their original spin state after half a rotation (n=1/2). Thus, gravitons have a spin number of 2, or more precisely, |2|, as they lack polarization or chirality, meaning no spin direction (left or right-handed).

The EMs can be viewed as special gravitons with polarization or chirality, thus having a spin number of ±2. Negative EMs are left-handed with a spin of -2, while positive EMs are right-handed with a spin of +2.

Spin-1 particles

In the context of NPM, photons, W bosons, and Z bosons exhibit a spin number of ±1 due to their composition of two identical particles (EMs) with intrinsic spin. When these internal EMs complete a rotation around each other, the bosons return to their original spin state. Left-handed photons, W bosons, or Z bosons possess a spin number of -1, whereas right-handed bosons have a spin number of +1.

As mentioned in Sec. 2.5, neutrinos are a type of photon with the same spin number: -1 for left-handed and +1 for right-handed. Thus, in NPM, neutrinos are not fermions (spin-1/2 particles).

Gluons (g_e, g_μ, g_τ, $g_{*\mu}$, $g_{*\tau}$) consist of two identical particles, either photons or neutrinos, which possess spin. Consequently, their spin number is also ±1.

Spin-0 particles

Axions (Ax), which are considered cold dark matter particles, consist of two photons analogous to gluons. However, the internal photons within Ax exhibit a closer and more intense coupling, resulting in highly dynamic relative motions. These interactions can be interpreted as four intertwined electromagnetic fields. Regardless of how many times the two photons rotate around each other, the overall spin state never returns to its original configuration ($n \to \infty$), leading to a spin number of 0.

The Higgs particle (H) consists of two Z bosons, with an interior situation like Ax, resulting in a spin number of 0. However, the Z boson is highly unstable, which causes the H particle to be extremely unstable as well.

Spin-1/2 particles

Charged leptons (e, μ, τ, e*, μ*, τ*) and their antiparticles are composed of two distinct spinning particles: a photon (or neutrino) and a W boson. The spins of the photon and the W boson are asynchronous, requiring the internal particles to complete at least two rotations for the charged lepton to restore its spin state. Consequently, the spin number of charged leptons can be ±1/2 or ±1/n (where $n \geq 2$). For left-handed charged leptons, the spin number is negative, while it is positive for right-handed charged leptons. Further research is necessary to definitively determine the exact spin number for charged leptons. For instance, the electron's spin number could be precisely ±1/2 as its charge rotates twice as fast as its mass (*17*). The charge rotation originates from the W^- boson, and the mass rotation is influenced by the interactions between the W boson and the photon.

As detailed in Section 2.4, a quark is a charged lepton bound by a gluon, resulting in a spin number of ±1/2 or ±1/n (where $n \geq 2$).

Protons and neutrons each consist of two distinct internal components: the core structure and the virtual particle sea. The relative motion between the core and the "sea" can be compared to the movement between the Earth and its cloud atmosphere or the interaction between interior photons and W bosons within leptons. Consequently, the spin numbers of protons and neutrons are ±1/2 or ±1/n (where $n \geq 2$).

3.3 Layer Associated Spin

The spin number of gluons is the same (spin-1) as that of photons, W bosons, and Z bosons, but they present a spin state at different layers. Similarly, the spin number of protons and neutrons is identical to that of quarks (spin-1/2), yet they also display spin states at different layers. The spin number is a discontinuous quantum number that reflects the state of relative motion or orbital state between the interior components rather than the sum of the spin numbers of its interior particles. For example, a photon consists of an EM^- with spin number -2 and an EM^+ with spin number +2, but its spin number is either +1, or -1, never 0. Similarly, the spin number of a proton or neutron is not the sum of all interior particles' spin.

The spin angular momentum of particles is largely determined by the orbital angular momentum of their primary sublayer components, such as the uud core and virtual particle sea in protons. At deeper sublayers, the spin and orbital angular momentum of interior particles can be neglected. Therefore, the proton's spin is mainly influenced by the orbital angular momentum of the uud core and surrounding "sea", not by the valence quarks' spins. This suggests that the EMC experiment findings (*18*, *19*) which showed nearly equal numbers of valence quarks spinning in both directions, should not be considered a "proton spin crisis."(*20-22*).

In NPM, valence quarks and gluons form a stable uud core in the proton, with both contributing only to the core's collective orbital angular momentum. Sea (anti)quarks and non-massless sea gluons exist as quantum fluctuations and contribute solely to the sea's orbital angular momentum. Both the core and the sea together determine the proton's overall orbital

angular momentum at an upper layer, an aspect often neglected in theoretical and experimental analyses (23-27).

3.4 Spin Momentum of "Point-like" Particles

In the Standard Model (SM), elementary particles are point-like entities that do not exhibit true spinning. This concept is based on two key assumptions: the theory of relativity, which states that nothing can travel faster than the speed of light (C), and the Heisenberg uncertainty principle, a fundamental principle of quantum theory.

For a particle as small as an electron or even smaller, it would need to rotate at speeds faster than light to achieve the observed angular momentum and magnetic moment. The uncertainty principle indicates that when examining objects or structures smaller than photons and electrons, the momentum of these internal particles becomes too large for precise measurement. Additionally, the general theory of relativity suggests that a significant amount of energy concentrated in a very small space could result in sharp space-time curvature, potentially leading to the formation of a black hole.

A recent study on electrons indicates that the superluminal velocity of both mass flow and charge flow of electrons can be avoided due to the distribution of the electron's mass and charge over sufficiently large spaces (17)**.** In the NPM framework, electrons and other fundamental particles are not considered rigid point-like objects. Rather, the internal W and photon (or neutrino) components that constitute the electron progress in a spiral manner. The angular momentum of the electron is thus an average value produced by this spin-precession effect, ensuring that it does not exceed the speed of light.

Scientists acknowledge that every theory has its limits, including the uncertainty principle. The Planck size, based on the speed of light, is not necessary the finalized boundary. In NPM, yY particles and expandons existed before the electromagnetic field, possibly moving faster than light, which accounts for the superluminal phenomena observed in quantum entanglement, to be discussed further elsewhere.

4. About Particle Mass

4.1 The Origin of Mass

Essential mass

As delineated in Section 1, it is established that all known elementary particles contain electromagnetic particles (EMs), which can be considered as gravitons with polarization. Consequently, the mass of elementary particles originates from their internal gravitons and EMs through interactions with the gravitational field and the electromagnetic field.

A particle’s mass is its resistance to movement in the gravitational field and electromagnetic field. More mass means more resistance, causing slower movement. Particles have two types of mass: gravitational mass, determined by the number of gravitons they contain, and electromagnetic mass, defined by the structure and state of their internal EMs.

Elementary particles generally show a spiral precession within the electromagnetic field. In addition to their longitudinal motion, these particles also exhibit transverse movement, leading to both longitudinal and transverse electromagnetic mass.

Mass is a concept associated with observation and measurement. Gravitons and gravitational field, electromagnetic particles (EMs) and EM field could be the current technological boundary for measurement. Thus, particles such as yY particles and expandons that formed before the formation of gravitational field and electromagnetic field are outside the scope of the concept of mass. In Sec. 4.2, we will discuss that the energy is more fundamental than mass.

It is more accurate to refer to a particle's mass as intrinsic mass or net mass, rather than rest mass or static mass, because all elementary particles are perpetually in motion. Motion is an innate characteristic of these particles. Although gravitons and photons in a gravitational field and electromagnetic field may remain in a ground state, they do not remain at rest but instead undergo dynamic changes.

Many scientists, including Newton and Einstein, refer to the net mass of an object as its inertial mass. Newton defined inertia as the capacity or tendency of a substance to resist changes in its state, which is proportional to its mass (*28*).

Gravity is transmitted at the speed of light through the state transitions of adjacent gravitons in the gravitational field. Gravitons are fleeting, with zero gravitational mass.

Electromagnetic force travels at the speed of light via virtual photons in the EM field. These ground-state grid pairs of positive and negative EMs are also fleeting and massless.

The movement speed C of virtual gravitons and virtual photons is based on state transitions, determined by the transit frequency and the distance between adjacent particles (the Planck length). This allows for the calculation of the maximum frequency of a gamma ray.

Some EMs with longer lifespans were excited by the EM field and combined to form other particles, such as photons (γ), Z particles, and W particles, as described in Section 2.2. The excited photons in NPM have mass, so they are not the γ bosons in quantum theory, which are the same as the virtual photons discussed above.

Excited photons have a longer lifespan than virtual photons, but their existence remains brief. Their movement in the electromagnetic field is like that of virtual photons and is typically considered nearly instantaneous.

Masses of Composite Particles

Excited free photons contain only two electromagnetic particles (EMs), resulting in an extremely small gravitational mass. These photons share the same composition as virtual photons that lack

transverse electromagnetic mass; thus, their EM mass is also minimal. Consequently, free photons have a very small mass ($< 1\times10^{-18}$ eV) (29), measurable by experiments like the Eddington experiment (30).

In the Standard Model, elementary particles gain mass through electroweak symmetry breaking via the Higgs mechanism, a virtual process in which particles move in the Higgs field and couple with the Higgs particle to obtain mass through repeated conversion of positive and negative spin states (31). In the NPM, mass generation occurs similarly, with particles moving through the electromagnetic field and interacting with virtual photons or the positive and negative EM pairs.

In the electroweak theory, W^+, W^-, Z and γ are composed of a pair of four massless bosons (W1, W2, W3 and B). These bosons exist within weak isospin fields and weak supercharge fields. The particles W^+, W^- and Z acquire mass through the Higgs mechanism by interacting with the Goldstone boson, whereas γ remains massless as it does not interact with the Goldstone boson (32, 33).

While direct evidence for weak isospin and supercharge fields is lacking, electroweak theory implies that W, Z, and γ are composite particles (34), indirectly supporting the New Particle Model (NPM). NPM also treats the Higgs boson as an ordinary composite particle, which addresses the Standard Model's hierarchy problem (35-37).

Free photons have a structure like virtual photons, resulting in a large magnetic moment, small mass, and near-light speed movement. In contrast, W bosons have a different structure with a large mass and small magnetic moment, preventing fast movement.

In NPM, when paired with a W boson, a photon can increase the magnetic moment and reduce the mass of the composite particle. The spin and orbiting chirality of the W boson and photon inside a charged lepton primarily determine its properties such as flavour, mass, and magnetic moment. Leptons with different spin chirality between their interior W boson and photon have a larger magnetic moment and smaller mass compared to those with identical spin chirality.

Similarly, leptons with a linear interior photon have a much weaker magnetic moment and a larger mass. Thus,

$$m_\tau > m_\mu > m_e \quad (4.1)$$

$$m_\tau^* > m_\mu^* > m_e^* \quad (4.2)$$

They are also applied to the three generations of quarks, hence

$$m_b > m_s > m_d \quad (4.3)$$

$$m_t > m_c > m_u \quad (4.4)$$

$$m_b^* > m_s^* \quad (4.5)$$

$$m_t^* > m_c^* \quad (4.6)$$

4.2 Mass vs Energy

The analysis indicates that the net mass of elementary particles is derived from underlying particles and interactions, influenced directly by the gravitational field and the electromagnetic field. Consequently, hidden energy and fields play a crucial role in determining the particle's mass.

Einstein's renowned mass-energy equivalence formula, $E = mc^2$, posits that mass and energy are interchangeable.

Since energy is more fundamental, energy is always conserved, but mass is not. For instance, the low-energy positron and electron could annihilate each other and produce two or more photons and high-energy positron and electron annihilation could produce 10 mesons and a pair of proton and anti-proton (*38*). The extra particles and mass here are converted by the kinetic energy of the positron and electron, and their interior particles and binding energy.

Gravitons become EMs by attracting and approaching each other. EMs retain the graviton's gravitational mass and convert their internal angular kinetic energy or circular energy into EM mass. Excited elementary particles gain both gravitational and electromagnetic mass from their internal EMs, coupling with the grid gravitons of the gravitational field and the grid EMs of the electromagnetic field.

The mass and internal energy of a particle are primarily determined by its internal components, yet these properties are typically observed or measured externally. Consequently, the mass and energy of a particle's internal components may not be observable. For instance, the significant mass of internal W particles and the binding energy of internal photons within an electron are entirely concealed from observation and measurement. Likewise, numerous masses and energies exist within fundamental particles and hidden fields in the universe, which is essential for understanding and addressing the cosmological constant problem (*39*, *40*).

The contributions of gravitational field and electromagnetic field to an object's total mass vary across different levels. Elemental particles are significantly influenced by both fields, while hadrons are mainly affected by the EM field. Atoms primarily derive their mass from nucleons, with minimal impact from EM interactions between electrons and nucleons.

4.3 Masses of Quarks (d, u and s)

Spin-orbit coupling causes particles in the same generation of charged leptons and quarks to have different masses. When the orbiting chirality is opposite to the W's spin chirality, the particle has a higher mass (heavy state) than when they are aligned. Therefore, the following equations apply:

$$m_{\tau^*} > m_{\tau} \quad (4.7)$$

$$m_{\mu^*} > m_{\mu} \quad (4.8)$$

$$m_{e^*} > m_{e} \quad (4.9)$$

$$m_{t} > m_{b} \quad (4.10)$$

$$m_{c} > m_{s} \quad (4.11)$$

$$m_{u} > m_{d} \quad (4.12)$$

$$m_{t^*} > m_{t} \quad (4.13)$$

$$m_{b^*} > m_{b} \quad (4.14)$$

$$m_{c^*} > m_{c} \quad (4.15)$$

$$m_{s^*} > m_{s} \quad (4.16)$$

As stated in Section 4.2, the binding energy of gluons increases the mass of quarks compared to their corresponding leptons. Therefore, the following predictions are made:

$$m_{u} > m_{e^{*+}} \quad (4.17)$$

$$m_{d} > m_{e} \quad (4.18)$$

$$m_{c} > m_{\mu^{*+}} \quad (4.19)$$

$$m_{s} > m_{\mu} \quad (4.20)$$

$$m_{t} > m_{\tau^{*+}} \quad (4.21)$$

$$m_{b} > m_{\tau} \quad (4.22)$$

Since both m_u and m_d are increased by the same factors from $m_{e^{*+}}$ and m_e, the difference between them is likely to be proportionally magnified. Therefore, we deduce:

$$m_{u} - m_{d} > m_{e^{*+}} - m_{e} \quad (4.23)$$

About the Mass of Down Quark and Up Quark

Equation (4.12) suggests $m_u > m_d$, which contradicts the Particle Data Group data: $m_u = 2.16 \pm 0.07$ MeV and $m_d = 4.70 \pm 0.07$ MeV, with $m_d - m_u \approx 2.54$ MeV([41]). These PDG values are inconsistent with the mass of the neutral pion π^0 also provided by PDG, $m_{\pi^0} = 134.9768 \pm 0.0005$ MeV([41]). Considering the composition of π^0 ($u\bar{u}$ or $d\bar{d}$), the uncertainty indicates that $|m_{u\bar{u}} - m_{d\bar{d}}| < 0.0005$ MeV, suggesting $|m_u - m_d|$ is much less than 0.0005 MeV.

In NPM, the value of $|m_u - m_d|$ has been found to be up to 5 orders of magnitude less than 0.0005 MeV. The core composition of a proton is the uud structure or similar combinations that include $\bar{u}$ and $\bar{d}$, such as $uu\bar{u}$, $ud\bar{d}$, $ud\bar{u}$, $dd\bar{u}$, and $dd\bar{d}$. Since $m_u = m_{\bar{u}}$ and $m_d = m_{\bar{d}}$, the largest mass difference among these combinations is between $uu\bar{u}$ and $dd\bar{d}$, which is $3n|m_u - m_d|$, where $n > 1$ represents the mass enlarging factor due to gluons and the "sea" of virtual particles in the

proton. According to CODATA 2022 (42), the mass of a proton is 938.27208943(29) MeV. The precision level suggests that $3n|m_u - m_d| < 0.00000001$ MeV, implying $|m_u - m_d| < 0.000000003$ MeV.

The eq. (4.23) also induces that $m_{e^{*+}} - m_e < 0.000000003$ MeV, which is why it would be difficult to separate e^* from e.

We also found that the core structure of proton and neutron in NPM could explain the mass difference between the proton and neutron better than that in the SM. According to the value of CODATA 2022 (43), the mass of neutron is 939.56542194(48) MeV, resulting in $m_N - m_P = 1.29333251(19)$ MeV. This difference primarily arises from the mass of the additional down quark in the uud+d core structure of the neutron. This is consistent with considering eq. (4.18) $m_d > m_e$ and the electron mass $m_e = 0.51099895069(16)$ MeV (44).

About the Mass of Strange Quark

According to 2024 PDG data (41), $m_s = 93.5 \pm 0.8$ MeV, $m_\mu = 105.6583755 \pm 0.0000023$ MeV, indicating $m_s < m_\mu$, contrary to NPM's prediction of eq.(4.20) $m_s > m_\mu$. Since m_μ is experimentally well-established, any issue likely arises from the value of m_s, which combines measurement data and model calculations. Recent research shows that it could get $m_s = 120$ MeV by setting $m_c = 1.35$ GeV and $m_b = 4.0$ GeV under certain conditions, implying $m_s > m_\mu$ (45).

When the masses of d quark, u quark, and s quark are adjusted based on NPM predictions, they align more consistently with their respective masses as presented in the SM.

5. About Particle Charge

5.1 Integer Charge vs Fractional Charge

In NPM, only EM^+ and EM^- particles have fractional charges of +1/2e and -1/2e, respectively. These particles can bind to form ±1e or neutral particles. Therefore, NPM does not allow for particles with fractional charges of ±1/3e or ±2/3e, like quarks in the SM. Quarks are considered charged leptons bound by gluons and will be detected as such when escaping gluon bond, like electrons and positrons in beta decay. If particles with charges of -1/3e and +1/3e are allowed, as assumed with down and bottom quarks and their antiparticles, then particles carrying charges of integer multiples of 1/3e—such as the up, charm, and top quarks, as well as leptons and their antiparticles—would have to be composite. This observation suggests an inconsistency within the Standard Model theory. Additionally, in certain meson decays such as $J/\psi(1s)$, an intermediate γ can produce hadrons or leptons but never fractionally charged quarks—why is this the case?

The fractional charges of quarks were determined during the development of Quantum Chromodynamics (QCD) theory and were initially attributed to integer charges (46, 47). However, scientists have not observed fractionally charged quarks directly. Consequently, the theory of quark confinement (or gluon confinement) was developed to explain this phenomenon.

Studies suggest that quarks can move freely and bind to form hadrons in the early universe (48, 49), and a free up quark combining with a free down quark would form a meson with charge +1/3e and a different mass than the down quark. As a result, scientists theorized that fractionally charged particles (FCP) might be found in remnants of the Big Bang or other cosmic events. However, despite numerous experiments, including oil drop, high atmosphere experiments like BESS (50), space missions like AMS-01 and DAMPE (51), and underground experiments like CUORE (52), no FCPs were detected.

The fractional charges of quarks do not entirely align with observations about the composition of protons. Recent research, along with several previous studies, has identified approximately 50% more anti-down quarks than anti-up quarks in the proton. Existing models of the proton have yet to explain the mechanics behind this anti-matter asymmetry (53). According to NPM, the asymmetry could arise from assigning a 50% smaller fractional charge (1/3e) to down quarks compared to up quarks (2/3e). This requires 50% more down quarks in calculations to match charge measurements.

Anomalous Magnetic Moment (AMM)

In the SM, the relationship between the charge, mass and the magnetic moment of a charged lepton with spin-1/2 can be expressed as (54):

$$\vec{\mu}_\ell = g_\ell \left(\frac{q}{2m_\ell} \right) \vec{s}$$

where $g_\ell = 2(1+a_\ell)$, which is the gyromagnetic factor of ℓ (e, μ), a_ℓ is the anomalous magnetic moment (AMM).

The Dirac equation (11) predicts g = 2, Schwinger increased the g value with a radiative correction and predicted the electron AMM $a_e = \alpha/2\pi$ (55). In 2020 the international g-2 community predicted the muon AMM $a_\mu(\text{SM}) = 116\ 591\ 810(43) \times 10^{-11}$ (0.37ppm) based on a data-driven approach (56), which is 4.2 standard deviations with measurement of experiments. While the magnetic moment is considered an intrinsic property of particles in the framework of NPM, current theories predict and calculate the muon's anomalous magnetic moment by incorporating several external factors such as hadronic vacuum polarization (57, 58), hadronic light-by-light scattering (59, 60), and electroweak interactions (61, 62).

The international g-2 community recently updated the Standard Model prediction for a_μ using new data-driven and lattice-QCD results, which raised the SM value and reduced its discrepancy with experiments (63). However, it is premature to say the muon AMM puzzle is resolved, given ongoing misconceptions regarding the SM in the lepton and hadron sectors discussed earlier and

in upcoming sections. For example, the muon interaction with the invisible free gluon g_e (see the eq. (9.2)) may have contribution to the g-2 experimentally, though current theories do not account for them. Additionally, the measurement of the $\pi^+\pi^-$ channel in the g-2 community is affected by significant statistical uncertainty, systematic uncertainty, and inconsistencies between different data sets (64). The issue is likely caused by misunderstandings about $\pi^{\pm}$ compositions (see details in Sec. 7.1).

The anomalous magnetic moment (AMM) of quarks in the presence of an external magnetic field has been a subject of study for over two decades (65-67). Similar to the research on muon AMM, most studies on quark AMM have concentrated on external contributions such as magnetic catalysis (68) and chirality magnetic effect (69). NPM suggests that the quark AMM may be directly affected by the problematic fractional charges and masses of quarks. A recent study shows that it mainly influences the electric $\sim iE3\sigma3$ component under strong magnetic fields, and up and down quarks have proportionally different AMMs (65).

5.2 Indirect Measurement of Quark Charge

In 2014, D0 collaborations reported measuring the electric charge of top quarks in $\overline{t}t$ events from $\overline{p}p$ collisions at the Tevatron. This measurement is model-dependent and involves complex calculations. It assumes the Standard Model process $t \rightarrow W^+b$, and determines the b jets' charge using a jet charge algorithm developed by Feynman (70).

When reporting the discovery of the top quark, the authors noted that energetic scattering at wide angles, like Rutherford scattering, offers insights into the structure of colliding objects. One interpretation is that excess jets are caused by collisions of smaller objects within quarks, which no other experiment has observed (see Fig. 4 (71)). Fractionally charged particles like t and b quarks should contain smaller charges due to charge conservation, but the suspicious result shows they split into excess jets with larger, integer charges.

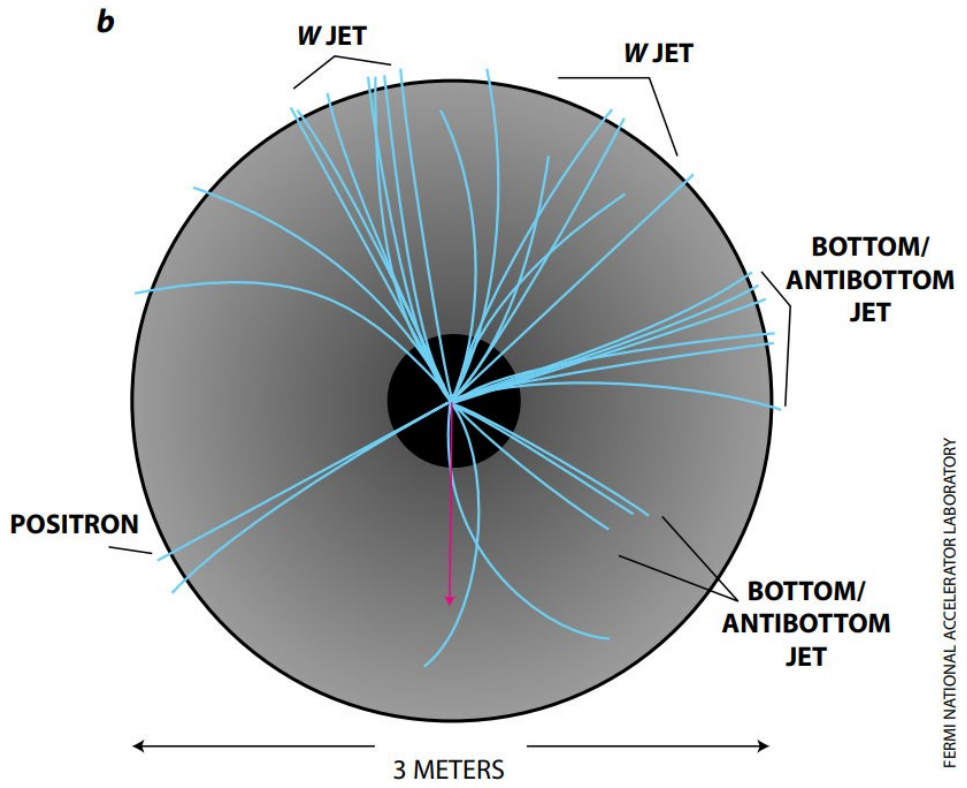

Fig.4| $\bar{t}t$ collision event. This was described as $\bar{p}p \rightarrow \bar{t}t \rightarrow W^+W^- \bar{b}b$.

5.3 Interior Charge Distribution of Hadrons

In the Standard Model (SM), mesons are either neutral or possess integer charges, such as $\pi^+(+1e) \equiv u(+2/3e)\,\bar{d}(+1/3e)$ and $K^-(-1e) \equiv s(-1/3e)\bar{u}(-2/3e)$. When considering charge coupling without the constraints of the meson definition and the "color" hypothesis of Quantum Chromodynamics (QCD) (see details in Sec.6.2), a question arises: why is there no meson with fractional charge combinations such as $\bar{d}(+1/3e)\bar{d}(+1/3e)$, $u(+2/3e)u(+2/3e)$, $\bar{u}(-2/3e)\bar{d}(+1/3e)$ and $u(+2/3e)d(-1/3e)$? What mechanism prevents these from existing in nature? This phenomenon is clearly explained within the New Particle Model (NPM), where all quarks have integer charges (+1e or -1e).

Similarly, why is there no baryon with fractional charge combinations like $u(+2/3e)\bar{u}(-2/3e)\bar{d}(+1/3e)$ and $\bar{d}(+1/3e)u(+2/3e)d(-1/3e)$? In NPM, the answer is straightforward as discussed. Furthermore, in contrast to mesons, what fundamental factors preclude the existence of particles composed of electron-positron pairs, muon-antimuon pairs, or tau-antitau pairs, held together by gluons? What mechanisms are responsible for inhibiting the formation of such composite particles? Section 7 will explain that these lepton pairs are actual compositions of common mesons.

In NPM, quarks with identical charge rarely combine to form a meson due to the strong repulsive force of the same charge, which prevents the gluon from holding them together. Therefore, combinations such as uu, $\overline{dd}$, $u\overline{d}$, $\overline{u}d$, $u\overline{s}$ and $\overline{u}s$ is not allowed in NPM. This makes the compositions of mesons like π^+, π^-, K^+, K^-, $\rho^+$and ρ^- significant for further study. For example, both π^+ and ρ^+ have the same composition of $u\overline{d}$ in the SM, yet they have different masses and decay modes. The cause of mass difference between π meson and ρ meson is explained by different G-parity and different J^{PC} (*72*) or different number of massive gluons involved (*73*). However, NPM reveals that π meson and ρ meson have totally different components that can easily explain their mass difference. More detailed analysis of these phenomena will be provided in Section 7.

6. About Strong Interaction

6.1 Actual Gluons in Strong Interaction

The strong force, classified as one of the four fundamental forces in the Standard Model, is responsible for binding quarks into hadrons through gluon exchange. The residual strong force maintains the cohesion of nucleons by means of virtual mesons. In the Standard Model, descriptions of gluons vary: they are sometimes likened to rubber bands in relation to quark confinement, occasionally referenced as possessing mass (*73*), yet also described as massless particles traveling at the speed of light when defined as gauge bosons.

In NPM, gluons consist of two photons or neutrinos and possess mass, so they don't travel at light speed. The strong force operates through the coupling of gluon’s internal photons with bound particles.

At a nucleon or sub-nucleon scale, gluons act like rubber bands between particles. Their binding force weakens as particles get closer and strengthens as they move apart, but not enough to achieve confinement as described by the Standard Model (*74*). With enough energy, bound particles like quarks can escape their binding force and become independent, as seen in pion decay and free quarks in Quark-Gluon Plasma (*75*). We can better understand it when we know that quarks are charged leptons bound by gluons.

The magnitude of the strong force is predominantly influenced by electromagnetic interactions between the two bound particles, as well as the electromagnetic effects from external factors or the environment. For example, in the proton's uud core structure, the binding forces between the three valence quarks are significantly strong due to the mediating gluons counteracting the repulsive Coulomb effects generated by the two up quarks (even influencing the interaction between up quark and down quark), thereby ensuring the stability of the uud core. Conversely, in the neutron's duu-d core structure, the binding force between the duu structure and the additional down quark is weak because the connecting gluon becomes less taut owing to the

reduction of repulsive Coulomb force. Consequently, the extra down quark is more susceptible to being displaced by neutrino impacts (as detailed in Section 9).

Similarly, in a neutral meson, the binding force is also weak because the channeling gluon is less constrained due to the presence of only attractive Coulomb force between the quark and anti-quark pair, rendering most mesons unstable (as detailed in Section 7).

6.2 Empirical Meaning of Colour Charges in QCD

In quantum chromodynamics (QCD), color charges describe and calculate the strong force, but their physical meaning is not well understood.

In NPM, "colors" in QCD represent different coupling modes between quarks and gluons: ν mode (gluon couples with the interior ν of the quark), W mode (gluon couples with the interior W of the quark), and νW mode (gluon couples with the entire quark). A quark's state, considering both coupling and electric charge, is termed colour charge.

According to the Pauli Exclusion Principle, a gluon's two neutrinos cannot couple quarks with the same mode or colour. Therefore, in baryons like protons and neutrons, there are 6 types of colour charges based on three coupling modes and two electric charges.

Inside mesons, quarks often change coupling modes due to the loose binding of gluons, creating a superposition state that appears "colorless." Despite this undifferentiated state, there are still two sequences of transitions between positive and negative quarks, resulting in two colour-charges. Adding these with the six colour charges in baryons, there are a total of eight colour charges in NPM, matching the QCD theory.

In Quantum Chromodynamics (QCD), "colors" for quarks or antiquarks denote their energy states, which can be described by wave functions. For gluons, "color" is an intrinsic attribute, with each type of gluon facilitating the conversion between specific pairs of "colors". Consequently, there are 8 distinct types of gluons. In the uud structure at the proton core, theoretically, 3x6 gluons are involved in strong interactions, as it necessitates 6 different gluons between each pair of valence quarks.

In NPM, a single gluon can handle all "color" conversions with quarks by adjusting its coupling modes. Thus, only three gluons are needed in the proton's uud core structure. Simplifying the calculation of strong forces is possible if we can constrain the coupling constant for each mode.

In QCD, gluons act as virtual bosons that move between quarks and antiquarks and change their “colors”. In NPM, gluons are considered real particles that respond to mode changes between quarks or antiquarks and can be classified into three different flavours with varying masses and binding strengths.

In Section 11, we will explain that nuclear forces are better described by the electromagnetic interactions and coupling between nucleon quarks via real gluons or mesons, rather than the exchange of virtual mesons as in QCD.

6.3 Strong CP Problem and Yang-Mills Mass Gap Problem

The strong CP problem (76) concerns why quantum chromodynamics (QCD) seems to preserve CP-symmetry, and it's commonly referred to as "the most underrated puzzle in all of physics."

CP combines charge conjugation (C) and parity (P) symmetries. While QCD theory permits CP violation in strong interactions, experiments have not detected it, leading to a "fine tuning" problem in particle physics.

The NPM does not have a strong CP problem. As described in Sec. 6.1, the strong interaction is based on electromagnetic processes that involve gluon internal photons coupling with bound particles. The strong interaction keeps CP symmetry intact by allowing changes in color charge (coupling mode) without affecting charge conjugation or parity.

The Yang-Mills mass gap problem (77) refers to the apparent paradox wherein classical Yang-Mills equations suggest that strong force carriers, such as gluons (the gauge fields), are massless. However, experimental evidence indicates that these combine through confinement into massive particles (hadrons), which requires the existence of massive bound gluons.

NPM does not encounter this issue. In NPM theory, strong interactions involve massless photons within gluons coupling with bound particles, while gluons themselves are always massive. The mass gap between photons and gluons is not problematic. Unlike the Standard Model, NPM does not exhibit confinement: if binding forces are disrupted, quarks transition into charged leptons.

7. About Mesons

In NPM, mesons are composed of certain (anti)leptons and gluons, thus not in any superpositions that mix different pair of (anti)leptons as described in the SM. However, mesons may have different coupling modes, thus may decay differently when caused by different external impacts. It is always better to treat them as different mesons because they have different components.

In the NPM framework, the strong force binds (anti)leptons together via gluons within mesons. Consequently, meson decay occurs through the disruption of the gluon bond, rather than through weak interaction as described in the Standard Model (SM). Although W bosons are passively involved in meson decays in NPM, they do not actively emit or decay.

Quarks can theoretically be bound by glueballs or gluon chains, forming heavy states of mesons. This paper focuses on some common light states of mesons with a single mediating gluon.

7.1 Mesons with e or e*

In most mesons composed of e and e^+ (or e* and e^{*+}), only the g_e gluon acts as a bond. The g_μ (g^*_μ) and g_τ(g^*_τ) gluons are excluded due to their incompatible size and coupling properties.

When e and e^+ have opposite chirality

In the SM, the neutral pion π^0 is a superposition of $u\bar{u}$ and $d\bar{d}$; in NPM, π^0 consists of a pair of e and e^+ (or e* and e^{*+}) with opposite chirality, which can be expressed as:

$$\pi^0 \equiv (eL)(g_e)(e^+R),\ (eR)(g_e)(e^+L) \text{ or } dL(g_e)\bar{d}R,\ dR(g_e)\bar{d}L \qquad (7.1)$$

Note: for present purposes, $(eL)(g_e)(e^{*+}R)$, $(e^*R)(g_e)(e^+L)$ and $dL(g_e)uR$, $uL(g_e)\bar{u}R$, $uR(g_e)\bar{u}L$ are not listed.

When π^0 decays, e and e^+ annihilate due to the close coupling within the meson, releasing 2γ with a (98.823±0.034)% probability (*41*).

When e and e^+ have same chirality

In theory, π meson may also consist of a pair of e and e^+ (or e* and e^{*+}) with same chirality. This meson is called π' and can be expressed as:

$$\pi' \equiv (eL)(g_e)(e^+L),\ (eR)(g_e)(e^+R) \text{ or } dL(g_e)\bar{d}L,\ dR(g_e)\bar{d}R \qquad (7.2)$$

When π' decays, the electron (e) and positron (e^+) separate due to a bit loose coupling within the meson, while the gluon may either merge with the background field or convert into a photon. Thus:

$$\pi' \rightarrow e + e^+ + (\gamma) \qquad (7.3a)$$

In the SM, π' is π^0 that has decay mode with a (1.174±0.035) % fraction(*41*); in NMP, $\pi'$and π^0 should be treated as different mesons due to their different components.

The π^0 can also decay into an electron and a positron when interacting with a neutrino, like the process observed in β^+ decay (refer to Section 9.4 for more information).

Theoretically, when π'decays, the gluon may also split into two neutrinos that briefly bind with e and e^+. This creates intermediate states like $e\nu$ and $e^+\nu$, which eventually decay into e, e^+ and 2ν. Thus,

$$\pi' \rightarrow e + e^+ + (\gamma) \qquad (7.3b)$$

About $\pi^+$and π^-

As mentioned in Section 5.3, couplings like $u\bar{d}$ and $\bar{u}d$ are not allowed in NPM. A charged pion acts as an intermediate state of a broken meson, such as $\rho^0(770)$ and $\omega(782)$, when the binding gluon splits into two neutrinos, each temporarily pairing with μ and μ^+. Thus,

$$\pi^{\pm} \equiv \mu^{\pm}\nu \tag{7.4}$$

This is why $\pi^{\pm}$ decays to $\mu^{\pm} + \nu$ with a fraction of (99.98770±0.00004) % (41).

If a meson is defined as a particle consisting of a lepton and anti-lepton pair (or quark and anti-quark), then $\pi^{\pm}$ particles would not be classified as mesons. Their designated names may not be appropriate, as they do not share characteristics with π^0 particles. The mean lifetime of $\pi^{\pm}$ particles and π^0 particles differs by approximately 9 orders of magnitude, and their masses vary significantly more than the mass difference between protons and neutrons (41). The measurement of the $\pi^+\pi^-$ channel in the g-2 community is affected by substantial statistical uncertainty, systematic uncertainty, and inconsistencies between different data sets (64). This issue is most likely due to misconceptions regarding the compositions of $\pi^{\pm}$.

Similarly, the $K^{\pm}$, $\rho^{\pm}$, $D^{\pm}$ and $B^{\pm}$ should also not be classified as mesons due to their actual compositions (see more introductions in Sec. 7.3 and 7.4).

7.2 Mesons with μ

When μ and μ^+ have opposite spin chirality

Just like π^0, when the constituent μ and μ^+ have opposite chirality in a meson, they tend to annihilate each other. However, the meson is more complex than π^0 due to the involvement of two types of gluons (g_e and g_μ). By analyzing decay modes, we find that they correspond well to the eta meson η(548) and the eta prime meson η′(958), which can be expressed as:

$$\eta(548) \equiv (\mu L)(g_e)(\mu^+ R),\ (\mu R)(g_e)(\mu^+ L) \text{ or } sL(g_e)\bar{s}R,\ sR(g_e)\bar{s}L \tag{7.5}$$

$$\eta'(958) \equiv (\mu L)(g_\mu)(\mu^+ R),\ (\mu R)(g_\mu)(\mu^+ L) \text{ or } sL(g_\mu)\bar{s}R,\ sR(g_\mu)\bar{s}L \tag{7.6}$$

Since the g_e can bind effectively with the interior neutrinos of μ and μ^+ with opposite chirality, the η(548) possesses a relatively small mass and primarily decays into 2γ (from $\mu\mu^+$ annihilation) or pions (possibly inspired from the 2γ) (41). Conversely, due to the same chirality of interior neutrinos, the g_μ cannot bind μ and μ^+ as effectively and closely as the g_e, resulting in the η′(958) having a significantly larger mass than the η(548), which provides a straightforward explanation for the "η – η′ puzzle" (78) without requiring a complex hypothesis. The majority of η′(958) decay modes produce charged particles, including π^+ and π^- (or $\mu^+\nu$ and $\mu\nu$) (41).

We predict that μ and μ^+ with opposite chirality might couple with g^*_μ to form heavy η′ mesons in rare situations.

When μ and μ^+ have same spin chirality

1) Bound with g_e

It may be uncommon and challenging for a g_e to bind μL and $\mu^+ L$ (or μR and $\mu^+ R$) together. However, we propose that the observed $f_0(500)$ could serve as an appropriate candidate for this combination, expressed as:

$$f_0(500) \equiv (\mu L)(g_e)(\mu^+ L),\ (\mu R)(g_e)(\mu^+ R) \text{ or } sL(g_e)\bar{s}L,\ sR(g_e)\bar{s}R \tag{7.7}$$

2) Bound with g_μ

The g_μ binds μ and μ^+ in a meson due to their same flavour, forming two coupling states. One state has the same chirality for g_μ and bound μ and μ^+, making it more stable and lighter. The other state has different chirality, resulting in higher mass. This can be represented by $\rho^0(770)$ and $\omega(782)$ accordingly as:

$$\rho^0(770) \equiv (\mu L)(g_\mu L)(\mu^+ L),\ (\mu R)(g_\mu R)(\mu^+ R);\ \text{or } sL(g_\mu L)\bar{s}L,\ sR(g_\mu R)\bar{s}R \tag{7.8}$$

$$\omega(782) \equiv (\mu L)(g_\mu R)(\mu^+ L),\ (\mu R)(g_\mu L)(\mu^+ R);\ \text{or } sL(g_\mu R)\bar{s}L,\ sR(g_\mu L)\bar{s}R \tag{7.9}$$

The $\rho^0(770)$ decays to $\pi^- + \pi^+$ with a 100% fraction (*41*). during which the g_μ splits into 2ν that bind with μ and μ^+ separately and temporarily. According to the eq. (7.4) , the decay can be expressed as (for present purposes, in the rest of work, we will present process using only right-handed gluon or only left-handed gluon because both have the same patten):

$$\rho^0(770) \equiv (\mu R)(g_\mu R)(\mu^+ R) \equiv (\mu R)(\underline{\nu} R + \underline{\nu} R) R(\mu^+ R)$$

$$\rightarrow (\mu R)(\underline{\nu} R) + (\underline{\nu} R)(\mu^+ R) \equiv \mu\nu + \mu^+\nu \equiv \pi^- + \pi^+ \tag{7.10}$$

$\omega(782)$ may decay with more intense, thus g_μ breaks into 2ν and excites an additional π^0 with a fraction of $(89.2 \pm 0.7)\%$ (*41*):

$$\omega(782) \equiv (\mu R)(g_\mu L)(\mu^+ R) \equiv (\mu R)(\underline{\nu} L + \underline{\nu} L) L(\mu^+ R)$$

$$\rightarrow (\mu R)(\underline{\nu} L) + (\underline{\nu} L)(\mu^+ R) + \pi^0 \equiv \mu\nu + \mu^+\nu + \pi^0 \equiv \pi^- + \pi^+ + \pi^0 \tag{7.11a}$$

There is an intermediate state before the final decay of $\omega(782)$, where π^0 is bound with either π^- or π^+. The former combination forms ρ^-, and the latter forms ρ^+. Both combinations will decay into two π with a 100% fraction (*41*), which can be expressed as:

$$\rho^\pm \equiv \pi^\pm \pi^0 \rightarrow \pi^\pm + \pi^0 \tag{7.12}$$

Equations (7.10) and (7.12) indicate that $\rho^\pm$ differs from ρ^0, and their mass difference should be at least as large as that between $\pi^\pm$ and π^0.

The second common decay of $\omega(782)$ occurs via $\mu\mu^+$ annihilation into a γ and the bound g_μ producing a π^0 with a (8.33 ± 0.25) % fraction (*41*).

$$\omega(782) \rightarrow \gamma + \pi^0 \tag{7.11b}$$

3) Bound with g^*

In rare instances, a g^*_μ may bind the μ and μ^+ (or s^* and s^{*+}) to form heavy states of ρ meson and ω meson.

7.3 Mesons with μ*

μ* decay modes

We predict that μ* has a shorter lifetime than μ and may decay to μ, e or e* through interactions with various gluons. Here are some examples of μ* decay modes:

$$\mu^*R + g_eL \equiv (W^-L + \nu L')R + (\nu L'' + \nu R'')L$$
$$\rightarrow (W^-L + \nu R'')L + (\nu L'' + \nu L')R \equiv eL + g^*_\mu R;$$

$$\mu^*R + g_eR \equiv (W^-L + \nu L')R + (\nu L'' + \nu R'')R$$
$$\rightarrow (W^-L + \nu R'')R + (\nu L'' + \nu L')R \equiv e^*R + g^*_\mu R;$$

$$\mu^*R + g_\mu L \equiv (W^-L + \nu L')R + (\nu L'' + \nu L'')L$$
$$\rightarrow (W^-L + \nu L'')L + (\nu L'' + \nu L')R \equiv \mu L + g^*_\mu R;$$

$$\mu^*R + g_\mu R \equiv (W^-L + \nu L')R + (\nu R'' + \nu R'')R$$
$$\rightarrow (W^-L + \nu R'')R + (\nu R'' + \nu L')R \equiv e^*R + (g_e)R;$$

$$\mu^*L + g^*_\mu R \equiv (W^-R + \nu R')L + (\nu L'' + \nu L'')R$$
$$\rightarrow (W^-R + \nu L'')R + (\nu L'' + \nu R')L \equiv eR + (g_e)L;$$

$$\mu^*R + g^*_\mu L \equiv (W^-L + \nu L')R + (\nu R'' + \nu R'')L$$
$$\rightarrow (W^-L + \nu R'')L + (\nu R'' + \nu L')R \equiv eL + (g_e)R$$

Note: the marks ′, ″ and ‴ in this paper are for tracking locations and improving readability.

Gluons may further decay into π^0 or $(\pi^- + \pi^+)$ depending on the cause of the decay. Thus, the μ* decay modes above can be simply expressed as:

$$\mu^* + g_e \rightarrow e + g^*_\mu \rightarrow e + \pi^0 \quad (7.13a)$$

$$\mu^* + g_e \rightarrow e + g^*_\mu \rightarrow e + \pi^- + \pi^+ \quad (7.13b)$$

$$\mu^* + g_\mu \rightarrow \mu + g^*_\mu \rightarrow \mu + \pi^0 \quad (7.14a)$$

$$\mu^* + g_\mu \rightarrow \mu + g^*_\mu \rightarrow \mu + \pi^- + \pi^+ \quad (7.14b)$$

$$\mu^* + g_\mu \rightarrow e^* + g_e \rightarrow e^* + \pi^0 \quad (7.15a)$$

$$\mu^* + g_\mu \rightarrow e^* + g_e \rightarrow e^* + \pi^- + \pi^+ \quad (7.15b)$$

$$\mu^* + g^*_\mu \rightarrow e + g_e \rightarrow e + \pi^0 \quad (7.16a)$$

$$\mu^* + g^*_\mu \rightarrow e + g_e \rightarrow e + \pi^- + \pi^+ \qquad (7.16b)$$

The exchange of neutrinos can alter the chirality of newly produced leptons and gluons. However, sometimes the exchange results in two separate neutrinos without affecting the chirality of the new lepton:

$$\mu^*R + g_eL \equiv (W^-L + \nu_\mu L')R + (\nu_e L'' + \nu_e R'')L$$

$$\rightarrow (W^-L + \nu_e R'')L + \nu_e L'' + \nu_\mu L' \equiv eL + \nu_e L'' + \nu_\mu L' \qquad (7.17a)$$

$$\mu^*R + g_\mu L \equiv (W^-L + \nu_\mu{}^* L')R + (\nu_\mu L'' + \nu_\mu L'')L \rightarrow (W^-L + \nu_\mu{}^* L')R\ \nu_\mu L'' + \nu_\mu L''$$

$$\rightarrow (W^-L + \nu_\mu L'')L\ \nu_\mu{}^* L' + \nu_\mu L'' \equiv \mu L + \nu_\mu L'' + \nu_\mu{}^* L' \qquad (7.18a)$$

or simply expressed as:

$$\mu^* + g_e \rightarrow e + \nu_e + \nu_\mu \qquad (7.17b)$$

$$\mu^* + g_\mu \rightarrow \mu + \nu_\mu + \nu_\mu{}^* \qquad (7.18b)$$

Equation (7.18b) suggests the existence of a heavy muon neutrino, $\nu_\mu{}^*$.

When the μ^* is in an excited state, it may inspire additional neutral particles such as π^0 or ρ^0 during its decay process.

Equation (7.18a) can be stated as follows, considering the intermediate states and referencing equations (7.4) and (7.22):

$$\mu^* + g_\mu \rightarrow K^- + \nu_\mu \rightarrow \pi^- + \nu_\mu{}^* \rightarrow \mu + \nu_\mu + \nu_\mu{}^* \qquad (7.18c)$$

The μ^* and μ^{*+} bound by g_e is rare due to their mass and instability, which prevents finding mesons fitting this coupling. Hence, we assume that μ^* and μ^{*+} are only bound with g_μ and g^*_μ.

When μ^* and μ^{*+} have opposite chirality

1) Bound with g^*_μ

Our analysis indicates that the particle generated through the coupling between g^*_μ and μ^*/μ^{*+}(with opposite chirality) corresponds effectively to the observed J/ψ(1s) meson. This can be articulated as:

$$J/\psi(1s)(c^*\bar{c}^*) \equiv (\mu^*L)(g^*_\mu)(\mu^{*+}R),\ (\mu^*R)(g^*_\mu)(\mu^{*+}L)$$

$$\text{or } c^*L(g^*_\mu)\bar{c}^*R,\ c^*R(g^*_\mu)\bar{c}^*L \qquad (7.19)$$

Like π^0 and η(548), g^*_μ tightly binds μ^*L and $\mu^{*+}R$, thus when J/ψ(1s) decays, μ^* and μ^{*+} generally annihilate, emitting photons that can convert into hadrons or leptons (41), while g^*_μ may decay to g_μ (or g_e), or inspire hadrons or leptons.

The J/ψ(1s) was found to have an unexpected lifetime roughly 1000 times greater than the ρ^0 meson (79), which is obvious in NPM due to its stronger internal coupling.

Recent studies indicate that the observed J/ψ productions do not match the theoretical predictions (80-82), possibly because of differences between the assumed $c\bar{c}$ component and the actual $c^*\bar{c}^*$ component.

2) Bound with g_μ

Similarly, we find that the particle formed through coupling between g_μ and μ^*/μ^{*+}(with opposite chirality) matches the observed η_c meson, which can be expressed as:

$$\eta_c(c\bar{c}) \equiv (\mu^*L)(g_\mu)(\mu^{*+}R),\ (\mu^*R)(g_\mu)(\mu^{*+}L) \text{ or } cL(g_\mu)\bar{c}R,\ cR(g_\mu)\bar{c}L \qquad (7.20)$$

ηc has a shorter lifetime than J/ψ because of its weaker internal coupling. According to equation (7.18c), interactions between $\mu^{*\pm}$ and g_μ have several phases, so ηc may decay into pairs of K, π, μ, or combinations thereof, depending on the phase and energy from an incident particle, likely a neutrino.

When μ^* and μ^{*+} have same chirality

The pair of μ^* and μ^{*+}(with the same chirality) coupling with g^*_μ and g_μ fits well with various versions of the ϕ(1020) meson. Our prediction is as follows:

$$\phi(1020) \equiv (\mu^*R)(g^*_\mu R)(\mu^{*+}R),\ (\mu^*R)(g^*_\mu L)(\mu^{*+}R),\ c^*R(g^*_\mu R)\bar{c}^*R,\ c^*R(g^*_\mu L)\bar{c}^*R$$
$$\text{or } (\mu^*R)(g_\mu R)(\mu^{*+}R),\ (\mu^*R)(g_\mu L)(\mu^{*+}R),\ cR(g_\mu R)\bar{c}R,\ cR(g_\mu L)\bar{c}R \qquad (7.21)$$

Note: for present purposes, we do not include the μ^*L in the list.

1) Bound with g^*_μ

There are two versions of ϕ(1020) meson with different decay modes in this coupling. In the first version, when $\mu^{*\pm}$ and g^*_μ have same chirality, g^*_μ simply breaks to two neutrinos and couple with the μ^* and μ^{*+}:

$$\phi(1020)1 \equiv (\mu^*R)(g^*_\mu R)(\mu^{*+}R) \equiv (W^-L + \nu L')R\ (\nu L'' + \nu L'')R\ (W^+L + \nu L''')R$$
$$\rightarrow (W^-L + \nu L')R\ (\nu L'') + (W^+L + \nu L''')R\ (\nu L'') \equiv \mu^*\nu + \mu^{*+}\nu$$

In NPM, we predict and define:

$$K^\pm \equiv \mu^{*\pm}\nu \qquad (7.22)$$

Thus, this decay mode can be described as:

$$\phi(1020)1 \rightarrow K^- + K^+ \qquad (7.23)$$

The fraction of this decay mode is (49.1±0.5)% (41).

The $K^\pm$ decays to $\mu^\pm + \nu_\mu$ with a (63.56±0.11) % fraction (41). It is observed that the decay products are identical to those of $\pi^\pm$ decay, raising significant questions given the distinct masses and compositions of K and π particles. According to equation (7.18), it appears more plausible that $K^\pm(\mu^{*\pm}\nu)$ decays into $\mu^\pm + \nu_\mu + \nu_\mu^*$ suggesting that additional neutrinos may have been missed in previous observations.

Based on equations (7.14a and 7.14b), $K^{\pm}(\mu^{*\pm}\nu)$ may also decay to $\mu^{\pm}\nu + \pi^0 \equiv \pi^{\pm} + \pi^0$ or $\mu^{\pm}\nu + \pi^- + \pi^+ \equiv \pi^{\pm} + \pi^- + \pi^+$ depending on the level of impacting energy. This phenomenon is a well-known instance of parity violation in the τ–θ puzzle (*83*, *84*). This is obvious in NPM because $\pi^{\pm}$ are different types of particles from π^0, as explained in Sec. 7.1.

The second version of ϕ(1020) occurs when $\mu^{*\pm}$ and g^*_{μ} exhibit different chirality. In this scenario, if μ^* transitions to e first and μ^{*+} transitions to μ^+ afterwards, then ϕ(1020) decays to K^0. Conversely, if μ^{*+} transitions to e^+ first and μ^* transitions to μ subsequently, then ϕ(1020) decays to $\bar{K}^0$:

$$\phi(1020)2 \equiv (\mu^*R)(g^*_{\mu}L)(\mu^{*+}R) \equiv (W^-L + \nu L')R\ (\nu R'' + \nu R'')L\ (W^+L + \nu L''')R$$
$$\rightarrow (W^-L + \nu R'')L\ (\nu L' + \nu R'')L\ (W^+L + \nu L''')R$$
$$\rightarrow (W^-L + \nu R'')L\ (\nu L''' + \nu R'')L\ (W^+L + \nu L')L$$
$$\equiv (eL)(g_eL)(\mu^+L) \equiv d\bar{s} \equiv K^0 \qquad (7.24a)$$

or

$$\phi(1020)2 \equiv (\mu^*R)(g^*_{\mu}L)(\mu^{*+}R) \equiv (W^-L + \nu L')R\ (\nu R'' + \nu R'')L\ (W^+L + \nu L''')R$$
$$\rightarrow (W^-L + \nu L')R\ (\nu R'' + \nu L''')L\ (W^+L + \nu R'')L$$
$$\rightarrow (W^-L + \nu L''')L\ (\nu R' + \nu L')L\ (W^+L + \nu R'')L$$
$$\equiv (\mu L)(g_eL)(e^+L) \equiv s\bar{d} \equiv \bar{K}^0 \qquad (7.24b)$$

The total fraction of ϕ(1020)2 decay modes is (33.9±0.4)% (*41*), which is about 15% less than the fraction of ϕ(1020)1 decay modes. According to NPM, the ϕ(1020)2 combination is less popular due to its harsher interior or because its two-step decay process is more difficult than the one-step decay of ϕ(1020)1. Alongside the neutron's uud-d core described in Sec.2.5, the different compositions of charged $K^{\pm}$ and neutral K^0 ($\bar{K}^0$) account for the isospin-symmetry violation, a phenomenon that existing QCD models have yet to fully explain (*10*).

K^0 and $\bar{K}^0$ can oscillate through neutrino exchange via gluon, known as **K^0 - $\bar{K}^0$ Oscillation**:

$$K^0 \equiv d\bar{s} \equiv (eL)(geL)(\mu^+L) \equiv (W^-L + \nu R')L\ (\nu L'' + \nu R'')L\ (W^+L + \nu L''')L$$
$$\leftrightarrow (W^-L + \nu L'')L\ (\nu R' + \nu L''')L\ (W^+L + \nu R'')L$$
$$\equiv (\mu L)(geL)(e^+L) \equiv s\bar{d} \equiv \bar{K}^0$$

The oscillation can be clarified using two inverse cyclic processes, during these, unstable $\mu^{\pm}$ changes to stable $e^{\pm}$, and the released energy transfers $e^{\pm}$ to $\mu^{\pm}$ via the gluon channel:

$$K^0 \equiv d\bar{s} \equiv (eL)(geL)(\mu^+L) \equiv (W^-L + \nu R')L\ (\nu L'' + \nu R'')L\ (W^+L + \nu L''')L$$
$$\rightarrow (W^-L + \nu R')L\ (\nu L'' + \nu L''')L\ (W^+L + \nu R'')L$$
$$\rightarrow (W^-L + \nu L'')L\ (\nu R' + \nu L''')L\ (W^+L + \nu R'')L$$

$$\equiv (\mu L)(g_e L)(e^+ L) \equiv s\bar{d} \equiv \bar{K}^0 ,$$

$$K^0 \equiv d\bar{s} \equiv (eL)(g_e L)(\mu^+ L) \equiv (W^- L + \nu R')L\ (\nu L'' + \nu R'')L\ (W^+ L + \nu L''')L$$

$$\leftarrow (W^- L + \nu R')L\ (\nu L'' + \nu L''')L\ (W^+ L + \nu R'')L$$

$$\leftarrow (W^- L + \nu L'')L\ (\nu R' + \nu L''')L\ (W^+ L + \nu R'')L$$

$$\equiv (\mu L)(g_e L)(e^+ L) \equiv s\bar{d} \equiv \bar{K}^0$$

Oscillation can be interrupted by various environmental impacts, causing $K^0(\bar{K}^0)$ to decay in different ways. K^0_S(K-short) decays due to low-energy impacts shortly after K^0 generation, while K^0_L(K-long) requires higher energy impacts, occurring with lower probability over a longer period.

2) Bound with g_μ

In the first version of this bound ($\mu^{*\pm}$ and g_μ with different chirality), the μ^* and μ^{*+} decay to μ and μ^+ through the neutrino exchange and chirality change while the g_μ breaks and initializes a π^0:

$$\phi(1020)3 \equiv (\mu^* R)(g_\mu L)(\mu^{*+} R) \equiv (W^- L + \underline{\nu} L')R\ (\underline{\nu} L'' + \underline{\nu} L'')L\ (W^+ L + \underline{\nu} L''')R$$

$$\rightarrow (W^- L + \underline{\nu} L')R\ (\underline{\nu} L'')L + (W^+ L + \underline{\nu} L''')R\ (\underline{\nu} L'')L + \pi^0$$

$$\rightarrow (W^- L + \underline{\nu} L'')L\ \underline{\nu} L' + (W^+ L + \underline{\nu} L'')L\ \underline{\nu} L''' + \pi^0$$

$$\equiv \mu\nu + \mu^+\nu + \pi^0 \equiv \pi^- + \pi^+ + \pi^0 \ \ (\text{or } \rho^0 + \pi^0)$$

or simply expressed as:

$$\phi(1020)3 \rightarrow \pi^- + \pi^+ + \pi^0 \ \ (\text{or } \rho^0 + \pi^0) \qquad (7.25)$$

In the second version of this bound ($\mu^{*\pm}$ and g_μ with same chirality), μ^* and μ^{*+} decay to e and e^+ through the neutrino exchange. Afterwards, e and e^+ may either separate or annihilate to produce γ, while the gluon can decay into neutrinos or generate a neutral hadron such as η, ω, or π^0:

$$\phi(1020)4 \equiv (\mu^* R)(g_\mu R)(\mu^{*+} R) \equiv (W^- L + \nu L')R\ (\nu R'' + \nu R'')R\ (W^+ L + \nu L''')R$$

$$\rightarrow (W^- L + \nu R'')R\ (\nu L' + \nu L''')R\ (W^+ L + \nu R'')R$$

$$\rightarrow (W^- L + \nu R'')R\ (\nu L') + (W^+ L + \nu R'')R\ (\nu L''')$$

$$\equiv e\nu + e^+\nu,$$

or,

$$\phi(1020)4 \equiv (\mu^* R)(g_\mu R)(\mu^{*+} R) \equiv (W^- L + \nu L')R\ (\nu R'' + \nu R'')R\ (W^+ L + \nu L''')R$$

$$\rightarrow (W^- L + \nu R'')R\ (\nu L' + \nu L''')R\ (W^+ L + \nu R'')R$$

$$\rightarrow \eta + \gamma \ (\text{or } \omega + \gamma, \ \pi^0 + \gamma)$$

or simply expressed as:

$$\phi(1020)4 \rightarrow e\nu + e^{+}\nu \qquad (7.26)$$

$$\phi(1020)4 \rightarrow \eta + \gamma \text{ (or } \omega + \gamma,\ \pi^{0} + \gamma) \qquad (7.27)$$

The fraction of $\phi(1020)3$ decay modes plus the fraction of $\phi(1020)4$ decay modes is about (15.4±0.4)%([41](#)).

From equations (7.23) and (7.24a, 7.24b), both $\phi(1020)1$ and $\phi(1020)2$ decays produce kaons, with their combined decay fraction totaling about 83%. This is expected since μ^{*} and μ^{*+} (of the same chirality) are more likely to combine with g^{*}_{μ} than with g_{μ} due to stronger coupling. Therefore, it is unnecessary to invoke the complicated Okubo–Zweig–Iizuka (OZI) rule ([85](#), [86](#)) to explain why decay modes $\phi(1020)1 + \phi(1020)2 \rightarrow K$ (K^{0} or $K^{+} + K^{-}$) would be more common than decay mode $\phi(1020)3 \rightarrow \pi^{-} + \pi^{+} + \pi^{0}$.

D Mesons and D^{0}-$\bar{D}^{0}$ oscillation

In both SM and NPM, $D^{0} \equiv c\bar{u}$, $\bar{D}^{0} \equiv \bar{c}u$. Similar to K^{0}-$\bar{K}^{0}$ oscillation, the D^{0}-$\bar{D}^{0}$ oscillation is described as follows:

$$\begin{aligned} D^{0} \equiv c\bar{u} \equiv (\mu^{*+}L)(g_{e}L)(e^{*}L) &\equiv (W^{+}R + \underline{\nu}R')L\ (\underline{\nu}L'' + \underline{\nu}R'')L\ (W^{-}R + \underline{\nu}L''')L \\ &\leftrightarrow (W^{+}R + \underline{\nu}L'')L\ \ (\underline{\nu}R' + \underline{\nu}L''')L\ (W^{-}R + \underline{\nu}R'')L \\ &\equiv (e^{*+}L)(g_{e}L)(\mu^{*}L) \equiv u\bar{c} \equiv \bar{D}^{0} \end{aligned} \qquad (7.28)$$

In the SM, $D^{+} \equiv c\bar{d}$, $D^{-} \equiv \bar{c}d$ and $Ds^{+} \equiv c\bar{s}$, which is prohibited in NPM.

7.4 Mesons with τ and τ*

τ* decay

We anticipate that τ* will possess a lifetime shorter than that of τ and will decay into τ, μ*, μ, e, or e* through interactions involving g_{τ}, g^{*}_{μ}, g_{μ}, or g_{e}. Below are examples illustrating possible decay processes:

$$\tau^{*}R + g_{\tau}L \equiv (W^{-}L + \nu|')R + (\nu L'' + \nu|'')L$$

$$\rightarrow (W^{-}L + \nu|'')L + (\nu L'' + \nu|')R \equiv \tau L + g^{*}_{\tau}R\ ;$$

$$\tau^{*}R + g^{*}_{\mu}R \equiv (W^{-}L + \nu|')R + (\nu L'' + \nu L'')R$$

$$\rightarrow (W^{-}L + \nu L'')R + (\nu L'' + \nu|')R \equiv \mu^{*} + g^{*}_{\tau}R;$$

$$\tau^{*}R + g_{\mu}L \equiv (W^{-}L + \nu|')R + (\nu L'' + \nu L'')L$$

$$\rightarrow (W^{-}L + \nu L'')L + (\nu L'' + \nu|')R \equiv \mu + g^{*}_{\tau}R;$$

$$\tau^{*}R + (ge)L \equiv (W^{-}L + \nu|')R + (\nu L'' + \nu R'')L$$

$$\rightarrow (W^{-}L + \nu R'')L + (\nu L'' + \nu|')R \equiv e + g^{*}_{\tau}R;$$

$$\tau^{*}R + (ge)R \equiv (W^{-}L + \nu|')R + (\nu L'' + \nu R'')R$$

$$\rightarrow (W^{-}L + \nu R'')R + (\nu L'' + \nu|')R \equiv e^{*} + g^{*}_{\tau}R$$

They can be stated more simply as:

$$\tau^{*} + g_{\tau} \rightarrow \tau + g^{*}_{\tau} \qquad (7.29)$$

$$\tau^{*} + g^{*}_{\mu} \rightarrow \mu^{*} + g^{*}_{\tau} \qquad (7.30)$$

$$\tau^{*} + g_{\mu} \rightarrow \mu + g^{*}_{\tau} \qquad (7.31)$$

$$\tau^{*} + g_{e} \rightarrow e + g^{*}_{\tau} \qquad (7.32)$$

$$\tau^{*} + g_{e} \rightarrow e^{*} + g^{*}_{\tau} \qquad (7.33)$$

The neutrino exchange in these decay reactions theoretically produces a new lepton and gluon; however, it could instead yield two separate neutrinos:

$$\tau^{*}R + g_{\tau}L \equiv (W^{-}L + \nu_{\tau^{*}}|')R + (\nu_{\tau}L'' + \nu_{\tau}|'')L$$

$$\rightarrow (W^{-}L + \nu_{\tau}|'')L + \nu_{\tau}L'' + \nu_{\tau^{*}}|' \equiv \tau L + \nu_{\tau}L'' + \nu_{\tau^{*}}|';$$

or simply expressed as:

$$\tau^{*} + g_{\tau} \rightarrow \tau + \nu_{\tau} + \nu_{\tau^{*}} \qquad (7.34)$$

Therefore, it suggests the possible existence of an additional tau neutrino flavour, the heavy tau neutrino, $\nu_{\tau^{*}}$. Likewise, the following straightforward equations for τ^{*} decays can be derived:

$$\tau^{*} + g_{\tau} \rightarrow \tau + \nu_{\tau} + \nu_{\tau^{*}} \qquad (7.35)$$

$$\tau^{*} + g^{*}_{\mu} \rightarrow \mu^{*} + \nu_{\mu}^{*} + \nu_{\tau^{*}} \qquad (7.36a)$$

or $$\tau^{*} + g^{*}_{\mu} \rightarrow K + \nu_{\tau^{*}} \qquad (7.36b)$$

$$\tau^{*} + g_{\mu} \rightarrow \mu + \nu_{\mu} + \nu_{\tau^{*}} \qquad (7.37a)$$

or $\tau^* + g_\mu \longrightarrow \pi^0 + \nu_{\tau^*}$ (7.37b)

$\tau^* + g_e \longrightarrow e + \nu_e + \nu_{\tau^*}$ (7.38)

$\tau^* + g_{*e} \longrightarrow e^* + \nu_{e^*} + \nu_{\tau^*}$ (7.39)

When the τ^* is in an excited state , these decays would inspire extra neutrals like π^0 and ρ^0, etc, and the gluon g^*_τ may break into $\nu_\tau + \nu$. Thus, if omitting the gluons and neutrinos for the present purposes, the τ^* may decay to so many combinations of particles:

$$\tau^* \longrightarrow \tau,\ \mu^*,\ \mu,\ e,\ e^*,\ K,\ \pi^0,\ \tau + \pi^0,\ \mu^* + \pi^0,\ \mu + \pi^0,\ e + \pi^0,\ e^* + \pi^0\ ,$$

$$\tau + \rho^0,\ \mu^* + \rho^0,\ \mu + \rho^0,\ e + \rho^0,\ e^* + \rho^0 \ldots$$

Currently, most of these decay modes are classified as τ decay (41) because τ^* is not recognized. There are also uncertainties related to measuring and defining the top quark mass (87). Between 2011 and 2024, LHC physicists conducted multiple measurements of the top quark mass, obtaining results that varied across a significant span of about 6.5 GeV(88). Progress may be possible if the existence of a heavy top quark and tau particle is confirmed.

τ decay

The τ particle has a relatively short lifetime and can decay into μ^*, μ, e, or e^* through interactions involving g^*_μ, g_μ, or g_e. Examples of some decay processes are as follows:

$$\tau L + g^*_\mu R \equiv (W^- L + \nu|')L + (\nu L'' + \nu L'')R$$

$$\longrightarrow (W^- L + \nu L'')R + (\nu L'' + \nu|')R \equiv \mu^* R + g^*_\tau R;$$

$$\tau L + (g_\mu)L \equiv (W^- L + \nu|')L + (\nu L'' + \nu L'')L$$

$$\longrightarrow (W^- L + \nu L'')L + (\nu L'' + \nu|')L \equiv \mu L + g_\tau L;$$

$$\tau L + (g_e)R \equiv (W^- L + \nu|')L + (\nu L'' + \nu R'')R$$

$$\longrightarrow (W^- L + \nu R'')R + (\nu L'' + \nu|')L \equiv e^* R + g_\tau L$$

$$\tau L + (g_e)L \equiv (W^- L + \nu|')L + (\nu L'' + \nu R'')L$$

$$\longrightarrow (W^- L + \nu R'')L + (\nu L'' + \nu|')L \equiv eL + g_\tau L$$

They can be simply stated as:

$$\tau + g^*_\mu \longrightarrow \mu^* + g^*_\tau \quad (7.40)$$

$$\tau + g_{\mu} \rightarrow \mu + g_{\tau} \quad (7.41)$$

$$\tau + g_{e} \rightarrow e^{*} + g_{\tau} \quad (7.42)$$

$$\tau + g_{e} \rightarrow e + g_{\tau} \quad (7.43)$$

Similar to τ^{*} decay, it may theoretically produce two distinct neutrinos rather than a new gluon:

$$\tau + g^{*}{}_{\mu} \rightarrow \mu^{*} + \nu_{\mu}{}^{*} + \nu_{\tau} \quad (7.44a)$$

$$\tau + g^{*}{}_{\mu} \rightarrow K + \nu_{\tau} \quad (7.44b)$$

$$\tau + g_{\mu} \rightarrow \mu + \nu_{\mu} + \nu_{\tau} \quad (7.45a)$$

$$\tau + g_{\mu} \rightarrow \pi^{0} + \nu_{\tau} \quad (7.45b)$$

$$\tau + g_{e} \rightarrow e^{*} + \nu^{*}{}_{e} + \nu_{\tau} \quad (7.46)$$

$$\tau + g_{e} \rightarrow e + \nu_{e} + \nu_{\tau} \quad (7.46)$$

Mesons with τ

Theoretically, there may be some possible mesons with $\tau\tau^{+}$ compositions, bound by g_{τ} or $g^{*}{}_{\tau}$:

$(\tau L)(g_{\tau}L)(\tau^{+}L)$; $(\tau L)(g_{\tau}R)(\tau^{+}L)$; $(\tau L)(g^{*}{}_{\tau}L)(\tau^{+}L)$; $(\tau L)(g^{*}{}_{\tau}R)(\tau^{+}L)$; $(\tau L)(g_{\tau}L)(\tau^{+}R)$; $(\tau L)(g^{*}{}_{\tau}R)(\tau^{+}R)$;

Of these, the first combination appears to be the most stable; therefore, we designate it as the $\Upsilon(1S)$ meson:

$$\Upsilon(1S)(bb^{+}) \equiv (\tau L)(g_{\tau}L)(\tau^{+}L) \equiv (W^{-}L+\nu|)L(\nu L+\nu|)L(W^{+}L+\nu|)L \quad (7.46)$$

Mesons with τ^{*}

Similarly, there may be some possible mesons with $\tau^{*}\tau^{*+}$ compositions, bound by g_{τ} or $g^{*}{}_{\tau}$:

$(\tau^{*}L)(g_{\tau}L)(\tau^{*+}L)$; $(\tau^{*}L)(g_{\tau}R)(\tau^{*+}L)$; $(\tau^{*}L)(g^{*}{}_{\tau}L)(\tau^{*+}L)$; $(\tau^{*}L)(g^{*}{}_{\tau}R)(\tau^{*+}L)$; $(\tau^{*}L)(g_{\tau}L)(\tau^{*+}R)$;
$(\tau^{*}L)(g^{*}{}_{\tau}R)(\tau^{*+}R)$;

The third combination could be the most stable, we designate it as the θ meson:

$$\theta(t^{*}t^{*+}) \equiv (\tau^{*}L)(g^{*}{}_{\tau}L)(\tau^{*+}L) \equiv (W^{-}R+\nu|)L(\nu R+\nu|)L(W^{+}R+\nu|)L \quad (7.47)$$

B^0-$\bar{B}^0$ oscillation and Bs^0-$\bar{B}s^0$ oscillation

The B^0-$\bar{B}^0$ and Bs^0-$\bar{B}s^0$ oscillations are analogous to K^0-$\bar{K}^0$ and D^0-$\bar{D}^0$ oscillations, all requiring quarks and gluons with matching chirality. They can be represented as:

$$B^0(d\bar{b}*) \equiv (eL)(g*_\tau L)(\tau^+ L) \equiv (W^- L + \underline{\nu}R')L\ (\nu|'' + \underline{\nu}R'')L\ (W^+ L + \nu|''')L$$

$$\leftrightarrow (W^- L + \nu|'')L\ (\underline{\nu}R' + \nu|''')L\ (W^+ L + \underline{\nu}R'')L \equiv (\tau L)(g*_\tau L)(e^+ L) \equiv \bar{B}^0(b*\bar{d}) \qquad (7.48)$$

$$Bs^0(s\bar{b}) \equiv (\mu L)(g_\tau L)(\tau^+ L) \equiv (W^- L + \underline{\nu}L')L\ (\nu|'' + \underline{\nu L}'')L\ (W^+ L + \nu|''')L$$

$$\leftrightarrow (W^- L + \nu|'')L\ (\underline{\nu}L' + \nu|''')L\ (W^+ L + \underline{\nu}L'')L \equiv (\tau L)(g_\tau L)(\mu^+ L) \equiv\ \bar{B}s^0(b\bar{s}) \qquad (7.49)$$

The following couplings of B charged mesons are present in the Standard Model (SM) but are not allowed in NPM: $B^+(u\bar{b})$ and $Bc^+(c\bar{b})$. The LHCb Collaboration has recently reported initial evidence for direct CP violation in beauty to charmonium decays (*89*). It is possible that the observed CP violation may be related to uncertainties in understanding the composition of π^+, K^+ and B^+ mesons.

8. About Neutrinos

8.1 Particular Type of Photons

Neutrinos are photons that are produced under specific conditions. In the early universe, neutrinos only emerged after second-generation particles—such as gluons, leptons, and Higgs bosons—had formed. Typically, neutrinos result from gluon fragmentation, lepton decay, or meson decay, taking on flavours based on their previous tendency of coupling, which in turn influences how they interact with other particles.

In comparison, ordinary photons are usually produced during processes such as particle-antiparticle annihilation, electromagnetic decay, and bremsstrahlung; they do not possess flavour, and under certain conditions can merge with other photons or divide into new ones. For example, during electron-positron annihilation, the interior W^- of the electron annihilates with the interior W^+ of the positron, resulting in the production of two EM^+ and two EM^- particles that dissipate into the background field, while the interior γ components of both the electron and the positron are released and subsequently lose their coupling tendency (flavour). In electromagnetic decay or bremsstrahlung, the electron's internal γ splits into two photons—one remains coupled with W^-, while the other is emitted from the electron as a gamma or X-ray photon, rather than as a coupling-prone neutrino.

8.2 Sources of Neutrinos

Neutrinos can result from the breakup of unstable fermions, bound gluons, or free gluons under extreme conditions. As discussed in Section 7, many neutrinos are emitted from bound gluons and unstable quarks during meson decay processes.

In nature, both free and bound gluons exist in and around objects like stars. Many solar neutrinos may result from gluon breakup in the solar core under extreme conditions. Neutrinos are not produced by pure fusion, which only adds binding gluons without splitting them (see Section 11 for details).

Neutrinos from gluon breakup, as predicted by NPM, may address unresolved issues in astrophysics. For example, it is unclear how neutrinos are generated during massive star core-collapse, what are the explosion mechanism of core-collapse supernovae (CCSNe), and why explosive energy growth rates fail to account for observed ^{56}Ni mass (*90-94*).

There is another example. White dwarfs are stellar remnants that have depleted their nuclear energy sources and cool gradually, emitting light from residual heat over billions of years (*95*). However, recent scientific studies have found that some cooling white dwarfs exhibit a constant luminosity for a longer period than previously expected. This extended cooling process suggests the possibility of an unidentified energy source influencing the rate at which these stars freeze (*96*, *97*). The breakdown of unknown gluons has been proposed as one possible explanation for this cooling behavior observed in high-mass white dwarfs.

So, one of the main sources of neutrinos in nature is the gluons. As the mediates of strong interactions, gluons are well-known in current theories; but as a participant of weak interactions, the existence and function of gluons are not well known at present. To address various phenomena in the neutrino sector that extend beyond the Standard Model (SM), physicists have introduced numerous theoretical particles and models involving neutrinos and gluons. These include heavy neutral leptons (HNL) (*98*), dark photon coupling (*99*), heavy neutrino (HN) (*100*) and SM gauge-singlet fermions (sterile neutrinos) (*101*), which could be explained by the features and behaviors of different free gluons (dark matters) in NPM.

The next subsection will discuss gluon channel functions in relation to neutrino oscillations.

8.3 Mechanism of Neutrino Oscillation

Neutrino oscillation resembles meson oscillation; both involve gluons mediating neutrino exchange, with the former using free gluons and the latter involving bound gluons.

The interactions between three flavours of gluons and three flavours of neutrinos can be expressed as following (note: for the present purposes, here the chirality of the gluons and the heavy states of neutrinos and gluons are not presented here, which follow the same patterns of neutrino transmutation):

$$\nu_eR + g_\mu \equiv \nu_eR + (\nu_\mu L + \nu_\mu L) \leftrightarrow (\nu_eR + \nu_\mu L) + \nu_\mu L \equiv g_e + \nu_\mu L \quad (8.1a)$$

$$\nu_eL + g_\mu \equiv \nu_eL + (\nu_\mu R + \nu_\mu R) \leftrightarrow (\nu_eL + \nu_\mu R) + \nu_\mu R \equiv g_e + \nu_\mu R \quad (8.1b)$$

$$\nu_eR + g_\tau \equiv \nu_eR + (\nu_\tau L + \nu_\tau|) \leftrightarrow (\nu_eR + \nu L) + \nu_\tau| \equiv g_e + \nu_\tau| \quad (8.2a)$$

$$\nu_eL + g_\tau \equiv \nu_eL + (\nu_\tau R + \nu_\tau|) \leftrightarrow (\nu_eL + \nu_\tau R) + \nu_\tau| \equiv g_e + \nu_\tau| \quad (8.2b)$$

$$\nu_\mu L + g_\tau \equiv \nu_\mu L + (\nu_\tau L + \nu_\tau|) \leftrightarrow (\nu_\mu L + \nu_\tau L) + \nu_\tau| \equiv g_\mu + \nu_\tau| \quad (8.3a)$$

$$\nu_\mu R + g_\tau \equiv \nu_\mu R + (\nu_\tau R + \nu_\tau|) \leftrightarrow (\nu_\mu R + \nu_\tau R) + \nu_\tau| \equiv g_\mu + \nu_\tau| \quad (8.3b)$$

Equations (8.1a) and (8.1b) show that ν_e and ν_μ helicity or chirality changes during oscillation. Recent studies on relic neutrinos confirm this shift with significant probability (*102*).

In the Standard Model, neutrinos propagate as superposition states, but in NPM, their state remains fixed during propagation and interaction. While flavour conversion may seem to create a new neutrino with different properties, it is an exchange of position between the traveling and bound neutrinos in the gluon.

The mass hierarchy of τ, μ, and e matches that of their respective g and ν counterparts. Mass (energy) conversion typically occurs stepwise, so most transitions between ν_τ and ν_e proceed via ν_μ, making direct ν_τ–ν_e conversions (as in eq. 8.2a and 8.2b) rare. These repeated conversions resemble oscillations.

The likelihood of neutrinos interacting with free gluons decreases as their energy increases. Because ν_τ and ν_μ often originate from heavy or high-energy particle decays, they tend to have higher energies and travel farther before interacting with gluons compared to ν_e. For example, a recent KM3NeT detection captured an ultra-high-energy cosmic neutrino that had traveled an exceptionally long distance and time (*103*).

We propose that the three neutrino mass eigenstates predicted by the PMNS matrix theory (*104*, *105*) correspond to the masses of the three gluon flavours (including heavy states). Determining gluon flavour masses from other sources could enhance the accuracy of the PMNS matrix, and improvements in this theory may, in turn, yield more precise values for both gluon and neutrino masses.

Free gluons are also widely distributed in ordinary matter, so neutrino oscillations may occur in other areas rather than the core area of the sun and the earth with the Mikheyev–Smirnov–Wolfenstein (MSW) effect (*106*). Because of their strong weak-force and gravitational interactions with regular matter, gluons can follow baryon distribution closely. This may help address the "mass discrepancy" in ΛCDM (*106*, *107*) and account for observations explained by Modified Newtonian Dynamics (MOND) theory (*108*).

9. About Weak Interaction

9.1 Violation of Charge Conservation and Energy Conservation

In the Standard Model, weak interactions involve W or Z boson exchange between fermions. For instance, in neutron β^- decay: $d \rightarrow u + W^-$, and $W^- \rightarrow e + \bar{\nu}_e$, resulting overall in $d \rightarrow u + e + \bar{\nu}_e$, $ddu \rightarrow duu + e + \bar{\nu}_e$, or $N \rightarrow P + e + \bar{\nu}_e$.

In NPM, as noted in Section 2, the up quark has a +1 charge and the down quark a -1 charge, so the process $d \rightarrow u + W^-$ violates charge conservation. It also breaks energy conservation unless external energy is provided, making spontaneous occurrence impossible. While the SM uses quantum tunneling to address energy violations, its low probability cannot account for the rapid decay of many unstable particles.

Similarly, the reactions $u + W^- \rightarrow d$, $u \rightarrow W^+ + d$, $W^+ \rightarrow e^+ + \nu_e$ and $W^+ + \bar{\nu}_e \rightarrow e^+$ are invalid. The down and up quarks, considered as electron and heavy electron (e and e^{*+}) bound by gluons, should be as stable as e and e^{*+}, and not decay under normal conditions. In NPM, since up and down quarks' composition implies that $u \rightarrow d$ requires $W^+ \rightarrow W^-$, this would violate charge conservation.

Processes such as $d \rightarrow u + W^-$ and $W^+ \rightarrow e^+ + \nu_e$ may conform to the weak isospin conservation law mathematically but not align with the charge conservation law and energy conservation law in physics. This indicates that the weak isospin hypothesis may have limitations even when applied to weak interactions.

Although W^- is unstable, the process $W \rightarrow \ell\nu$ does not occur in practice. The actual decay involves W^- interacting with an invisible gluon, for instance,

$$W^-R + g_e \equiv W^-R + (\nu_eL + \nu_eR) \rightarrow (W^-R + \nu_eL) + \nu_eR \equiv e + \nu_e \qquad (9.1a)$$

or $$W^-R + g_\mu \equiv W^-R + (\nu_\mu R + \nu_\mu R) \rightarrow (W^-R + \nu_\mu R) + \nu_\mu R \equiv \mu + \nu_\mu \qquad (9.1b)$$

The CDF collaboration's 2022 report measured the W boson mass at 7 standard deviations above the Standard Model (SM) prediction (*109*), hinting at new physics. While recent ATLAS (*110*) and CMS (*111*) results align with SM expectations, the anomaly is unresolved since there are no clear issues with the CDF measurement. Other experiments like LEP combination (*112*), D0 (*113*) and LHCb (*114*) also show W boson masses higher than the SM value. One possible explanation is the W boson's interaction with invisible gluons in processes like (9.1a) and (9.1b). The influence of these interactions on measurement outcomes can be affected by variables such as gluon type, the specific final state particles detected, and the momentum of the W boson. Consequently, experiments that utilize different collision pairs, collision energies, or detection particles may observe varying degrees of impact.

A more popular process is the μ decay process $\mu \rightarrow e + \bar{\nu}_e + \nu_\mu$, which also has an invisible g_e involved, for example,

$$\mu + g_e \equiv (W^{-}R + \nu_{\mu}R) + (\nu_eL + \nu_eR) \rightarrow (W^{-}R + \nu_eL) + \nu_eR + \nu_{\mu}R \equiv e + \nu_e + \nu_{\mu} \qquad (9.2)$$

9.2 Neutrino-Induced Beta Decay

Neutrinos typically pass through matter without interaction or detection because of their neutral charge, very small mass, and lack of participation in electromagnetic and strong interactions. However, they can collide and scatter with other particles, and studies indicate that many β decays may be initiated by neutrino interactions rather than occurring spontaneously.

There are two main types of beta decay: β^- decay, where a neutron turns into a proton via a W^- boson as a down quark becomes an up quark, and β^+ decay, where a proton becomes a neutron via a W^+ boson. While the Standard Model attributes beta decay to weak interactions, the exact cause and mechanism in nature remain uncertain (*115*).

In 1973, experiments in CERN's Gargamelle chamber observed that a neutrino altered the trajectory of an electron via the neutral current (virtual Z) (*116*). This was interpreted as a direct interaction between the neutrino and the electron, similar to the elastic neutrino-electron scattering studied by MINERvA experiments across various energy scales (*117-120*).

As outlined in Section 2, the down quark is described as an electron bound by a gluon, while the up quark is characterized as a heavy positron similarly bound. Consequently, both particles may participate in scattering events with neutrinos akin to those observed with electrons. This interpretation is further supported by data obtained from studies and measurements of coherent elastic neutrino-nucleus scattering (CEνNS) (*121*, *122*).

We observe that neutrinos are the primary cause of most beta decays, rather than beta decays generating neutrinos. The following observations support neutrino-induced beta decay:

1. Many fully ionized atoms experience much faster beta decay (*123*), as the absence of outer electrons leaves nucleons more exposed to incoming neutrinos.
2. The β^+decay rate increases with the number of neutrons and protons in the nucleus (*124*). This occurs because more nucleons lead to greater excitation of binding pions, weakening nuclear forces among protons and raising the likelihood of β^+ decay, as more pions are susceptible to neutrino interactions (see Sec. 9.4 for details). A single isolated proton cannot undergo β^+ decay since no pions are excited.
3. Some nuclei can undergo ββ decay, in which the charge of the nucleus changes by two units; this is considered the rarest form of radioactive decay. As of 2019, only 14 instances of ββ decay have been observed, with the isotopes exhibiting this decay having an average lifetime exceeding 10^{18} years (*125*). This is due to the extremely low probability of two neutrons' uud-d cores within a nucleus interacting simultaneously with two incoming neutrinos. Standard Model theories also predict the possibility of "neutrino-less ββ decay", though no experimental observations of this process have been reported to date (*126*). Under the neutrino-induced beta decay hypothesis in NPM, it is suggested that this type of decay does not occur.

9.3 About β^- Decay

As discussed in Section 2, following early universe evolution, protons and neutrons formed with the structures shown in Fig. 3.

At any given time, countless neutrinos pass through each neutron, occasionally striking the uud-d core structure. While the stable uud segment typically remains intact, the extra down quark (or bound electron)—due to its weaker binding—can be ejected by a neutrino—typically an electron neutrino. The neutrino then loses some kinetic energy and changes direction, and the neutron transforms into a proton as it loses the additional d quark (or electron), as shown in Fig. 5. Thus, β^- decay can be represented as:

$$N + \nu_e(\text{incident}) \equiv uud+d + \nu_e(\text{incident}) \rightarrow uud + e + \nu_e(\text{incident}) \equiv P + e + \nu_e(\text{incident})$$

or more simply:

$$N + \nu_e(\text{incident}) \rightarrow P + e + \nu_e(\text{incident}) \qquad (9.3)$$

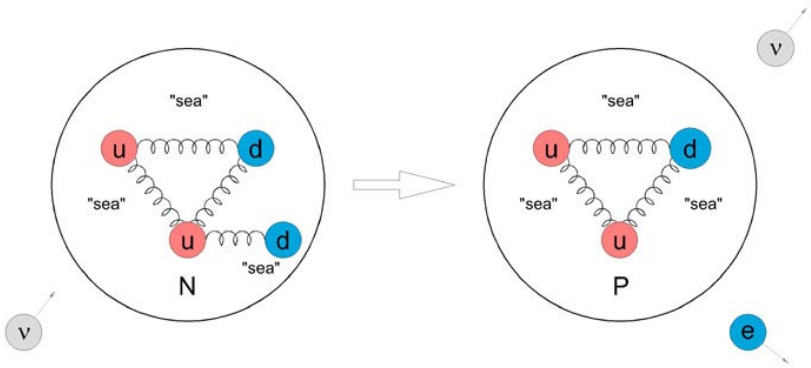

Fig.5| β^- decay. A neutron interacts with a neutrino, resulting in the transformation of the neutron into a proton as one of its down quarks is removed. The neutrino experiences elastic scattering, altering its trajectory and continuing onward with reduced kinetic energy.

A well-known example of β^- decay involves measuring the lifetime of free neutrons, typically about 15 minutes. Two main methods—beam and ultracold neutron storage—produce results that differ by roughly 9 seconds (4 standard deviations). Despite decades of refinement, this discrepancy persists (*127*, *128*). NPM suggests the difference is due to different movement: fast-moving beam neutrons have a lower chance of neutrino interaction and thus last longer, while ultracold neutrons are more likely to be struck and decay faster due to slow movement, maintaining the 9-second gap between methods. One approach to assess whether incoming neutrinos affect neutron lifetime measurements is to re-analyse historical data to check for the presence of annual or diurnal oscillations in decay rates.

Another popular example of the β^- decay is the Homestake experiment. But in the Standard Model, this experiment is described as charged current interaction, inverse β^- decay, or inverse electron capture reaction:

$$^{37}Cl + \nu_e \rightarrow {}^{37}Ar + e$$

The reaction is a neutrino impact, corresponding to a β^- decay, rather than a neutrino capture, and should be stated as such:

$$^{37}Cl + \nu_e(\text{incident}) \rightarrow {}^{37}Ar + e + \nu_e(\text{incident})$$

The threshold neutrino energy for this reaction is 0.814 MeV; consequently, the resulting νe typically remains undetectable because of the very limited kinetic energy available. An analogous β^- decay occurs in the gallium (Ga) to germanium (Ge) reaction, which has a substantially lower energy threshold of 0.233 MeV (refer to Section 10.4 for additional details).

A widely cited example of β^- decay is the Wu experiment (*129*):

$$^{60}Co \rightarrow {}^{60}Ni + e + \bar{\nu}_e + 2\gamma\ .$$

The experiment provided evidence of parity violation (P-violation) in weak interactions, which is attributed to the participation of only left-handed fermions through the exchange of virtual W bosons (*130*). However, as noted in Section 9.1, W exchange processes such as $d \rightarrow u + W^-$ and $W^- \rightarrow e + \bar{\nu}_e$ are not valid. It is proposed that P-violation may result from the presence of preferred spatial directions, where incident neutrinos can more effectively kick out the extra down quark in the duu-d core of the neutron, while associated binding gluons may dissociate into two photons emitted in opposite directions. The underlying cause of parity symmetry breaking may relate to structural features of the nucleus, specifically the existence of a closed end and an open (growing) end, with beta decay occurring predominantly at the open end (see further discussion in Section 11).

9.4 About β^+ Decay

The uud core of the proton represents one of the most stable configurations among all hadrons; it remains intact even when subjected to interactions with neutrinos or photons, so an isolated proton has not been observed to decay in nature. Consequently, physicists do not need to take proton decay into account when working with accelerated protons confined within the LHC.

In proton-rich nuclei, Coulomb forces may cause some protons to be ejected or held by the nucleus via excited mesons (mainly π^0) and gluons. An incoming neutrino can break an excited π^0 into an electron, positron, and gluon. The electron can bind to the proton's uud core, changing it into a neutron, while the positron escapes and may annihilate with a shell electron. This outlines the basic mechanism of β^+decay:

$$P + \pi^0 + \nu_e(\text{incident}) \equiv (uud) + (dd^+) + \nu_e(\text{incident}) \rightarrow (uud + d) + d^+ + \nu_e(\text{incident}) \equiv N + e^+ + \nu_e(\text{incident})$$

or more simply

$$P + \pi^0 + \nu_e(\text{incident}) \rightarrow N + e^+ + \nu_e(\text{incident}) \qquad (9.4)$$

where the associated gluon (g_e) may go undetected in the background.

The excited meson can also be either a ρ^0 or ω meson, both of which may decay into a μ and μ^+ upon interaction with ν_μ. The μ decays into an electron, which is then attracted and bound to the proton via a gluon, converting the proton into a neutron as the μ^+ exits the nucleus. This describes the reaction $p(\bar{\nu}_\mu, \mu^+)n$.

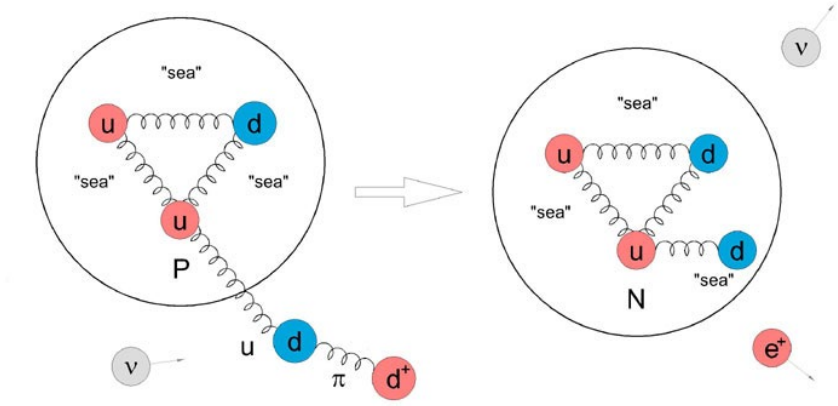

Fig. 6 |β^+ decay. When a neutrino interacts with a pion, the excited pion may decay into an electron and a positron. The electron can be absorbed by the proton's core, resulting in the conversion of the proton into a neutron, while the positron moves away from the nucleus.

In the SM, β^+ decay is typically written as:

$$P \rightarrow N + e^+ + \nu_e \, .$$

The process cannot happen spontaneously or with a lone proton, as extra energy is required to convert a proton into a neutron, positron, and neutrino. The subprocesses ($u \rightarrow W^+ + d$ and $W^+ \rightarrow e^+ + \nu_e$) are also invalid, as noted in Sec. 9.1. In NPM, this energy comes from the excited π0 and the incoming neutrino (see equation 9.4).

In the Standard Model, inverse β^+ decay (*131*) is given by $P + \bar{\nu}_e \rightarrow N + e^+$, based on the reaction $W^+ + \bar{\nu}_e \rightarrow e^+$, which can occur only in extreme high-energy environments like those present early in the universe. Electron capture (EC), another form of inverse β^+ decay, will be discussed next.

The Cowan–Reines neutrino experiment involves an (inverse) β^+ decay process (*132*). It is proposed that the electron captured and the emitted positron in this experiment originate not from the hydrogen nuclei, but from the Cl nuclei or Cd nuclei of the liquid scintillator ($CdCl_2$), where there are excited π^0 mesons required for the β^+ decay.

9.5 About Electron Capture

Electron capture (EC) is an alternative to β^+ decay in proton and electron-rich atoms. It is the sole option when a proton binds to a nucleus via a gluon, as in ^{7}Be (see Fig. 21c), rather than through a light meson and gluon, as in ^{8}B (see Fig. 22c). In EC, a K- or L-shell electron is captured by a nucleus proton.

In the Standard Model, an electron converting a proton to a neutron via weak interactions involves processes like $e \rightarrow W^- + \nu_e$ and $u + W^- \rightarrow d$. However, as noted in Sec. 9.1, $u + W^- \rightarrow d$ violates charge and energy conservation, and $e \rightarrow W^- + \nu_e$ cannot occur spontaneously because the electron is stable.

Some may suggest that the energy to overcome the barrier is provided by the binding energy difference between the parent and daughter nuclide (*133*). However, this differential binding energy is typically released after electron capture, usually as one or two gamma rays.

In NPM, electron capture has two forms. One involves a K- or L-shell electron being absorbed by the nucleus, often after γ ray impact. This process may release γ rays (from nuclear de-excitation) or X-rays (from electron shell transitions and bremsstrahlung), which can be described as:

$$P + e + \gamma(\text{incident}) \equiv uud + e + \gamma(\text{incident}) \rightarrow (uud+d) + \gamma(\text{incident}) + (\gamma\text{s or X-rays})(\text{released}) \equiv N + \gamma(\text{incident}) + (\gamma\text{s or X-rays})(\text{released})$$

or more simply:

$$P + e + \gamma(\text{incident}) \rightarrow N + \gamma(\text{incident}) + (\gamma\text{s or X-rays})(\text{released}) \qquad (9.5a)$$

Another form of electron capture occurs when a neutrino strikes an electron in the K- or L-shell, causing it to be captured by a proton in the nucleus (see Fig. 7). This may lead to γ emission from nuclear de-excitation, X-ray release from electronic de-excitation, and electron bremsstrahlung. The process can be summarized as follows:

$$P + e + \nu(\text{incident}) \equiv uud + e + \nu(\text{incident}) \rightarrow (uud+d) + \nu(\text{incident}) + (\gamma\text{s or X-rays})(\text{released}) \equiv N + \nu + (\gamma\text{s or X-rays})(\text{released})$$

or more simply:

$$P + e + \nu(\text{incident}) \rightarrow N + \nu(\text{incident}) + (\gamma\text{s or X-rays})(\text{released}) \qquad (9.5b)$$

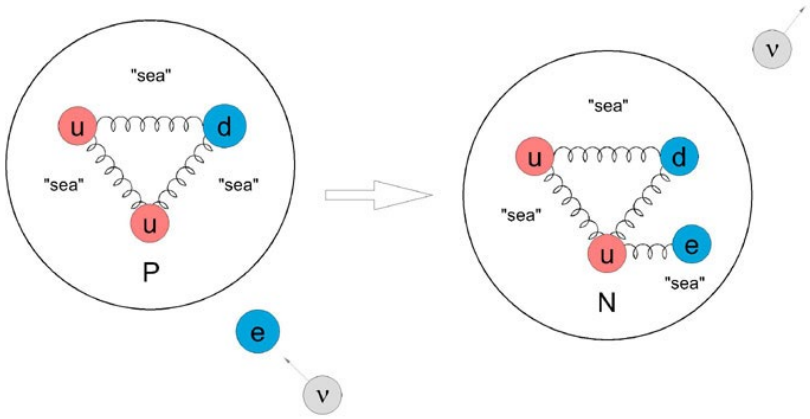

Fig. 7 | Neutrino-induced Electron Capture. In a proton-rich and electron-rich atom, an electron is knocked by a neutrino and captured by the proton, then bound to the core by a gluon, which makes the proton transmute to a neutron.

The reaction $^{7}Be \rightarrow {}^{7}Li$ may represent one of the earliest electron capture (EC) processes occurring during Big Bang nucleosynthesis. The EC reactions $^{51}Cr \rightarrow {}^{51}V$, $^{37}Ar \rightarrow {}^{37}Cl$ and $^{71}Ge \rightarrow {}^{71}Ga$ are commonly studied in Ga anomaly experiments, as will be discussed in Sec.10.4.

It may be more accurate to consider β^{+}decay as a specific form of electron capture, where the captured electron originates from a different source, such as an excited π^{0} bound to the nucleus, rather than from the electron shell.

Analysis of various forms of beta decay indicates that the influence of ambient neutrino flux has been insufficiently addressed in current theoretical frameworks. As a result, the calculated cross-section for neutrino interactions with nucleons and electrons may be erroneously estimated at approximately 10^{-46} cm^{2} (*134*), thereby rendering neutrino-induced beta decay seemingly implausible.

10. Neutrino Associated Anomalies

10.1 Decay Rate Variability

Although some studies link variability in radioactive decay to changes in solar and cosmic neutrino flux (*135*), others disagree (*136*). These conflicting findings may result from differences in experimental conditions, methods, equipment, measurement sensitivity, or misinterpretation of results. Here, we present some evidence supporting Falkenberg's conjecture of neutrino-induced beta decay (*137*), noting that opposing studies have yet to provide compelling counter-evidence.

Determination of solar neutrino variability

The Borexino (138), SNO (139) and Super-Kamiokande (140) have observed annual modulation in solar neutrino interaction rates, consistent with changes in the Earth-Sun angle. Super-Kamiokande also reported a day/night asymmetry in solar neutrino flux (141). Therefore, observing annual or diurnal oscillations in neutrino-induced decay rates is plausible, provided experiments control for weather and environmental factors.

The GSI and Bellotti radon experiments

The GSI radon experiments have demonstrated diurnal variation in radon beta decay data that does not appear to be attributable to local environmental factors (142). Similar patterns were recorded in experiments conducted at different locations, where conditions included gas radon sealed within closed volumes, gamma detectors shielded with lead, and an additional detector monitoring environmental gamma rays.

Other specialized GSI experiments using a goniometer design (see Fig. 8) have demonstrated that radon beta-decay measurements exhibit directional characteristics (143).

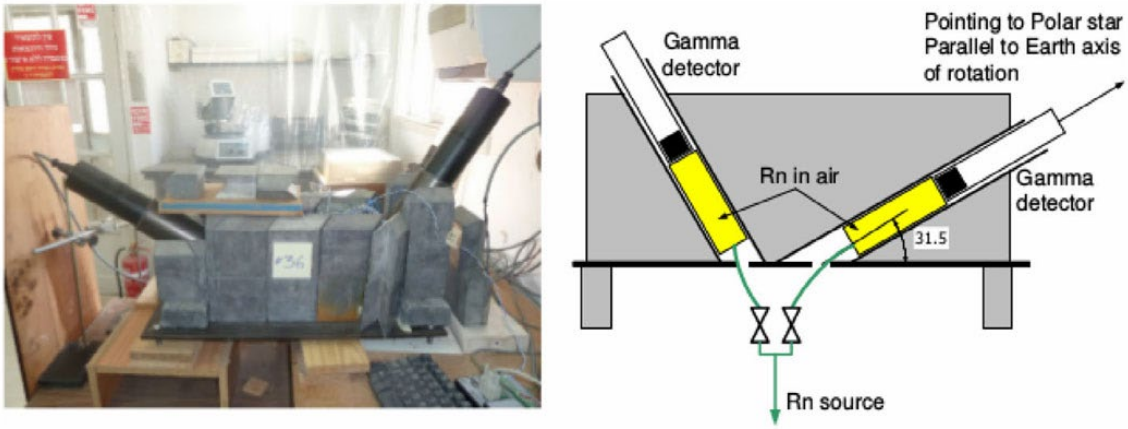

Fig.8| The GSI goniometer experiment. In the diagram, north is to the right, while in the photo (left), north is to the left. The Pb shield appears as grey in the diagram and is visible in the photo. Figure source:(143).

The vertical and perpendicular channels measured different results for radon beta decay, showing variations in both the pattern and pace. These results also differed from the environmental gamma ray measurement patterns. The experimental outcomes indicate that solar radiation flux may influence radon beta decay processes.

There were two versions of the Bellotti radon beta decay experiments: one with radon in air and another with radon in olive oil, both in spherical containers (144). The first experiment showed diurnal oscillations like those observed in the GSI experiments.

However, the second Bellotti radon experiment did not observe a diurnal variation, unlike the first experiment. The addition of olive oil appears to have contributed to this difference. In paper (144), Bellotti and colleagues suggest that displacement of radon within the gas volume may cause diurnal variation by affecting detection efficiency, and the use of olive oil may have mitigated this effect. Alternatively, it is possible that the in-air setup of the initial experiment kept

the radon nucleus closer to its original state, while introducing a medium such as olive oil might alter the nuclear binding environment at the open end of the radon nucleus. A similar phenomenon was noted in the Cowan–Reines neutrino experiment, where β^+ decay was rare in pure water but became more prominent when a liquid scintillator like $CdCl_2$ was added (see Sec. 9.4).

Reactor-status effect on the β^+ decay rate of ^{22}Na

To examine the potential effect of electron antineutrinos on beta decay and address limitations of earlier experiments, β-decay counting with ^{22}Na and ^{60}Co sources was performed at the Koeberg Nuclear Power Station in South Africa. Measurements spanned approximately three years during reactor ON-OFF cycles (*145*). The Pb-shielded sources were in the seismic vault beneath the reactor core containment building (see Fig. 9).

After excluding system uncertainties and background factors such as fast neutron-induced reactions, a reduced neutrino effect on the beta decay rate was detected in the ^{22}Na source, while no reactor status effect appeared with the ^{60}Co source—an outcome current theories cannot explain.

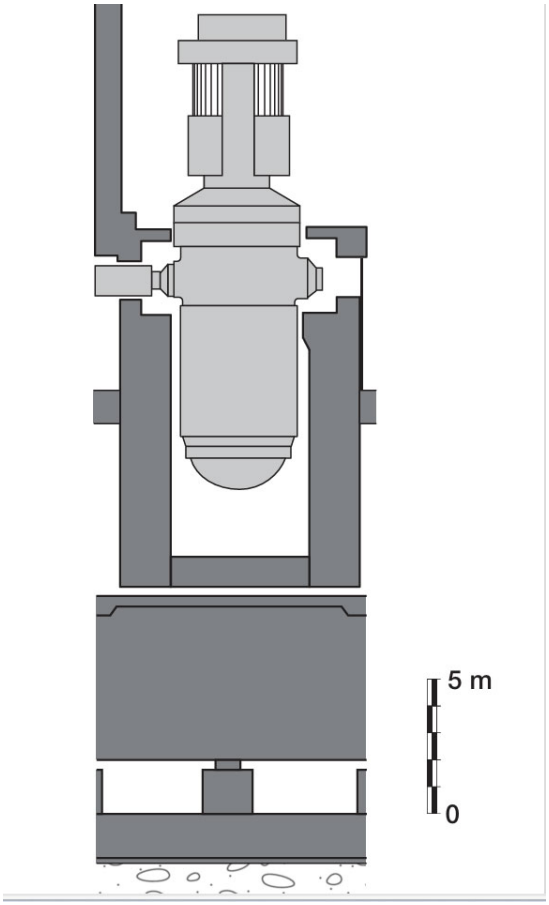

Fig. 9|Schematic cross section of the relevant parts of the reactor building at Koeberg. Total thickness of concrete layers between reactor vessel and seismic vault is approx. 8 m. Figure taken from Ref.(*145*).

However, the observations in NPM provide a qualitative explanation for the observed differences between the ^{22}Na source and the ^{60}Co source.

First, as discussed in Section 9, most beta decays are influenced by neutrinos. When the reactor is ON, many neutrinos emitted from the reactor are "second-hand" solar neutrinos with reduced energy. With the reactor OFF, solar neutrinos directly affect both ^{22}Na and ^{60}Co source. However, when the reactor is ON, especially around noon, solar neutrinos interact with dense fission materials in the core; only those retaining enough kinetic energy can reach and impact the ^{22}Na and ^{60}Co sources. This interaction may reduce the beta decay rates of both sources, particularly for ^{22}Na, due to its higher neutrino interaction cross section.

Secondly, while fast neutron capture on the ^{22}Na source could raise 1275 keV gamma ray counts by converting ^{22}Na to ^{23}Na, it would also lower the β^+ decay rate for the same reason. The paper overlooked fast neutron capture interference with ^{60}Co (*145*); yet, neutron capture turns ^{60}Co into ^{61}Co, which has a much higher β^- decay rate.

Although fast neutron capture slightly increases the beta decay rate as background for the ^{22}Na source, it does not offset the reduction caused by fewer neutrinos; thus, the reactor neutrino effect on ^{22}Na β^+ decay is negative. For ^{60}Co β^- decay, the negative impact of reduced neutrinos is mostly counterbalanced by the opposing effect of fast neutron capture, so the change in decay rate between the reactor's ON and OFF states may fall below detectable levels.

10.2 RAA and 5 MeV Bump

In 2011, the Huber-Mueller model's revised calculations of reactor antineutrino flux (*146*, *147*) and neutron lifetime predicted values about 5% higher than previous short-baseline experiment measurements, a discrepancy known as the reactor antineutrino anomaly (RAA)(*148-151*).

The RAA has prompted extensive experimental and theoretical studies, many of which found that flux deficits vary between fission isotopes (*152-155*), a result not explained by the sterile neutrino oscillation hypothesis and suggesting issues with the Huber-Muller model.

Extensive studies of reactor antineutrinos have revealed an excess near 5 MeV in the prompt energy spectrum, known as the 5 MeV bump or shape anomaly, first observed by RENO in 2014 (*156*) and later confirmed by over ten other experiments (*157-168*). Comparisons indicate this anomaly is independent of fission isotope.

Although recent summation models that incorporate updated nuclear data have largely replaced the RAA, the 5 MeV bump persists and remains insufficiently explained (*169*). Consequently, these new models do not fully account for all observed reactor neutrino data.

We suggest that both the RAA and the shape anomaly are related to "second hand" solar neutrinos, which are not accounted for in the Huber-Muller or newer models. These reactor neutrinos are solar neutrinos scattered by fission isotopes—hence, the RAA's isotope dependence

arises from varying cross sections with different solar neutrinos. The 5 MeV bump is likely due to ^{8}B and hep solar neutrinos, which peak near 6.8 MeV (see Fig. 10 from (170)).

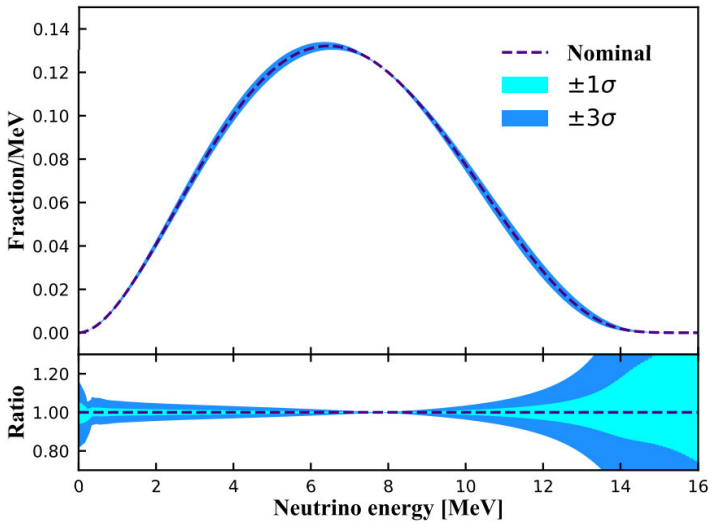

Fig. 10 | ^{8}B and hep ν_e spectrum with the shape uncertainties. Figure taken from Ref.(170).

As discussed in Sec. 9.4, within the Standard Model (SM), inverse beta decay (IBD) is represented as:

$$P + \bar{\nu}e \rightarrow N + e^{+}.$$

Accordingly, the energy of incoming neutrinos and the prompt positron energy are given by the equation (171):

$$E_{\nu e} = E_{prompt} + 0.78MeV + T_n ,$$

where T_n represents the kinetic energy of the recoil neutron, which can typically be neglected. This expression does not account for the undetectable outgoing neutrino. Therefore, the difference between the incoming neutrino energy and the prompt energy may exceed 1 MeV.

The 5 MeV bump strongly suggests that beta decays are caused by neutrinos, since it is unlikely that various fission isotopes would spontaneously emit neutrinos with similarly distorted energy spectra.

One method to evaluate whether incoming neutrinos are associated with the RAA and the 5 MeV bump is to re-examine historical data for evidence of annual or diurnal oscillations in beta decay rates.

10.3 LSND and MiniBooNE Anomaly

The LSND (172-174) and MiniBooNE (175, 176) experiments have observed anomalous excesses of ν_e-like and $\bar{\nu}_e$-like events within ν_μ beams at short baselines. The combined significance of these anomalies has reached approximately 6.1σ (177). While these observations remain under active discussion and investigation, numerous theoretical models—such as 3+N and resonant neutrino oscillations (178), sterile neutrino decay (179) —have been proposed to account for the results.

The origins of these anomalies in NPM can be attributed to the hypothesis that neutrinos are Majorana particles, meaning neutrinos and antineutrinos are identical in their properties and behavior. As a result, both ν_e-like and $\bar{\nu}_e$-like events are considered equivalent, and both ν_e and $\bar{\nu}_e$ running modes should include both types of events, leading to an expectation of increased event counts. Consequently, the observed anomaly is absent in the dump mode, which does not differentiate between neutrinos and antineutrinos (180).

The following observation from the MiniBooNE experiment indicates similar behavior between neutrinos and antineutrinos: a) beam timing data shows that most of the excess events occur in coincidence with neutrinos interacting in the detector; b) the radial distribution demonstrates that the excess is present throughout the detector volume, and applying more restrictive fiducial volume cuts increases the significance of the observed excess (180).

10.4 Gallium Anomaly

The measured neutrino capture rate on ^{71}Ga from an intense source in the four original calibration experiments showed approximately a 2.5σ deviation from theoretical predictions (181), which has increased to 6σ with the results of the BEST experiment (182, 183). Various studies have examined possible explanations for this gallium anomaly, including the 3+1 active-sterile neutrino mixing scheme (184, 185), re-evaluation of the neutrino capture cross section (186), potential unknown excited states of Ge, and overestimation of the source intensity (187), among others.

From the NPM perspective, measuring source intensity is a promising approach to addressing the Ga anomaly. As (187) notes, if the actual branching ratio for ^{51}Cr decays to the excited state of ^{51}V were just ~2% higher, source intensity could be overestimated by ~20%—sufficient to account for the anomaly. As mentioned in Sec. 9.5, not all electron capture (EC) events are neutrino-induced; some result from γ-ray interactions, leading to an overestimation of source neutrinos due to incomplete understanding of the EC process.

11. Nuclear Forces and Binding Structures

11.1 Current Models of Nuclear Forces

Currently, various models of nuclear forces exist, including shell model (188), meson exchange model (189), electromagnetic hydrogen model (190), Gamow's alpha decay model (191), Weizsäcker formula and the liquid drop model (192) , alpha cluster model (193), collective model (194), collective-motion model (195) and residual chromo dynamic model (196). Most models focus on particular features of nuclear forces rather than offering a full explanation (197), treating protons and neutrons equally according to QCD's isospin symmetry.

A recently developed electromagnetic model (198) describes nuclear behaviours with consideration of the electromagnetic energies and forces of quarks within nucleons, an aspect that previous models may not have addressed.

The nuclear force can be viewed as the attraction between up and down quarks in different nucleons. Electromagnetic models, supported by detailed explanations and calculations, indicate that nuclei form chain-like alpha-cluster structures—an idea both theorized and experimentally observed by various researchers (199-208). Significant experimental quadrupole moments across nuclides (A = 0 to 250) challenge models that assume a spherical nucleus shape (198, 209). The electromagnetic model suggests that internucleon quark binding, governed purely by electromagnetic forces with a single variable, yields calculated binding energies closely matching experimental values within a few percent (198).

As discussed in Section 6, NPM suggests that nuclear binding forces primarily result from electromagnetic interactions among quarks inside nucleons and environmental electromagnetic effects. Like the electromagnetic model, NPM accounts for various nuclear force behaviors and predicts most nuclei have a chain-like alpha cluster structure. However, significant differences exist between the two models regarding quark charge and composition, gluon properties, and neutron core structure. For instance, NPM offers more detail about interior structure variations among nuclides and isotopes (see Sec.11.4 and Appendix-I).

11.2 Types of Nuclear Forces

Most standard models view nuclear forces as collective, while NPM and similar models describe them as independent interactions between neighbouring nucleons. For example, the meson exchange model sees nuclear forces as bonds formed through virtual meson exchange between two nucleons. NPM identifies three types of nuclear forces:

1) Direct Gluon Bond: This main nuclear force holds nucleons together in nuclides. A stable nuclide requires each core nucleon to have at least two strong Direct Gluon Bonds. If any nucleon at the growing end is connected only by one Direct Gluon Bond, the nuclide becomes radioactive; neutrons may β^- decay and protons may undergo electron capture.
2) Meson/Gluon Bond: this is the binding force between a proton and the growing end of the nuclide via an excited meson and two gluons. This type of nuclear force usually exists in a proton-rich nuclide, where the excited meson may be generated by the electromagnetic

interaction between nucleons. The proton with a meson/gluon bond to the open end (or growing end) of the nuclide may undergo β^+ decay.
3) Sea Gluon Bond: This refers to a collective nuclear force acting between the sea gluons of an independent nucleon and those of core nucleons within a nuclide. Such interactions typically occur when the independent nucleon occupies a central concave region among a cluster of core nucleons, as observed in structures like ^{3}H and metastable ^{4m}He within certain nuclides. Owing to the inherently weak binding associated with this configuration, these states are highly unstable, often resulting in neutron or proton emission, examples of which include ^{4}H (see Fig.18d), ^{5}H (see Fig.18e), ^{5}He (see Fig.19d) and ^{10}He (see Fig.19i).

Several rules have been identified or proposed regarding various nuclear forces:

a) the valence quark of a core nucleon can only bond with one valence quark in another core nucleon, thus a core nucleon can maximumly binds three neighbouring nucleons with the Direct Gluon Bond.
b) the extra down quark in the duu-d core of the neutron has more freedom than another down quark in the same core, thus it has more chance to bind an up quark of neighbouring nucleons with a Direct Gluon Bond.
c) when the number of protons in the core of the nuclei is fixed, the more the neutrons with Direct Gluon Bond to the growing end of the nuclide, the weaker the bonds, thus the higher the rate of β^- decay these neutrons will undergo.
d) Following beta decay or electron capture, the nuclide promptly rearranges its gluon bonds to reach the lowest energy state.
e) In halo nuclei, the halo neutrons or protons are not orbiting the core of the nuclide in the traditional sense but are instead bound to the core via gluon or meson/gluon interactions. These nucleons exhibit orbital-like behavior due to several factors: **first,** the gluons involved in this binding are not directly detectable; **second,** the matter and charge radius of ^{4m}He (see Fig. 11) exceeds that of ^{4}He (the anticipated core, further discussed in the next subsection), making nucleons attached to the ^{4m}He core look more extended than expected, for example, in ^{6}He (see Fig.19e) and ^{8}He (see Fig.19g); **third**, in certain light nuclei, two or three correlated neutrons may be bound to the nuclide core in a chain-like configuration, resembling halo particles as they appear to orbit a relatively compact core, such as in ^{14}Be (see Fig.21p) and ^{21}B (see Fig.22r). Consequently, similar bound nucleons do not display halo characteristics in larger nuclei.

Researchers have recently reported a 23-sigma anomaly in ytterbium isotope shifts (*210*) and an approximately 1000-sigma anomaly in calcium isotope shifts (*211*). These findings have led to hypotheses that the anomalies may result from a “fifth force” between orbiting electrons and the nucleus or from nuclear polarization. However, we suggest that these anomalies could be due to nuclear deformation (stemming from variety of nuclear forces), not yet fully understood thus significantly underestimated by current Standard Model theories.

11.3 Nuclear Building Blocks

In the early universe, after most particles and anti-particles annihilated, the expanding and cooling cosmos formed hydrogen (^{2}H, ^{3}H) and helium (^{3}He, ^{4}He) nuclides from a hot plasma of

gluons, (anti)electrons, protons, and neutrons. These nuclides became the building blocks for heavier elements created through nucleosynthesis during events like star formation, supernovae, and neutron star mergers.

Protons and neutrons are fundamental components of nuclei. Figure 11 shows other common nuclides, categorized by their internal binding structures of protons and neutrons.

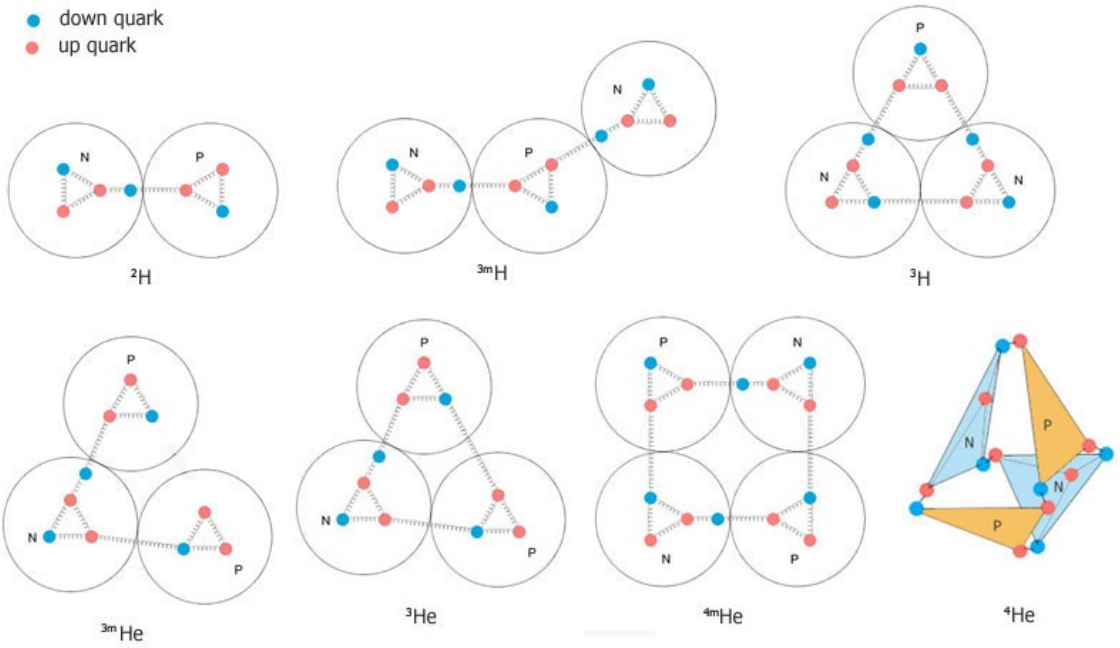

Fig. 11|Basic nuclides and their internal binding structures. Nucleons are bound by Direct Gluon Bonds between down quark and up quark of their core structures.

^{2}H (deuterium) is stable because its proton and neutron are held together by a symmetric Direct Gluon Bond.

^{3}H (tritium) is expected to be stable due to its structure and higher average binding energy per nucleon compared to ^{3}He, yet it has a measured half-life of 12.33(2) years (*212*). This suggests the existence of a metastable state, ^{3m}H, with only two interior bonds. Despite having a comparable average binding energy per nucleon to deuterium (^{2}H), ^{3m}H still undergoes beta decay because its binding structure is less balanced and symmetric.

The independent ^{4}He (alpha particle) is a highly stable nucleus with six interior bonds, making it unable to bond with additional nucleons. According to NPM, ^{4}He also has a metastable state, ^{4m}He, featuring four internal bonds and four spare valence quarks for bonding with nearby nucleons. It is ^{4m}He, not ^{4}He, that serves as the nuclear building block for heavier nuclides. When ^{4m}He is emitted during decay, it immediately transitions to the more stable ^{4}He state.

Likewise, ^{3}He has an isomer, ^{3m}He, which may appear in certain unstable nuclei or as a brief transitional state during isotope shifts.

11.4 Nuclear Behaviours Explained

Based on the nuclear force rules from Sec.11.2, we determined the binding structures for isotopes ranging from ^{2}H to ^{22}C, shown as simplified graphics in Appendix I. These structures can account for observations in isotope transformation and can also be used to predict possible, as-yet-unidentified states of isotopes. The following sub-section will provide several examples.

Why is ^{5}H so extremely unstable?

Similar to ^{4}H, ^{5}He, ^{7}He, ^{4}Li, ^{5}Li, ^{6}Be, ^{15}Be, ^{7}B, ^{9}B and ^{8}C, etc, ^{5}H (Fig.18e) contains a Sea Gluon Bond nucleon whose stability relies on the overall balance of the system, residing in the concave region of the nucleus. Minor vibrations or external impacts may disrupt this equilibrium, resulting in the ejection of the Sea Gluon Bond nucleon. Consequently, most isotopes of this type exhibit half-lives on the order of zeptoseconds(zs) or yoctoseconds(ys).

Why is ^{8}Be so extremely unstable?

The isotope ^{8}Be exhibits two distinct energy states: the open state and the bent isomeric state (^{8m}Be). As illustrated in Figure 21, the U-shaped ^{8m}Be can be incorporated within other isotopes. When ^{8m}Be separates from a parent nuclide and transitions to the open configuration of ^{8}Be, the associated release of energy or internal stress may cause it to dissociate into two ^{4m}He nuclei (see Fig. 19b), which promptly transition to their ground states as alpha particles.

Why is ^{11}He not observed?

As illustrated in Fig. 19i, from a system balance perspective, ^{10}He containing two Sea Gluon Bond neutrons is considered neutron-saturated, which results in the nucleus expelling any additional neutrons.

Why does ^{18}B not have halo neutron while both ^{17}B and ^{19}B does?

As shown in Fig. 22n, ^{17}B features a symmetric structure with two halo neutrons. Adding a neutron to an open-end chain disrupts this symmetry but placing it to the concave area at the nucleus's closed end preserves balance, as seen in ^{18}B (Fig. 22o). Adding one neutron to each halo tail maintains symmetry and creates ^{19}B (Fig. 22p), which has four halo neutrons. Therefore, while ^{18}B possesses two halo neutrons like ^{17}B, its notably brief half-life—attributed to the Sea Gluon Bond neutron—leads to unique characteristics and manifestations. As a result, ^{18}B may appear to lack halo neutrons.

Why does ^{11}Be and ^{14}Be decay differently?

Although there are several differences between the decay of ^{11}Be and ^{14}Be, this discussion addresses why the majority of ^{11}Be undergoes β^- decay, while most ^{14}Be decays through the β^-n mode (*212*).

As shown in Fig. 21j, ^{11}Be contains a halo neutron. When this outer neutron becomes a proton via β^- decay and combines with nearby nucleons to form a ^{4m}He component at the nuclide's open end, another chain neutron can join other nucleons to create a ^{3m}H component at the same end. This process forms ^{11}B (Fig. 22g) without ejecting any neutrons.

As shown in Fig. 21p, ^{14}Be contains two neutron chains ending with halo neutrons. When one halo neutron undergoes β^- decay and becomes a proton, forming a ^{4m}He component, its adjacent neutron is ejected due to lack of space and difficulty joining another chain. Therefore, ^{14}Be typically experiences β^-n decay.

What causes the spikes in the binding energy curve?

Certain isotopes, such as ^{4}He, ^{8}Be, ^{12}C, ^{16}O and ^{20}Ne, show distinct peaks in nuclear binding energy per nucleon (see Fig. 12). We suggest these peaks arise from unknown isomers of these isotopes that have even numbers of protons and structures composed of integer multiples of ^{4m}He.

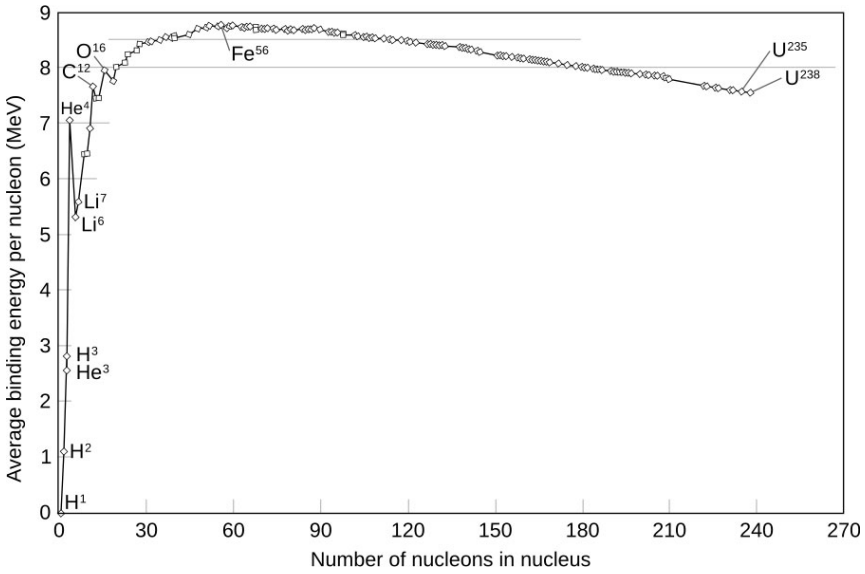

Fig.12. Binding energy per nucleon. Source: Wikipedia (https://en.wikipedia.org/wiki/Nuclear_binding_energy). Data available from the NuDat 2 database (*213*).

We have determined the structures of ^{4}He, ^{8}Be, ^{12}C and their isomers (see Appendix I). Using β^- decays, we can also identify the structures of ^{16}O and ^{20}Ne isomers as shown in Fig.13. As transition states, these isomers' binding energies better reflect relationships with neighbouring isotopes than independent states. Their average binding energy per nucleon is lower due to fewer bonds or open structures. Measuring the binding energies of these isomers and updating current data may smooth out or correct spikes in the binding energy curve.

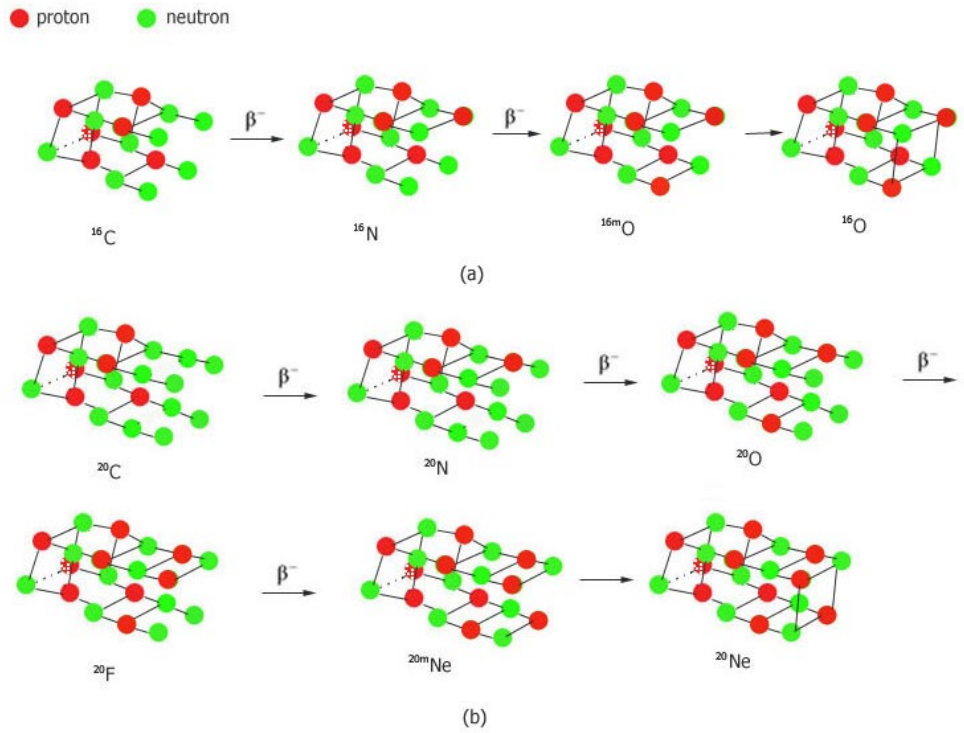

Fig. 13. Beta decay studies have shown that ^{16}O and ^{20}Ne have transition isomers, ^{16m}O and ^{20m}Ne.

11.5 Misconceptions About Fusion

Fusion is not exothermic reaction

A common misconception is that nuclear fusion is exothermic. For instance, in the hydrogen burning process ($4^1H \rightarrow {}^4He$), mainstream scientists argue that the mass deficit between four hydrogen nuclei and one helium nucleus is released as energy, per $E = mc^2$ (*214-217*). However, if the binding energy remains within the helium to keep it stable, it cannot also be released externally. If fission releases binding energy, fusion—the reverse process—should logically require energy input, making it endothermic rather than exothermic.

For example, we will look at the deuterium–tritium (DT) reaction, a highly favourable nuclear reaction (*218*):

$$^2D + {}^3T \rightarrow {}^4He\ (3.5MeV) + n(14.1MeV).$$

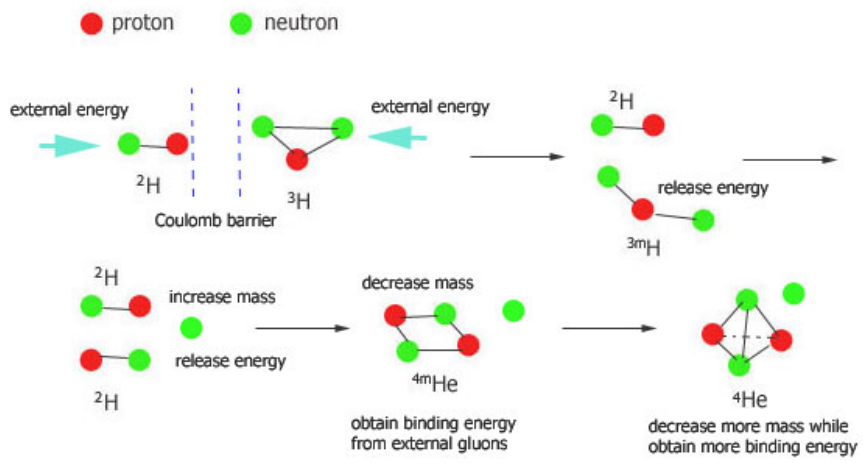

Fig.14. Several processes in the D-T reaction involve changes in binding energy.

In NPM, the D-T fusion reaction consists of several processes (see Fig. 14) and can be described by a set of equations:

$$^2\text{H} + {}^3\text{H} + \text{E1} \rightarrow {}^2\text{H(K1)} + {}^3\text{H(K2)} \rightarrow {}^2\text{H(K1)} + {}^{3m}\text{H(K3)} + \text{E2} \rightarrow {}^2\text{H(K1)} + \text{E2} + {}^2\text{H(K4)} + \text{n} + \text{E3} \rightarrow {}^{4m}\text{He(K5)} + \text{n(K6)} \rightarrow {}^4\text{He(K7)} + \text{n(K6)},$$

where E1 is the external energy required for ^{2}H and ^{3}H to overcome the Coulomb barrier. K1 and K2 are the kinetic energies gained by ^{2}H and ^{3}H during this process. K3 is the kinetic energy passed from ^{3}H to ^{3m}H, while E2 is the energy released when a bond in ^{3}H breaks due to some of E1. K4 is the kinetic energy transferred from ^{3m}H to the second ^{2}H, and E3 is the energy released from breaking a bond in ^{3m}H. K5 is the kinetic energy inherited by ^{4m}He from both ^{2}H, K6 is the neutron's kinetic energy derived from E2, E3, and partly K3, and K7 is the kinetic energy ^{4}He inherits from ^{4m}He.

The kinetic energies K6 (14.1 MeV) and K7 (3.5 MeV) of the final particles originate from the external energy E1 and the energy E2 and E3 released during the fission of ^{3}H and ^{3m}H, not from nuclear fuel mass deficits.

As shown in Fig. 14, the mass loss of nuclear materials results from added binding energy, sourced entirely from environmental gluons. The D-T reaction theoretically involves both fission and fusion: fusion consumes energy, while fission releases it. In practice, the overall reaction is exothermic only if the energy from fission exceeds that consumed by fusion.

Similarly, the following fusion reactions involve both fission and fusion processes, with the release of binding energy primarily resulting from the fission steps:

$$^3\text{He} + {}^3\text{He} \rightarrow {}^4\text{He} + 2\text{p},$$

$$^2\text{He} + {}^3\text{He} \rightarrow {}^4\text{He} + \text{p},$$

$$p + {}^{11}B \rightarrow 3{}^{4}He.$$

Fusion-only processes, such as those below, theoretically do not release binding energy:

$${}^{2m}H + {}^{2m}H \rightarrow {}^{4}He,$$

$${}^{3m}H + {}^{3m}He \rightarrow {}^{6}Li.$$

More observations and discussions about fusion

If fusion doesn't produce net energy, what stellar reactions generate such immense energy? In a star's early development, its growing mass led to contraction (*219*), converting gravitational energy into particle kinetic energy in the core. This raised core density and temperature enough to trigger gluon fission, releasing photons, neutrinos, and binding energy. This energy started fusion, while photons and neutrinos contributed to decay processes in the hot plasma.

Fission of various gluons can result in the release of different types of neutrinos in distinct regions of a star. The heavier g_μ and g_τ may undergo breakup at lower temperatures and densities, whereas g_e is more likely to break apart under higher temperature and density. The neutrinos produced in these processes may interact with remaining gluons, potentially resulting in flavour transitions similar to those observed in neutrino oscillations and the MSW effect (*220*).

The lack of net energy from fusion-only reactions may explain why commercial fusion has remained elusive for over sixty years. Recently, Lawrence Livermore National Laboratory (LLNL) achieved a burning plasma with its best fusion-to-laser energy ratio (1.5) (*221*). However, some of this output could be attributed to gluon fission at extreme temperatures and pressures from multiple laser impacts, resembling the H-bomb process.

Tokamak reactors, such as ITER, may struggle to achieve break-even fusion because their toroidal magnetic confinement design could hinder fusion initiation. NPM suggests that stronger magnetic fields make it harder for isotopes to fuse, as nucleon alignment prevents binding.

11.6 Misconceptions in Nucleosynthesis

Numerous misconceptions in nucleosynthesis arise from incomplete understanding of nuclear internal structures and the forces responsible for nuclear binding.

In NPM, protons can more readily convert to neutrons by capturing electrons, especially in high-temperature, high-density plasma. As a result, neutron and proton abundances are similar during events like star formation, core-collapse, and mergers. Since nuclei experience less Coulomb repulsion when capturing neutrons than protons, neutron capture is generally more frequent than proton capture throughout all nucleosynthesis stages—not just in the r-process and s-process.

About p-p chain

The proton-proton chain (p-p chain) is one of two established sets of solar fusion reactions that convert hydrogen into helium; the other is the CNO cycle. The p-p chain includes four branches, and current theoretical models do not incorporate neutron capture in any branch of this process.

1. pp-I branch

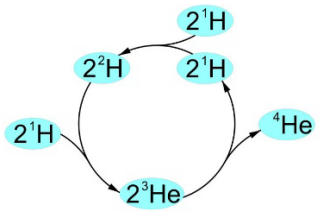

Fig.15 pp-I branch. ^{1}H is converted to ^{2}H, then to ^{3}He and finally to ^{4}He by proton capture.

In SSM theory, the pp-I branch initiates three processes, as depicted in Fig.15:

$$p + p \rightarrow {}^{2}H + e^{+} + \nu e\ ,$$

$$^{2}H + p \rightarrow {}^{3}He + \gamma,$$

$$^{3}He + {}^{3}He \rightarrow {}^{4}He + 2p.$$

The initial pp reaction underlies all branches of the pp-chain. However, it relies on two rare events—pp fusion and β^{+} decay—occurring simultaneously, which is statistically highly unlikely.

According to the SSM, roughly 91% of solar neutrinos come from pp fusion, but this process is extremely slow—only one proton undergoes the reaction every 10 billion years (*222*). As a result, pp fusion remains hypothetical and has never been observed in laboratories.

Producing ^{2}H (deuteron) via neutron capture is likely easier and faster than proton capture in the solar core's neutron-rich environment:

$$p + n \rightarrow {}^{2}H.$$

Similarly, as another reaction that generates ^{2}H, the pep process might occur more frequently in NPM than is indicated by the SSM theory:

$$p + e + p \rightarrow {}^{2}H.$$

In the hot, dense cores of solar systems, the D-D reaction ($^{2}H + {}^{2}H \rightarrow {}^{4m}He \rightarrow {}^{4}He$) also contributes to ^{4}He production.

2. pp-II branch

In SSM, these reactions occur in the pp-II branch:

$$^{3}He + {}^{4}He \rightarrow {}^{7}Be + \gamma,$$

$$^{7}Be + e \rightarrow {}^{7}Li + \nu e,$$

$^{7}Li + p \rightarrow 2^{4}He.$

In NPM, it is more accurate to describe the initial process as follows:

$^{3}He + {}^{4m}He \rightarrow {}^{7}Be + \gamma,$

Since ^{7}Li (Fig. 20e) is a stable isotope without a growing end in its nucleus, the process $^{7}Li + p \rightarrow 2^{4}He$ is likely very rare. A more probable pathway for transmuting ^{7}Be to ^{4}He involves a different set of reactions:

$^{7}Be + n \rightarrow {}^{8m}Be \rightarrow 2^{4m}He \rightarrow 2^{4}He.$

Neutron capture, as a competing process to ^{7}Be electron capture, may help address the lithium depletion problem by reducing ^{7}Li production (223).

3. pp-III branch

According to current theories, the pp-III branch consists of four reactions:

$^{3}He + {}^{4}He \rightarrow {}^{7}Be + \gamma,$

$^{7}Be + p \rightarrow {}^{8}B + \gamma,$

$^{8}B \rightarrow {}^{8}Be + e^{+} + \nu e,$

$^{8}Be \rightarrow 2^{4}He.$

Similarly, the probability of neutron capture of ^{7}Be must be higher than the probability of p capture of ^{7}Be, thus the production of ^{8}B in nature could be lower than expected by current theory.

4. pp-IV (hep) branch

According to current theories, the pp-IV branch consists of a single reaction:

$^{3}He + p \rightarrow {}^{4}He + e^{+} + \nu e.$

This process, like $p + p \rightarrow {}^{2}H + e^{+} + \nu e$, is highly unlikely because it requires both fusion and β^{+} decay to occur simultaneously. A more plausible alternative involves the following set of processes:

$^{3m}He + n \rightarrow {}^{4m}He \rightarrow {}^{4}He.$

About CNO cycle

As shown in Fig.16, the CNO Cycle consists of four proton-capture fusion reactions and two β^{+} decay reactions in a continuous loop.

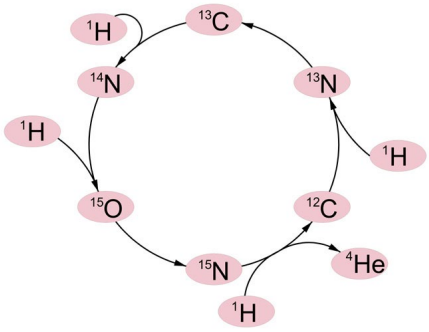

Fig.16|The CNO cycle consists of four proton-capture fusion reactions and two β^{+} decays.

It is assumed that the neutron abundance in the plasma at the core of the solar system is comparable to that of protons. Given that neutrons are more readily captured by positively charged nuclei than protons, it is therefore necessary to consider the following neutron capture processes within the CNO cycle:

$$^{12m}C + n \rightarrow {}^{13}C,\ {}^{13}N + n \rightarrow {}^{14}N,\ {}^{14}N + n \rightarrow {}^{15}N.$$

About alpha process

The alpha process, occurring in massive stars or supernovae, involves fusing helium to form heavier elements. The triple-alpha process, which creates carbon from three helium nuclei, is a specific example. All nuclides in this process have equal numbers of protons and neutrons, with atomic numbers that are multiples of 4 (see Fig. 17).

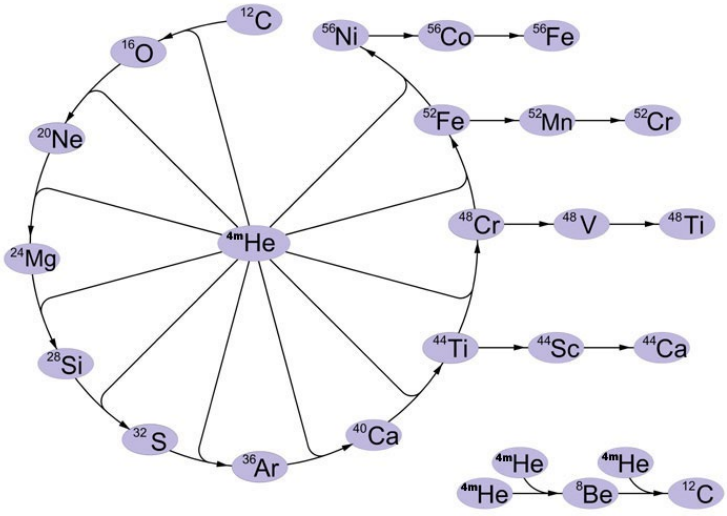

Fig.17|**Alpha-process:** all participating nuclides possess an equal number of protons and neutrons, with their atomic numbers being multiples of four.

In NPM, the alpha process involves ^{4m}He capture. Figures 23 and 13 show that ^{12}C, ^{16}O and ^{20}Ne all have a ^{4m}He at the growing end, making them suitable for alpha capture. Other nuclides, such as ^{10}B, ^{13}C, ^{14}C, ^{16}N and ^{20}C, lack the ^{4m}He at their nucleus growth end and therefore do not bond effectively with an additional ^{4m}He. We predict that all other nuclides involved in the alpha-process possess the ^{4m}He at their growing end.

It can also be inferred that the significant output from triple-alpha processes greatly limited the natural formation of the light element lithium, beryllium, and boron, which are positioned between helium and carbon in the periodic table.

11.7 Solar and Galaxy Abundance Problem

Solar abundance problem

The solar abundance problem refers to the difference between low-metallicity solar models and helioseismic measurements of the solar interior. This issue has been the subject of ongoing research and publications since approximately 2004 (*224-228*).

A recent study (*229*) attempted to match solar surface lithium levels in high-metallicity models using macroscopic transport. The updated models, however, conflict with helioseismic and neutrino data, indicating that the solar abundance problem involves both composition and complex physics.

Simple NPM answers

As introduced in Sec. 11.6, standard nucleosynthesis models (including SSMs) typically overlook neutron capture reactions in the pp-chain and CNO cycle while underestimating the triple-alpha process. Incorporating these processes could boost metal element production and lower lithium generation, leading to higher metallicity and improved alignment with observed solar lithium abundance. Additionally, accounting for neutrinos from gluon fission may help SSMs match measured neutrino fluxes.

Increased neutron capture and triple-alpha processes in nucleosynthesis may accelerate the evolution of the universe and sun beyond what BBN and SSM predict, as supported by recent observations.

The faint young Sun problem (*230*, *231*) refers to the paradox of early Earth having liquid water and life despite the Sun being expected to be dimmer at that time. While explanations such as cloud feedback (*232*) and solar mass loss (*233*) have been proposed, a simpler solution may be that the early Sun was brighter due to faster nucleosynthesis.

Recent JWST observations reveal ultra-massive, mature galaxies at redshifts $z >\sim 6$ (*234*) and at $z \sim 5.2$ (*235*) just 1 billion years after the Big Bang, with early galaxy oxygen detection as well (*236*). These findings are earlier and heavier than predicted by ΛCDM. In contrast, NPM suggests rapid nucleosynthesis, warm dark matter (gluons) interacting with normal matter, and

the absence of dark matter annihilation, enabling more massive galaxy formation and more rapid evolution early in the universe's history.

12. Conclusion and Outlook

The Standard Model (SM) describes fundamental particles and forces with high statistical accuracy over various sectors, but does not address phenomena like dark energy, dark matter, the lack of antimatter, neutrino oscillations and gravity. It also shows discrepancies with experimental results in various areas.

This paper presents a new particle model (NPM) that reveals internal structures and compositions of fundamental particles. It systematically addresses major issues in the SM concerning bosons, leptons, quarks, hadrons, and nuclides within both particle physics and astrophysics, while offering testable predictions.

NPM offers novel interpretations of weak and strong interactions, proposes empirical mechanisms for mass generation, beta decay, meson oscillation, and neutrino oscillation. It also uncovers isotope binding structures ranging from ^{2}H to ^{22}C, explaining diverse nuclear behaviors and offering predictions of new isotope states.

This paper offers qualitative solutions across various sectors as a foundation for future quantitative work. Based on the NPM framework, further research could include new interpretations of quantum phenomena, new cosmology models, exploration of fundamental force relationships, new space-time theory, unification of quantum theories with general relativity, and study of nuclear structures in isotopes beyond ^{22}C.

Acknowledgements

This manuscript presents the results of several years of independent research. The author acknowledges the contributions of scientists in the field, especially the physicists whose referenced works support this study.

Appendix 1 Nuclear Structures of Isotopes from ^{2}H to ^{22}C

Using assumed nuclear force types, structural models, and behavioral rules, we deduced and diagrammed the structures of isotopes from ^{2}H to ^{22}C (see Fig.18–23), laying groundwork for future study of other isotopes. Note: For clarity, dashed lines and dimmed colors indicate bindings or particles at the back.

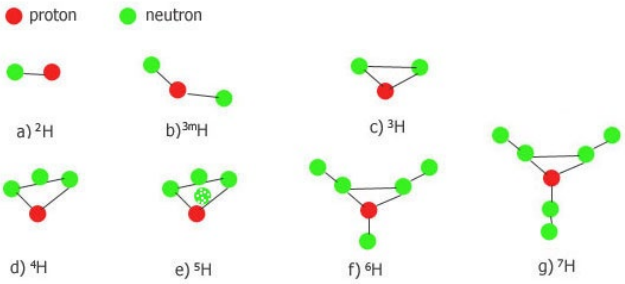

Fig.18. Binding structures of H isotopes.

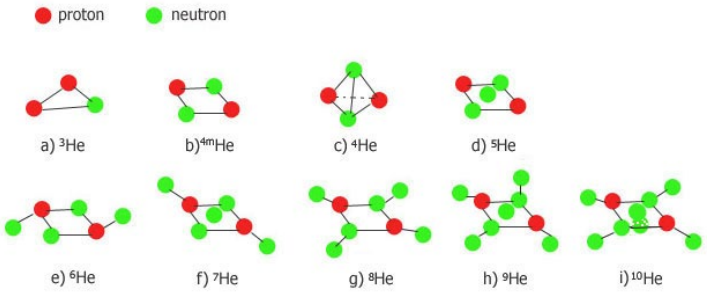

Fig.19. Binding structures of He isotopes.

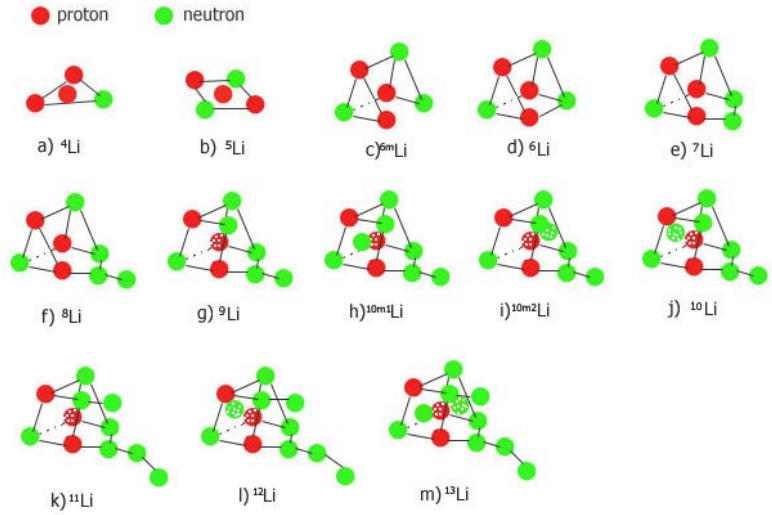

Fig.20. Binding structures of Li isotopes.

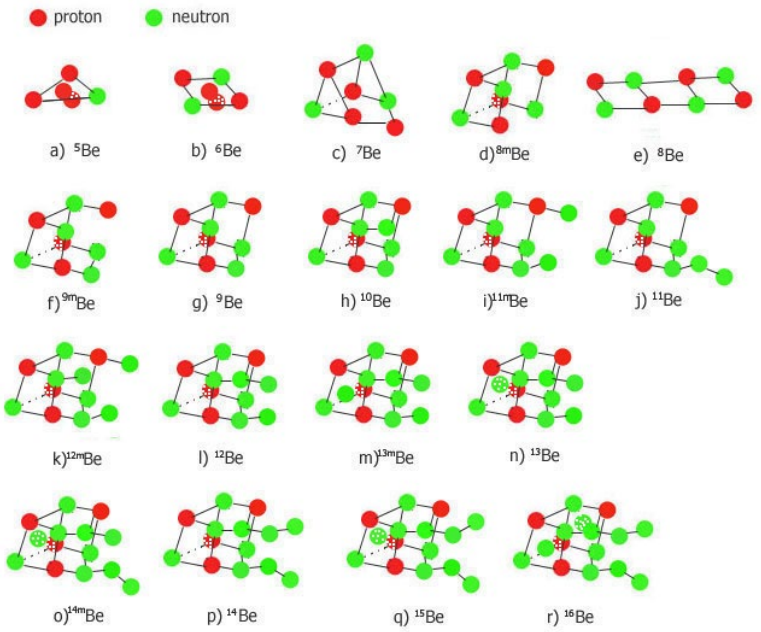

Fig.21. Binding structures of Be isotopes.

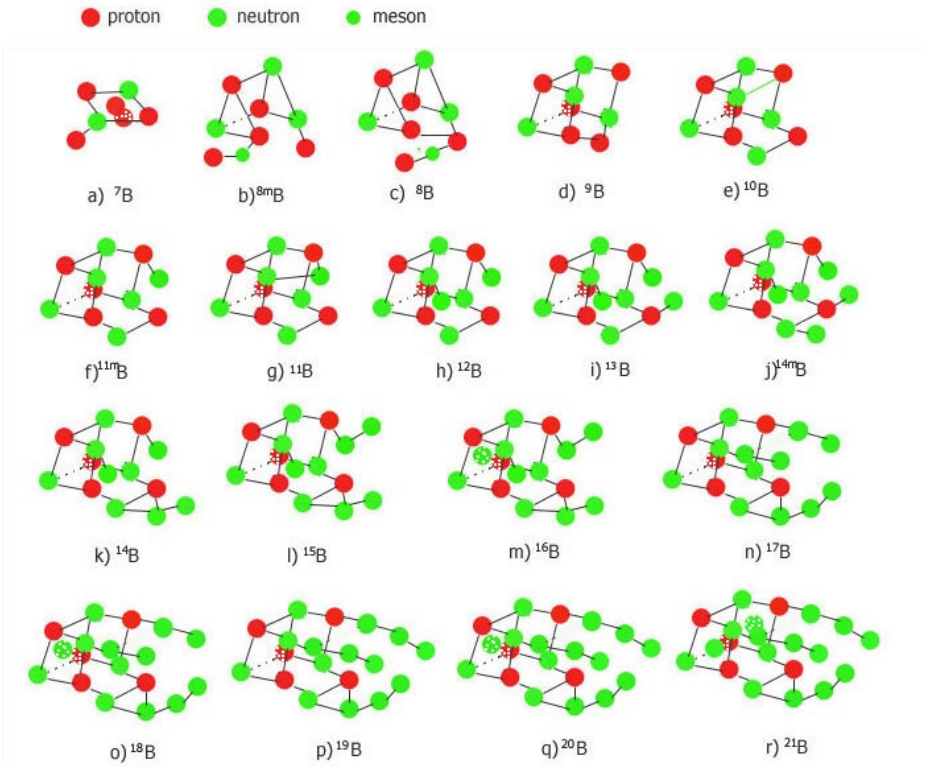

Fig.22. Binding structures of B isotopes.

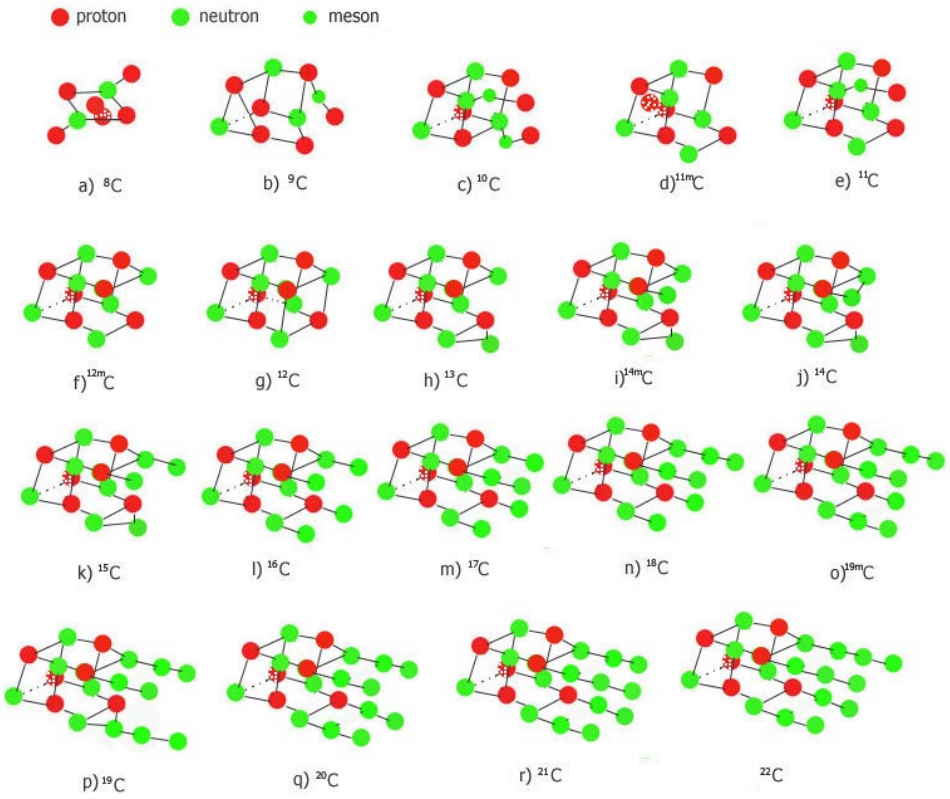

Fig.23. Binding structures of C isotopes

References

1. A. Djouadi, J.-L. Kneur, G. Moultaka, SuSpect: A Fortran code for the supersymmetric and Higgs particle spectrum in the MSSM. *Computer Physics Communications* **176**, 426–455 (2007).
2. C. Froggatt*, H. Nielsen, Trying to understand the Standard Model parameters. *Surveys in High Energy Physics* **18**, 55–75 (2003).
3. G. D. Orebi Gann, K. Zuber, D. Bemmerer, A. Serenelli, The future of solar neutrinos. *Annual Review of Nuclear and Particle Science* **71**, 491–528 (2021).
4. M. Kuster, G. Raffelt, B. Beltrán, *Axions: Theory, cosmology, and experimental searches*. (Springer Science & Business Media, 2007), vol. 741.
5. R. Aaij *et al.*, Observation of New Resonances Decaying to J/ψ K+ and J/ψ ϕ. *Physical Review Letters* **127**, 082001 (2021).
6. L. Collaboration, Observation of structure in the J/ψ-pair mass spectrum. *Science bulletin* **65**, 1983–1993 (2020).
7. I. Belov, A. Giachino, E. Santopinto, Fully charmed tetraquark production at the LHC experiments. *Journal of High Energy Physics* **2025**, 1–29 (2025).
8. C. Abel *et al.*, in *EPJ Web of Conferences*. (EDP Sciences, 2019), vol. 219, pp. 02001.
9. C. Abel *et al.*, Measurement of the permanent electric dipole moment of the neutron. *Physical Review Letters* **124**, 081803 (2020).

10. F. Giacosa, M. Gorenstein, R. Poberezhniuk, S. Samanta, Evidence of isospin-symmetry violation in high-energy collisions of atomic nuclei. *Nature Communications* **16**, 2849 (2025).
11. P. A. M. Dirac, The quantum theory of the electron. Part II. *Proceedings of the royal society of London. Series A, Containing papers of a mathematical and physical character* **118**, 351–361 (1928).
12. R. Penrose, *The road to reality*. Chapter 25.2 (Random house, 2006).
13. H. C. Ohanian, What is spin. *Am. J. Phys* **54**, 500–505 (1986).
14. B. Friedrich, D. Herschbach, Stern and Gerlach: How a bad cigar helped reorient atomic physics. *Physics Today* **56**, 53–59 (2003).
15. D. Castelvecchi, The stern–Gerlach experiment at 100. *Nature Reviews Physics* **4**, 140–142 (2022).
16. L. Kopf, R. Barros, S. Prabhakar, E. Giese, R. Fickler, Conservation of angular momentum on a single-photon level. *Physical Review Letters* **134**, 203601 (2025).
17. C. T. Sebens, How electrons spin. *Studies in History and Philosophy of Science Part B: Studies in History and Philosophy of Modern Physics* **68**, 40–50 (2019).
18. J. Ashman *et al.*, A measurement of the spin asymmetry and determination of the structure function g1 in deep inelastic muon-proton scattering. *Physics Letters B* **206**, 364–370 (1988).
19. R. L. Jaffe, Where does the proton really get its spin? *Physics today* **48**, 24–33 (1995).
20. A. W. Thomas, Interplay of spin and orbital angular momentum in the proton. *Physical review letters* **101**, 102003 (2008).
21. J. Hansson, The" Proton Spin Crisis"-a Quantum Query. *Progress in Physics* **3**, 51–52 (2010).
22. X. Ji, F. Yuan, Y. Zhao, Proton spin after 30 years: what we know and what we don't? *arXiv preprint arXiv:2009.01291*, (2020).
23. X. Ji, J.-H. Zhang, Y. Zhao, Physics of the gluon-helicity contribution to proton spin. *Physical Review Letters* **111**, 112002 (2013).
24. X. Ji, Proton tomography through deeply virtual Compton scattering. *National Science Review* **4**, 213–223 (2017).
25. S. D. Bass, Spinning gluons in the proton. *Physics* **10**, 23 (2017).
26. A. Deur, S. J. Brodsky, G. F. De Téramond, The spin structure of the nucleon. *Reports on Progress in Physics* **82**, 076201 (2019).
27. K.-F. Liu, Status on lattice calculations of the proton spin decomposition. *AAPPS Bulletin* **32**, 8 (2022).
28. I. Newton. (New York (London: Benjamin Motte, 1729), 1846).
29. C. Amsler, P. D. Group, partial update for the 2010 edition. *Cut-off date for this update was January* **15**, 2009 (2009).
30. F. Dyson, A. Eddington, C. Davidson, A Determination of the Deflection of Light by the Sun's Gravitational Field, from Observations made at the Total Eclipse of May 29, 1919. *Memoirs of the Royal Astronomical Society, Vol. 62, p. A1* **62**, A1 (1923).
31. G. Bernardi, M. Carena, T. Junk, Higgs bosons: theory and searches. *Reviews of Particle Data Group: Hypothetical particles and Concepts*, 10–11 (2007).
32. G. S. Guralnik, C. R. Hagen, T. W. Kibble, Global conservation laws and massless particles. *Physical Review Letters* **13**, 585 (1964).
33. P. D. Mannheim, Colloquium on the Higgs Boson. *arXiv preprint arXiv:1506.04120*, (2015).
34. M. Suzuki, The magnetic moment of W and the scale of composite weak bosons. *Physics Letters B* **153**, 289–293 (1985).
35. A. Collaboration, Observation of a new particle in the search for the Standard Model Higgs boson with the ATLAS detector at the LHC. *arXiv preprint arXiv:1207.7214*, (2012).
36. C. Collaboration, Observation of the Higgs boson decay to a pair of tau leptons with the CMS detector. *arXiv preprint arXiv:1708.00373*, (2017).
37. D. K. Hong, S. D. Hsu, F. Sannino, Composite Higgs from higher representations. *Physics Letters B* **597**, 89–93 (2004).

38. F. Wilczek, *The Lightness of Being*. Chapter 2 (Basic Book, 2008).
39. R. J. Adler, B. Casey, O. C. Jacob, Vacuum catastrophe: An elementary exposition of the cosmological constant problem. *American Journal of Physics* **63**, 620–626 (1995).
40. G. R. Bengochea, G. León, E. Okon, D. Sudarsky, Can the quantum vacuum fluctuations really solve the cosmological constant problem? *The European Physical Journal C* **80**, 1–12 (2020).
41. S. Navas *et al.*, Review of particle physics. *Physical Review D* **110**, 030001 (2024).
42. CODATA, in *Fundamental Physical Constants*. (2022).
43. CODATA, in *Fundamental Physical Constants*. (2022).
44. CODATA, in *Fundamental Physical Constants*. (2022).
45. H.-n. Li, Dispersive constraints on fermion masses. *Physical Review D* **107**, 094007 (2023).
46. R. Crewther, Quarks and anomalies. *International Journal of Modern Physics A* **30**, 1530012 (2015).
47. M.-Y. Han, Y. Nambu, Three-triplet model with double SU(3) symmetry. *Physical Review* **139**, B1006 (1965).
48. R. L. Thews, M. Schroedter, J. Rafelski, Enhanced J/ψ production in deconfined quark matter. *Physical Review C* **63**, 054905 (2001).
49. M. Schroedter, R. L. Thews, J. Rafelski, Bc-meson production in ultrarelativistic nuclear collisions. *Physical Review C* **62**, 024905 (2000).
50. H. Fuke *et al.*, Search for fractionally charged particles in cosmic rays with the BESS spectrometer. *Advances in Space Research* **41**, 2050–2055 (2008).
51. F. Alemanno *et al.*, Search for relativistic fractionally charged particles in space. *Physical Review D* **106**, 063026 (2022).
52. D. Adams *et al.*, Search for fractionally charged particles with CUORE. *Physical Review Letters* **133**, 241801 (2024).
53. J. Dove *et al.*, The asymmetry of antimatter in the proton. *Nature* **590**, 561–565 (2021).
54. B. Abi *et al.*, Measurement of the positive muon anomalous magnetic moment to 0.46 ppm. *Physical Review Letters* **126**, 141801 (2021).
55. J. Schwinger, On quantum-electrodynamics and the magnetic moment of the electron. *Physical Review* **73**, 416 (1948).
56. T. Aoyama *et al.*, The anomalous magnetic moment of the muon in the Standard Model. *Physics reports* **887**, 1–166 (2020).
57. M. Davier, A. Hoecker, B. Malaescu, Z. Zhang, Reevaluation of the hadronic vacuum polarisation contributions to the Standard Model predictions of the muon g-2 and α(mZ2) using newest hadronic cross-section data. *The European Physical Journal C* **77**, 1–12 (2017).
58. A. Kurz, T. Liu, P. Marquard, M. Steinhauser, Hadronic contribution to the muon anomalous magnetic moment to next-to-next-to-leading order. *Physics Letters B* **734**, 144–147 (2014).
59. K. Melnikov, A. Vainshtein, Hadronic light-by-light scattering contribution to the muon anomalous magnetic moment reexamined. *Physical Review D—Particles, Fields, Gravitation, and Cosmology* **70**, 113006 (2004).
60. G. Colangelo, M. Hoferichter, A. Nyffeler, M. Passera, P. Stoffer, Remarks on higher-order hadronic corrections to the muon g−2. *Physics Letters B* **735**, 90–91 (2014).
61. R. Jackiw, S. Weinberg, Weak-interaction corrections to the muon magnetic moment and to muonic-atom energy levels. *Physical Review D* **5**, 2396 (1972).
62. C. Gnendiger, D. Stöckinger, H. Stöckinger-Kim, The electroweak contributions to (g - 2) μ after the Higgs-boson mass measurement. *Physical Review D—Particles, Fields, Gravitation, and Cosmology* **88**, 053005 (2013).
63. R. Aliberti *et al.*, The anomalous magnetic moment of the muon in the Standard Model: an update. *Physics Reports* **1143**, 1–158 (2025).
64. M. Davier, A. Hoecker, B. Malaescu, Z. Zhang, A new evaluation of the hadronic vacuum polarisation contributions to the muon anomalous magnetic moment and to α (m Z 2). *The European Physical Journal C* **80**, 241 (2020).

65. E. S. Fraga, L. F. Palhares, C. Villavicencio, Quark anomalous magnetic moment in an extreme magnetic background from perturbative QCD. *Physical Review D* **109**, 116018 (2024).
66. P. J. d. A. Bicudo, J. E. F. Ribeiro, R. Fernandes, Anomalous magnetic moment of quarks. *Physical Review C* **59**, 1107 (1999).
67. J. Mei, S. Mao, Inverse catalysis effect of the quark anomalous magnetic moment to chiral restoration and deconfinement phase transitions. *Physical Review D* **102**, 114035 (2020).
68. V. Gusynin, V. Miransky, I. Shovkovy, Dimensional reduction and catalysis of dynamical symmetry breaking by a magnetic field. *Nuclear Physics B* **462**, 249–290 (1996).
69. D. E. Kharzeev, H. Warringa, The Chiral magnetic effect. *Phys. Rev. D* **78**, 074033 (2008).
70. D. Collaboration, Measurement of the Electric Charge of the Top Quark in $t\bar{t}$ Events. *arXiv preprint arXiv:1407.4837*, (2014).
71. T. M. Liss, P. L. Tipton, The discovery of the top quark. *Scientific American* **277**, 54–59 (1997).
72. C. Amsler, T. DeGrand, B. Krusche, Quark model. *Physics Letters B* **667**, 172–191 (2008).
73. J. Lan, C. Mondal, X. Zhao, T. Frederico, J. P. Vary, Gluonic contributions to the pion parton distribution functions. *Physical Review D* **111**, L111903 (2025).
74. J. Greensite, *An introduction to the confinement problem*. (Springer, 2011), vol. 821.
75. L. P. Fulcher, J. Rafelski, R. L. Thews, in *Heavy Ion Physics From Bevalac To Rhic-Proceedings Of The Relativistic Heavy Ion Symposium, Aps Centennial Meeting'99*. (World Scientific, 1999), pp. 156.
76. M. Lüscher, Chiral gauge theories revisited. *Subnucl. Ser* **38**, 41 (2002).
77. A. Dynin, On the Yang-Mills mass gap problem. *Russian Journal of Mathematical Physics* **21**, 326–328 (2014).
78. L. Del Debbio, L. Giusti, C. Pica, Topological susceptibility in su(3) gauge theory. *Physical review letters* **94**, 032003 (2005).
79. S. C. Ting, The discovery of the J particle: A personal recollection. *Reviews of Modern Physics* **49**, 235 (1977).
80. J. Mrazkova, Review on recent results of J/ψ production at STAR. *arXiv preprint arXiv:2507.23516*, (2025).
81. Q.-M. Feng, C.-F. Qiao, J/ψ Polarization and pT distribution in $c\bar{c}$ associated hadroproduction at O(α5 s). *arXiv preprint arXiv:2507.20654*, (2025).
82. L. Valencia Palomo, J/ψ and Υ (1S) production in jets at LHC energies. *The European Physical Journal Plus* **140**, 544 (2025).
83. R. Dalitz, Decay of τ mesons of known charge. *Physical review* **94**, 1046 (1954).
84. R. Dalitz, in *AIP Conference Proceedings*. (American Institute of Physics, 1994), vol. 300, pp. 141–158.
85. S. Okubo, φ-meson and unitary symmetry model. *Physics Letters* **5**, 165–168 (1963).
86. J. Iizuka, A systematics and phenomenology of meson family. *Progress of Theoretical Physics Supplement* **37**, 21–34 (1966).
87. G. Corcella, The top-quark mass: challenges in definition and determination. *Frontiers in Physics* **7**, 54 (2019).
88. C. collaboration, Review of top quark mass measurements in CMS. *Physics Reports*, (2025).
89. R. Aaij *et al.*, First evidence for direct CP violation in beauty to charmonium decays. *Physical review letters* **134**, 101801 (2025).
90. M. Liebendörfer, Fifty-Nine Reasons for a Supernova to not Explode. *arXiv preprint astro-ph/0405029*, (2004).
91. T. Foglizzo *et al.*, The explosion mechanism of core-collapse supernovae: progress in supernova theory and experiments. *Publications of the Astronomical Society of Australia* **32**, e009 (2015).
92. Y. Suwa, N. Tominaga, K. Maeda, Importance of 56Ni production on diagnosing explosion mechanism of core-collapse supernova. *Monthly Notices of the Royal Astronomical Society* **483**, 3607–3617 (2019).
93. A. Burrows, D. Vartanyan, Core-collapse supernova explosion theory. *Nature* **589**, 29–39 (2021).

94. R. Sawada, Y. Suwa, A consistent modeling of neutrino-driven wind with accretion flow onto a protoneutron star and its implications for 56ni production. *The Astrophysical Journal* **908**, 6 (2021).
95. H. M. Van Horn, The physics of white dwarfs. *Physics Today* **32**, 23–32 (1979).
96. S. Cheng, J. D. Cummings, B. Ménard, A cooling anomaly of high-mass white dwarfs. *The Astrophysical Journal* **886**, 100 (2019).
97. A. Bédard, S. Blouin, S. Cheng, Buoyant crystals halt the cooling of white dwarf stars. *Nature* **627**, 286–288 (2024).
98. R. A. Gustafson, R. Plestid, I. M. Shoemaker, Neutrino portals, terrestrial upscattering, and atmospheric neutrinos. *Physical Review D* **106**, 095037 (2022).
99. X. Geng *et al.*, Search for exotic interactions of solar neutrinos in the CDEX-10 experiment. *Physical Review D* **107**, 112002 (2023).
100. G. Vasquez, J. Zamora-Saa, Unveiling the heavy neutrino nature at LHCb. *Physical Review D* **108**, 053008 (2023).
101. K. Babu, V. Brdar, A. De Gouvea, P. A. Machado, Addressing the short-baseline neutrino anomalies with energy-dependent mixing parameters. *Physical Review D* **107**, 015017 (2023).
102. G. Baym, J.-C. Peng, Evolution of Primordial Neutrino Helicities in Astrophysical Magnetic Fields and Implications for Their Detection. *Physical review letters* **126**, 191803 (2021).
103. Observation of an ultra-high-energy cosmic neutrino with KM3NeT. *Nature* **638**, 376–382 (2025).
104. M. Czakon, J. Gluza, M. Zralek, Nonunitary neutrino mixing matrix and CP violating neutrino oscillations. *arXiv preprint hep-ph/0109245*, (2001).
105. S. Goswami, T. Ota, Testing nonunitarity of neutrino mixing matrices at neutrino factories. *Physical Review D—Particles, Fields, Gravitation, and Cosmology* **78**, 033012 (2008).
106. C. Lunardini, A. Y. Smirnov, Neutrinos from SN 1987A, Earth matter effects, and the large mixing angle solution of the solar neutrino problem. *Physical Review D* **63**, 073009 (2001).
107. S. S. McGaugh, A tale of two paradigms: the mutual incommensurability of ΛCDM and MOND. *Canadian Journal of Physics* **93**, 250–259 (2015).
108. A. O. Hodson, H. Zhao, Generalizing MOND to explain the missing mass in galaxy clusters. *Astronomy & Astrophysics* **598**, A127 (2017).
109. C. Collaboration†‡ *et al.*, High-precision measurement of the W boson mass with the CDF II detector. *Science* **376**, 170–176 (2022).
110. Measurement of the W-boson mass and width with the ATLAS detector using proton–proton collisions at s= 7 TeV. *The European Physical Journal C* **84**, 1309 (2024).
111. C. collaboration, High-precision measurement of the W boson mass with the CMS experiment at the LHC. *arXiv preprint arXiv:2412.13872*, (2024).
112. A. collaboration, D. Collaboration, L. Collaboration, O. collaboration, L. E. W. Group, Electroweak measurements in electron–positron collisions at W-boson-pair energies at LEP. *Physics reports* **532**, 119–244 (2013).
113. V. M. Abazov *et al.*, Measurement of the W Boson Mass with the D0 Detector. *Physical review letters* **108**, 151804 (2012).
114. R. Aaij *et al.*, Measurement of the W boson mass. *Journal of High Energy Physics* **2022**, 1–38 (2022).
115. S. Silaeva, V. Sinev, Test of beta and antineutrino spectra symmetry in beta-decay. *arXiv preprint arXiv:2102.12991*, (2021).
116. D. Cundy, "Neutrino Physics," *17th International Conference on High-energy Physics* (London, UK, 1974).
117. J. Park *et al.*, Measurement of neutrino flux from neutrino-electron elastic scattering. *Physical Review D* **93**, 112007 (2016).
118. L. Aliaga *et al.*, Neutrino flux predictions for the NuMI beam. *Physical Review D* **94**, 092005 (2016).

119. E. Valencia *et al.*, Constraint of the MINER ν A medium energy neutrino flux using neutrino-electron elastic scattering. *Physical Review D* **100**, 092001 (2019).
120. L. Zazueta *et al.*, Improved constraint on the MINER ν A medium energy neutrino flux using ν^{-} e-→ ν^{-} e-data. *Physical Review D* **107**, 012001 (2023).
121. D. Akimov *et al.*, The COHERENT experimental program. *arXiv preprint arXiv:2204.04575*, (2022).
122. J. Colaresi, J. Collar, T. Hossbach, C. Lewis, K. Yocum, Measurement of coherent elastic neutrino-nucleus scattering from reactor antineutrinos. *Physical Review Letters* **129**, 211802 (2022).
123. M. I. Smoliar, R. J. Walker, J. W. Morgan, Re-Os ages of group IIA, IIIA, IVA, and IVB iron meteorites. *Science* **271**, 1099–1102 (1996).
124. A. Kelić, N. Zinner, E. Kolbe, K. Langanke, K.-H. Schmidt, Cross sections and fragment distributions from neutrino-induced fission on r-process nuclei. *Physics Letters B* **616**, 48–58 (2005).
125. A. Barabash, Experiment double beta decay: Historical review of 75 years of research. *Physics of Atomic Nuclei* **74**, 603–613 (2011).
126. S. Bilenky, Neutrinoless double beta-decay. *Physics of Particles and Nuclei* **41**, 690–715 (2010).
127. F. E. Wietfeldt, Measurements of the neutron lifetime. *Atoms* **6**, 70 (2018).
128. R. Musedinovic *et al.*, Measurement of the free neutron lifetime in a magneto-gravitational trap with in situ detection. *Physical Review C* **111**, 045501 (2025).
129. C.-S. Wu, E. Ambler, R. W. Hayward, D. D. Hoppes, R. P. Hudson, Experimental test of parity conservation in beta decay. *Physical review* **105**, 1413 (1957).
130. J. Baez, J. Huerta, The algebra of grand unified theories. *Bulletin of the American Mathematical Society* **47**, 483–552 (2010).
131. A. Oralbaev, M. Skorokhvatov, O. Titov, in *Journal of Physics: Conference Series*. (IOP Publishing, 2016), vol. 675, pp. 012003.
132. F. Reines, C. Cowan Jr, Detection of the free neutrino. *Physical Review* **92**, 830 (1953).
133. E. M. Hussein, *Radiation mechanics: Principles and practice*. (Elsevier, 2010).
134. J. N. Bahcall, *Neutrino astrophysics*. (Cambridge University Press, 1989).
135. P. A. Sturrock, Neutrino-flux variability, nuclear-decay variability, and their apparent relationship. *Space Science Reviews* **218**, 23 (2022).
136. S. Pommé, K. Pelczar, Neutrino-induced decay: a critical review of the arguments. *Space Science Reviews* **218**, 64 (2022).
137. E. D. Falkenberg, Radioactive decay caused by neutrinos. *Apeiron* **8**, 32–45 (2001).
138. M. Agostini *et al.*, Seasonal modulation of the 7Be solar neutrino rate in Borexino. *Astroparticle physics* **92**, 21–29 (2017).
139. B. Aharmim *et al.*, Search for periodicities in the B 8 solar neutrino flux measured by the Sudbury Neutrino Observatory. *Physical Review D—Particles, Fields, Gravitation, and Cosmology* **72**, 052010 (2005).
140. K. Abe *et al.*, Search for Periodic Time Variations of the Solar B 8 Neutrino Flux between 1996 and 2018 in Super-Kamiokande. *Physical review letters* **132**, 241803 (2024).
141. Y. Suzuki, The Sun, neutrinos and Super-Kamiokande. *Proceedings of the Japan Academy, Series B* **96**, 204–233 (2020).
142. G. Steinitz, M. C. Martin-Luis, O. Piatibratova, Indications for solar influence on radon signal in the subsurface of Tenerife (Canary Islands, Spain). *The European Physical Journal Special Topics* **224**, 687–695 (2015).
143. G. Steinitz, P. Kotlarsky, O. Piatibratova, Observations of the relationship between directionality and decay rate of radon in a confined experiment. *The European Physical Journal Special Topics* **224**, 731–740 (2015).

144. E. Bellotti, C. Broggini, G. Di Carlo, M. Laubenstein, R. Menegazzo, Precise measurement of the 222Rn half-life: a probe to monitor the stability of radioactivity. *Physics Letters B* **743**, 526–530 (2015).
145. R. de Meijer *et al.*, First observation of a reactor-status effect on the beta+ decay rate of 22Na. *arXiv preprint arXiv:1610.01332*, (2016).
146. T. A. Mueller *et al.*, Improved predictions of reactor antineutrino spectra. *Physical Review C—Nuclear Physics* **83**, 054615 (2011).
147. P. Huber, Determination of antineutrino spectra from nuclear reactors. *Physical Review C—Nuclear Physics* **84**, 024617 (2011).
148. G. Mention *et al.*, Reactor antineutrino anomaly. *Physical Review D—Particles, Fields, Gravitation, and Cosmology* **83**, 073006 (2011).
149. K. Heeger, M. Tobin, B. Littlejohn, H. Mumm, Experimental parameters for a reactor antineutrino experiment at very short baselines. *Physical Review D—Particles, Fields, Gravitation, and Cosmology* **87**, 073008 (2013).
150. F. An *et al.*, Search for a light sterile neutrino at Daya Bay. *Physical review letters* **113**, 141802 (2014).
151. P. Vogel, L. Wen, C. Zhang, Neutrino oscillation studies with reactors. *Nature Communications* **6**, 6935 (2015).
152. H. Almazán *et al.*, Accurate Measurement of the Electron Antineutrino Yield of U 235 Fissions from the STEREO Experiment with 119 Days of Reactor-On Data. *Physical Review Letters* **125**, 201801 (2020).
153. F. An *et al.*, Evolution of the reactor antineutrino flux and spectrum at Daya Bay. *Physical review letters* **118**, 251801 (2017).
154. G. Bak *et al.*, Fuel-composition dependent reactor antineutrino yield at RENO. *Physical Review Letters* **122**, 232501 (2019).
155. D. Adey *et al.*, Extraction of the U 235 and Pu 239 antineutrino spectra at Daya Bay. *Physical review letters* **123**, 111801 (2019).
156. J. Choi *et al.*, Observation of energy and baseline dependent reactor antineutrino disappearance in the RENO experiment. *Physical review letters* **116**, 211801 (2016).
157. F. P. An *et al.*, Measurement of the reactor antineutrino flux and spectrum at Daya Bay. *Physical review letters* **116**, 061801 (2016).
158. Y. Abe *et al.*, Improved measurements of the neutrino mixing angle θ 13 with the Double Chooz detector. *Journal of High Energy Physics* **2014**, 1–44 (2014).
159. Y. Ko *et al.*, Sterile neutrino search at the NEOS experiment. *Physical review letters* **118**, 121802 (2017).
160. C. Zhang, X. Qian, M. Fallot, Reactor antineutrino flux and anomaly. *Progress in Particle and Nuclear Physics*, 104106 (2024).
161. Double Chooz θ 13 measurement via total neutron capture detection. *Nature Physics* **16**, 558–564 (2020).
162. M. Danilov, N. Skrobova, New results from the DANSS experiment. *arXiv preprint arXiv:2112.13413*, (2021).
163. A. Serebrov *et al.*, Search for sterile neutrinos with the Neutrino-4 experiment and measurement results. *Physical Review D* **104**, 032003 (2021).
164. H. Almazán *et al.*, First antineutrino energy spectrum from 235U fissions with the STEREO detector at ILL. *Journal of Physics G: Nuclear and Particle Physics* **48**, 075107 (2021).
165. M. Andriamirado *et al.*, Final Measurement of the U 235 Antineutrino Energy Spectrum with the PROSPECT-I Detector at HFIR. *Physical review letters* **131**, 021802 (2023).
166. G. Zacek *et al.*, Neutrino-oscillation experiments at the Gösgen nuclear power reactor. *Physical Review D* **34**, 2621 (1986).
167. V. Zacek, G. Zacek, P. Vogel, J.-L. Vuilleumier, Evidence for a 5 MeV spectral deviation in the Goesgen reactor neutrino oscillation experiment. *arXiv preprint arXiv:1807.01810*, (2018).

168. V. Kopeikin, L. Mikaelyan, V. Sinev, Spectrum of electronic reactor antineutrinos. *Physics of Atomic Nuclei* **60**, (1997).
169. V. Guadilla *et al.*, Large impact of the decay of niobium isomers on the reactor ν^{-} e summation calculations. *Physical review letters* **122**, 042502 (2019).
170. A. Abusleme *et al.*, Feasibility and physics potential of detecting 8B solar neutrinos at JUNO. *Chinese Physics C* **45**, 023004 (2021).
171. F. An *et al.*, Spectral measurement of electron antineutrino oscillation amplitude and frequency at Daya Bay. *Physical review letters* **112**, 061801 (2014).
172. C. Athanassopoulos *et al.*, Evidence for $\nu\ \mu \rightarrow \nu$ e Oscillations from the LSND Experiment at the Los Alamos Meson Physics Facility. *Physical Review Letters* **77**, 3082 (1996).
173. C. Athanassopoulos *et al.*, Results on $\nu\ \mu \rightarrow \nu$ e Neutrino Oscillations from the LSND Experiment. *Physical Review Letters* **81**, 1774 (1998).
174. A. Aguilar *et al.*, Evidence for neutrino oscillations from the observation of ν e appearance in a ν μ beam. *Physical Review D* **64**, 112007 (2001).
175. A. Aguilar-Arevalo, Event Excess in the MiniBooNE Search for $\bar{\nu}\mu \rightarrow \bar{\nu}$e Oscillations. *Physical review letters* **105**, (2010).
176. A. Aguilar-Arevalo *et al.*, Testing Meson Portal Dark Sector Solutions to the MiniBooNE Anomaly at CCM. *arXiv preprint arXiv:2309.02599*, (2023).
177. J. R. Jordan, Y. Kahn, G. Krnjaic, M. Moschella, J. Spitz, Severe constraints on new physics explanations of the MiniBooNE excess. *Physical review letters* **122**, 081801 (2019).
178. J. Asaadi, E. Church, R. Guenette, B. J. Jones, A. Szelc, New light Higgs boson and short-baseline neutrino anomalies. *Physical Review D* **97**, 075021 (2018).
179. A. Diaz, C. Argüelles, G. Collin, J. Conrad, M. Shaevitz, Where are we with light sterile neutrinos? *Physics Reports* **884**, 1–59 (2020).
180. A. A. Aguilar-Arevalo *et al.*, Updated MiniBooNE neutrino oscillation results with increased data and new background studies. *Physical Review D* **103**, 052002 (2021).
181. J. Abdurashitov *et al.*, Measurement of the response of a Ga solar neutrino experiment to neutrinos from a Ar 37 source. *Physical Review C—Nuclear Physics* **73**, 045805 (2006).
182. V. V. Barinov *et al.*, Results from the Baksan experiment on sterile transitions (BEST). *Physical review letters* **128**, 232501 (2022).
183. V. Barinov, D. Gorbunov, BEST impact on sterile neutrino hypothesis. *Physical Review D* **105**, L051703 (2022).
184. J. M. Berryman, P. Coloma, P. Huber, T. Schwetz, A. Zhou, Statistical significance of the sterile-neutrino hypothesis in the context of reactor and gallium data. *Journal of High Energy Physics* **2022**, 1–39 (2022).
185. C. Giunti, C. A. Ternes, Confronting solutions of the Gallium Anomaly with reactor rate data. *Physics Letters B* **849**, 138436 (2024).
186. S. R. Elliott, V. Gavrin, W. Haxton, The gallium anomaly. *Progress in Particle and Nuclear Physics* **134**, 104082 (2024).
187. V. Brdar, J. Gehrlein, J. Kopp, Towards resolving the gallium anomaly. *Journal of High Energy Physics* **2023**, 1–30 (2023).
188. M. Pryce, Nuclear shell structure. *Reports on Progress in Physics* **17**, 1 (1954).
189. H. Yukawa, On the interaction of elementary particles. I. *Proceedings of the Physico-Mathematical Society of Japan. 3rd Series* **17**, 48–57 (1935).
190. B. Schaeffer, Electric and magnetic Coulomb potentials in the deuteron. *Advanced Electromagnetics* **2**, 69–72 (2013).
191. G. Gamow, *The quantum theory of the atomic nucleus*. (US Atomic Energy Commission, Division of Technical Information Extension, 1963).
192. K. Pomorski, J. Dudek, Nuclear liquid-drop model and surface-curvature effects. *Physical Review C* **67**, 044316 (2003).

193. I. Hamamoto, B. R. Mottelson, Shape deformations in atomic nuclei. *arXiv preprint arXiv:1107.5248*, (2011).
194. B. Mottelson, Elementary modes of excitation in the nucleus. *Reviews of Modern Physics* **48**, 375 (1976).
195. K. S. Krane, *Introductory nuclear physics*. (John Wiley & Sons, 1991).
196. C. G. Vayenas, S. N.-A. Souentie, *Gravity, special relativity, and the strong force: A Bohr-Einstein-de Broglie model for the formation of hadrons*. (Springer, 2012).
197. J. Lilley, *Nuclear physics: principles and applications*. (John Wiley & Sons, 2013).
198. N. Bowen, The Electromagnetic Considerations of the Nuclear Force. *Journal of Condensed Matter Nuclear Science* **33**, 194–223 (2020).
199. H. Horiuchi, K. Ikeda, A Molecule-like Structure in Atomic Nuclei of 16O* and 10Ne. *Progress of Theoretical Physics* **40**, 277–287 (1968).
200. J.-J. Aubert *et al.*, The ratio of the nucleon structure functions F2n for iron and deuterium. *Physics Letters B* **123**, 275–278 (1983).
201. A. Wuosmaa *et al.*, Evidence for alpha-particle chain configurations in Mg 24. *Physical review letters* **68**, 1295 (1992).
202. A. Merchant, W. Rae, Systematics of alpha-chain states in 4N-nuclei. *Nuclear Physics A* **549**, 431–438 (1992).
203. B. Fulton, Clustering in nuclei: nuclear chains, nuclear molecules and other exotic states of nuclear matter. *Contemporary physics* **40**, 299–311 (1999).
204. T. Kawabata *et al.*, 2α+ t cluster structure in 11B. *Physics Letters B* **646**, 6–11 (2007).
205. D. Brink, in *Journal of physics: Conference series*. (IOP Publishing, 2008), vol. 111, pp. 012001.
206. H. Horiuchi, Coexistence of cluster states and mean-field-type states. *Clusters in Nuclei: Volume 1*, 57–108 (2010).
207. T. Ichikawa, J. Maruhn, N. Itagaki, S. Ohkubo, Linear Chain Structure of Four-α Clusters in O 16. *Physical Review Letters* **107**, 112501 (2011).
208. C. Beck, in *Journal of Physics: Conference Series*. (IOP Publishing, 2014), vol. 569, pp. 012002.
209. S. Raman, C. Nestor Jr, P. Tikkanen, Transition probability from the ground to the first-excited 2+ state of even–even nuclides. *Atomic Data and Nuclear Data Tables* **78**, 1–128 (2001).
210. M. Door *et al.*, Probing new bosons and nuclear structure with ytterbium isotope shifts. *Physical review letters* **134**, 063002 (2025).
211. A. Wilzewski *et al.*, Nonlinear calcium King plot constrains new bosons and nuclear properties. *Physical Review Letters* **134**, 233002 (2025).
212. F. Kondev, M. Wang, W. Huang, S. Naimi, G. Audi, The NUBASE2020 evaluation of nuclear physics properties. *Chinese Physics C* **45**, 030001 (2021).
213. A. A. Sonzogni, T. Burrows, B. Pritychenko, J. Tuli, D. Winchell, in *International Conference on Nuclear Data for Science and Technology*. (EDP Sciences, 2007), pp. 101–103.
214. A. S. Eddington, in *A Source Book in Astronomy and Astrophysics, 1900–1975*. (Harvard University Press, 1979), pp. 281–290.
215. Y. Suzuki, Solar neutrinos. *Space science reviews* **85**, 91–104 (1998).
216. S. Pourshahian, Mass defect from nuclear physics to mass spectral analysis. *Journal of The American Society for Mass Spectrometry* **28**, 1836–1843 (2017).
217. N. Bowen, Discrepancies with the Recent Models of Nucleons. *Journal of Condensed Matter Nuclear Science* **36**, 184–202 (2022).
218. J. J. Chapman, in *38th International Conference on Plasma Science (ICOPS)*. (2011).
219. W. Thomson, THE SUN'S HEAT. *Good words* **28**, 262–269 (1887).
220. A. Y. Smirnov, The MSW effect and solar neutrinos. *arXiv preprint hep-ph/0305106*, (2003).
221. W. Manheimer, Fusion It is time to color outside the lines. *arXiv preprint arXiv:2401.16442*, (2024).

222. A. M. Suliga, S. Shalgar, G. M. Fuller, A closer look at the pp-chain reaction in the Sun: constraining the coupling of light mediators to protons. *Journal of Cosmology and Astroparticle Physics* **2021**, 042 (2021).
223. B. D. Fields, The primordial lithium problem. *Annual Review of Nuclear and Particle Science* **61**, 47–68 (2011).
224. J. A. Guzik, K. Mussack, Exploring mass loss, low-Z accretion, and convective overshoot in solar models to mitigate the solar abundance problem. *The Astrophysical Journal* **713**, 1108 (2010).
225. J. N. Bahcall, A. M. Serenelli, M. Pinsonneault, How accurately can we calculate the depth of the solar convective zone? *The Astrophysical Journal* **614**, 464 (2004).
226. J. N. Bahcall, A. M. Serenelli, S. Basu, New solar opacities, abundances, helioseismology, and neutrino fluxes. *The Astrophysical Journal* **621**, L85 (2005).
227. M. Castro, S. Vauclair, O. Richard, Low abundances of heavy elements in the solar outer layers: comparisons of solar models with helioseismic inversions. *Astronomy & Astrophysics* **463**, 755–758 (2007).
228. A. M. Serenelli, W. C. Haxton, C. Pena-Garay, Solar models with accretion. I. Application to the solar abundance problem. *The Astrophysical Journal* **743**, 24 (2011).
229. G. Buldgen *et al.*, Higher metal abundances do not solve the solar problem. *Astronomy & Astrophysics* **669**, L9 (2023).
230. C. Sagan, G. Mullen, Earth and Mars: Evolution of atmospheres and surface temperatures. *Science* **177**, 52–56 (1972).
231. G. Feulner, The faint young Sun problem. *Reviews of Geophysics* **50**, (2012).
232. M. Yan, J. Yang, Y. Zhang, H. Huang, Cloud Feedback on Earth's Long-Term Climate Simulated by a Near-Global Cloud-Permitting Model. *Geophysical Research Letters* **49**, e2022GL100152 (2022).
233. E. J. Gaidos, M. Güdel, G. A. Blake, The faint young Sun paradox: An observational test of an alternative solar model. *Geophysical research letters* **27**, 501–503 (2000).
234. I. Labbé *et al.*, A population of red candidate massive galaxies~ 600 Myr after the Big Bang. *Nature* **616**, 266–269 (2023).
235. M. Xiao *et al.*, PANORAMIC: Discovery of an ultra-massive grand-design spiral galaxy at z~ 5.2. *Astronomy & Astrophysics* **696**, A156 (2025).
236. S. Schouws *et al.*, Detection of [O III] 88 μm in JADES-GS-z14-0 at z= 14.1793. *The Astrophysical Journal* **988**, 19 (2025).